Dear Editor,

First of all, we acknowledge both reviewers for their useful comments. We answered to all points raised by the reviewers but one (the third point of Reviewer 1 cannot be answered at the current development state of observations and data assimilation software and it is definitively out of the scope of this paper). We are also a bit surprised to see again the comment 2 of the Reviewer 1. We already answered to this point in the first review. Anyway, we added material to better answer to this point (Figure 18, Figure 19 and comments).

In order to keep the paper length short, most of the answers are provided in the supplemental material, and are discussed in the paper when necessary. This choice was made because most of the answers requested additional simulations with discussion and figures. Putting this material in the paper would result in a very long paper. We adjusted the paper according to the results of the supplemental material. In particular, we added the following sensitivity tests: a) increasing the observation error of radar reflectivity factor; b) changing the shape of the searching area to compute the relative humidity pseudo-profile; c) updating IC/BC as new observations are available; d) increasing the vertical resolution of RAMS@ISAC by using 42 vertical levels. All these tests generalized the results of the paper.

Both reviewers consider the English level poor. We did our best. We corrected some errors following the comments of Reviewer 1. The journal provides a copy-editing service that will solve most language problems. If requested, we could use an external copy-editing service if the paper reaches the minor revision status.

Reviewer #1:

Title: "Preliminary results of the impact of lightning and radar reflectivity factor data assimilation on the very short term rainfall forecasts of RAMS@ISAC: application to two case studies in Italy." by Federico et al.

Recommendation: Major revisions.

Main Comments:

(1) While the authors have gone at length to address some of my earlier concerns, I still found most of the analysis presented (especially on pages 19-22) relatively rudimentary. The text is essentially reduced to unnecessarily detailed and repetitive descriptions of rainfall plots. More targeted, concise descriptions clearly highlighting the pros and cons of each DA methods should be elaborated instead. As indicated in my original review, the authors should - in that regard - show Roebber performance diagrams in their analysis to provide clearer, concise estimates of the performance of their forecasts. Additionally and as also indicated in my original review, soundings complemented with horizontal cross- sections of RH/Qv should be provided to highlight, quantitively, how the RH/Qv field are adjusted by each respective DA approach at the analysis time (radar vs lightning). Such analysis is highly desired and, arguably, critical for readers to gain a better appreciation of the first order impact of the DA, especially given that both observations used essentially adjust the same field (cf main comment 2 below).

We added the Roebber performance diagram in the revised version of the paper. The discussion on the precipitation fields for different VSF was shortened, but we believe that information provided at this stage is essential and should not be further reduced. We included, for the second stage of the Livorno case, a map showing the averaged water vapor mixing ratio between 3 and 10 km for the different model settings (Figure 18) and vertical cross-sections of relative humidity (Figure 19). The specific VSF was chosen because more information about this phase of the storm can be found in the paper when discussing the cases studies (Section 2) and radar reflectivity factor data assimilation (Section 3.1). So, this VSF is better supported by the paper discussion. Results show clear differences between radar and lighting data assimilation despite they assimilate the same both the water vapour mixing ratio.

(2) Most importantly, as indicated in my original review, the current data assimilation set up suffers from one major drawback in that both the VAR assimilation of radar reflectivity factor and the nudging of lightning data essentially adjust the same variable (Qv ~ RH via Qv/QVsat) resulting in redundant overlap. A proper combined DA set up should ensure that adjustments from different observation sources are applied to different prognostic variables: E.g., lightning adjusts the Qv field while the reflectivity factor acts on specific hydrometeor mixing ratios (even through simple linear functional relationships). With this overlap, it is also unclear how the forecast results are impacted depending on whether the nudging of Qv is performed before or after the 3DVAR of reflectivity factor data. Until this critical point is not properly addressed, I will be inclined to maintain the current editorial decision of "Major Revisions".

The fact that different observations adjust the same field is appropriate. Of course, it could create redundancy (observations are of different type, however, and this redundancy often doesn't occur) but it avoids using simplified assumptions of the relationship between reflectivity and hydrometeors. Also, the method leave to the model the task of evolving water vapour added/subtracted, which is a good feature. The analyses of the two observations are different for two reasons: a) observations are different, as clearly stated in Section 3.3; b) lightning and radar data assimilation have different impacts on the relative humidity (or water vapor mixing ratio) via the data assimilation system.

The method used to assimilate radar reflectivity is well known in the bibliography and was shown to have a huge impact on the analysis also when compared to methods using reflectivity – hydrometeor's mixing ratios relationships (Fabry and Sun, 2010). The method used to assimilate lightning is well known in bibliography (Fierro et al., 2012) and widely applied. We are not discussing the methods, we are applying them in a way that is simple, straightforward and effective for rainfall VSF of two challenging cases.

It was clearly shown that assimilating lightning or radar reflectivity factor had a different impact on the precipitation field (3 VSF), on the evolution of water vapor (Section S1 of the supplemental material) and, in this version of the paper, on the maps of water vapor mixing ratio averaged between 3 and 10 km and on cross sections of relative humidity for one VSF. Differences are also apparent and interesting for other VSFs, but, as stated above, the VSF chosen is better supported by the paper.

The problem of assimilating first lightning and then radar and vice-versa is not very well understood because lightning is assimilated before and after radar data and vice-versa in the current setting (there is not a specific order). We could skip the first radar file to start with lighting data assimilation (we note that we did this experiment several times in the past, also for Serano and Livorno, and the results of this paper remain valid), but this is a different problem because part of the data are missing.

In summary, to better answer to this point compared to the already revised version of the paper, we added: a) a discussion in Section 3.3 to better support the results given in Section 4; b) maps of averaged mixing ratio between 3 and 10 km at the end of the assimilation period for one of the VSF; c) cross sections of relative humidity at the end of the assimilation period for one VSF.

(3) To complement (2), ideally, the Doppler (radial) winds should adjust the three Cartesian components of the wind field. Stating that such data "aren't yet ready" is, in my view, a succinct pretext to evade the (necessary) work.

This comment seems inappropriate considering the amount of work we did in the first and in this review. Again, radial velocity is not available at the moment for the motivation already provided in the paper and its assimilation is outside the scope of this paper.

(4) To provide a more equitable estimate of the performance of the DA method, the authors should also select at least one high impact weather event wherein the CTRL forecast performed reasonably well (e.g., a strongly forced case along a cold front). This point also was indicated in my original review but hasn't been satisfactorily addressed by the authors.

We considered this point in the new Section S.5 of the supplemental material. In particular, we considered a case study of a well predicted event in Rome (5 November 2017). We showed the limited impact of lightning data assimilation for this case, despite the large number of lightning observed for the event.

(5) For radar reflectivity factor, the DA should make use of 50-km disks instead of squares. This is easy to code in Fortran by using e.g., a 2-D mask array to find the grid points fitting within the disks.

We applied a well-known and widely accepted assimilation method. In the original formulation, a square is used. We agree that a circular shape could be also a good choice. However, the impact of this shape is expected to be small. We showed this point with a sensitivity experiment using a 50 km diameter disk rather than a square with 50 km edge in the assimilation of radar reflectivity factor. The experiment is discussed in Section S4 of the supplemental material: "Sensitivity to radar formulation".

(6) Last, I still found the level of English relatively poor and generally not suited/inappropriate for the level of a peer-reviewed journal. Because these issues are collectively substantial, I opted, for now, not to dwell on such editorial comments (including grammar).

We did our best to improve the English. Consider also that the journal provides a copy-editing service before the publication of the paper. If requested by the reviewer/editor we can use an external copy editing service if the paper goes to minor revision status.

Additional comments:

(1) Line 42: Radar data are far from being "unconventional".

The sentence was changed to avoid "unconventional".
(2) Line 44: Model "deficiencies" are by no means limited to oceanic regions.
Ok. We deleted "and model deficiencies".
(3) Line 47: "high spatio-temporal resolution"
Corrected.Thanks.
(4) Line 75: "Lightning is another source ...". Line 95: "convection-resolving"
Ok.
(5) Line 99: Not "extended" but "adopted".
Ok.
(6) Line 17-18, 39-40, 47,134, 249, 258-260, 266-267, 389, 711-712, 761 (among many other instances): Consider revising (grammar).
Ok. We changed/corrected these sentences. Also in other parts of the paper.
(7) Line 57-60: delete or include well known (seminal) studies such as those from Tong and Xue, Gao's, Aksoy's, Zhang's to name a few.
Deleted.
(8) Line 340: "subjectively as a compromise between increasing ..."
Ok.Thanks.
(9) Line 389: downscaled ? Please elaborate/explain.
Ok. We used downscaled. The explanation is already given.
(10) Line 414: This is reminiscent of the Gaspari and Cohn function for EnKF localization.
Ok. No actions were taken.
(11) Line 480: "With these settings, larger weights are given to". Line 489: "In contrast,". Line 497 "highlights the difficulty". Line 507: "reduce the relative". Line 703: "room for improvement"
Ok.Thanks.
(12) Lines 527-530: redundant; delete.
These lines were added for a specific request of Reviewer 2. We wouldn't delete them.

Reviewer #2:

„The impact of lightning and radar data assimilation on the performance of very short term rainfall forecasts for two case studies in Italy"

by

Stefano Federicio, Rosa Claudia Torcasio, Elenio Aviolo, Olivier Caumont, Mario Montopoli, Luca Baldini, Gianfranco Vulpiani and Stefano Dietrich

The study discusses the impact of the assimilation of lightning and radar reflectivity data on the performance of very short-range rainfall forecasts for two convective case studies in Italy. They showed that especially the combined assimilation of both observation types has a clear and positive impact on the forecast performance.

The manuscript is interesting and tackles a very important subject, since the forecast of severe precipitation is still a major weakness of current forecast systems. With the supplemental material, the methodology is now described with enough detail. In addition, most of my other comments are discussed in the new manuscript. I am nevertheless still concerned about your coarse vertical resolution. Since I guess that you anyway plan to increase the number of vertical levels in the future, the paper would greatly benefit when you include one first test with a higher horizontal resolution. If the results are similar or the same – fine.

Therefore, I stick to it. A **major revision** is needed before I can suggest the publication of the manuscript.

In the first review of this paper we answered to the points of Reviewer 2 by discussion, i.e. without the support of sensitivity tests. However, they are all good points and deserves further investigation, as requested by the reviewer. In this review, we answer to these points using the results of sensitivity tests.

Comments

- To generalize your results, a simulation with a larger number of vertical levels is needed for at least one of the cases. If it shows the same or similar results, you can be sure that your methodology works as expected.

  This point is discussed in Section S4: Sensitivity to model simulation. We considered a simulation with 42 vertical levels (the future operational setting of the model). We considered only the Livorno case. The results are similar to those of 36 levels showing that the findings of this paper are not sensitive to the number of vertical levels, at least for the numbers of levels considered. However, the results show that increasing the vertical levels from 36 to 42 should positively impact the rainfall VSF of the CTRL setting. This (small) improvement, however, is not transferred to the VSF assimilating both lightning and radar reflectivity factor, likely because the background error matrix in the 3D-Var is not optimally set for RAMS@ISAC with 42 levels.

- The error value of 1 to 3 dBz seems to be too small, making the system very sensitive to the radar data. Especially when combining this with a pure sampling of the radar data sounds dangerous to me. Please explain why you use this error value.

  This point is discussed in Section S4: Sensitivity to radar formulation. The choice of the error value when computing pseudo-profiles is not very important for the cases considered in this paper. Motivations are explained in section S4. In general, however, this error could be too small, as suggested by the reviewer. We highlighted this comment in the paper.

- You mention in the new manuscript that it is a limitation of the current manuscript that the R10 run is not updated after the acquisition of new data. True, but this needs to be quantified in a way. Depending on the situation, it is well possible that your very short forecasts are not influenced by this weakness. But it is necessary to show it.

  This point is discussed in Section S4: Sensitivity to model formulation. This sensitivity test did not show an important impact on the results of this paper. The motivations are discussed in Section S4.

- The readability of the original proposal was better. Therefore, the English needs considerable improvement before the manuscript can be accepted.

  We did our best to improve the English, and corrections have been also made by Reviewer 1. The journal provides a copy-editing service before the publication of the paper. If requested by the reviewer/editor we can contact an external copy editing service if the paper goes to minor revision status.

LIST OF RELEVANT CHANGES

We introduced the performance diagram in Figures 15-17 (panels f), as requested by Reviewer 1.

A discussion was put in Section 3.3 to clarify why we expect different results for very short term forecasts assimilating radar reflectivity factor or lightning.

Figure 18 and 19 are new and are used to show that, despite radar reflectivity factor and lightning data assimilation both adjust the water vapour mixing ratio, results of the experiment assimilating either radar reflectivity factor or lightning can be quite different. These figures, the discussion put in Section 3.3, and the results already presented in the paper should definitively answer to the major point 2 of Reviewer 1.

The sensitivity tests requested by Reviewer 2 were put in the supplemental material of the paper. The results of these sensitivity tests are recalled in the paper whenever necessary. The sensitivity tests are the following: a) increasing the observation error of radar reflectivity factor; b) updating IC/BC as new observations are available; c) increasing the vertical resolution of RAMS@ISAC by using 42 vertical levels.

Section S5 of the supplemental material discusses a case study well predicted by the model and the low impact of lightning data assimilation for this case. This case was added to provide a more equitable evaluation of DA.

A sensitivity test is discussed in the supplemental material to answer to the point 5 of Reviewer 1.

We corrected some English errors following the comments of Reviewer 1. More suggestions are welcome. The journal provides a copy-editing service that will solve most language problems.

The impact of lightning and radar reflectivity factor data assimilation on the very short term rainfall forecasts of RAMS@ISAC: application to two case studies in Italy

Eliminato: Preliminary results of t

Stefano Federico[1], Rosa Claudia Torcasio[1], Elenio Avolio[2], Olivier Caumont[3], Mario Montopoli[1], Luca Baldini[1], Gianfranco Vulpiani[4], Stefano Dietrich[1]

1. ISAC-CNR, via del Fosso del Cavaliere 100, Rome, Italy
2. ISAC-CNR, zona Industriale comparto 15, 88046 Lamezia Terme, Italy
3. CNRM UMR 3589, University of Toulouse, Météo-France, CNRS, 42 avenue G. Coriolis, 31057 Toulouse, France
4. Dipartimento Protezione Civile Nazionale Ufficio III - Attività Tecnico Scientifiche per la Previsione e Prevenzione dei Rischi, 00189 Rome

Abstract

In this paper, we study the impact of lightning and radar reflectivity factor data assimilation on the precipitation VSF (Very Short-term Forecast, 3 hours in this study) for two severe weather events occurred in Italy. The first case refers to a moderate and localised rainfall over central Italy occurred on 16 September 2017. The second case, occurred on 9 and 10 September 2017, was very intense and caused damages in several geographical areas, especially in Livorno (Tuscany) where nine people died.

Formattato: Interlinea: multipla 1,15 ri

Eliminato: relevant

Eliminato: case studies

The first case study was missed by several operational forecasts, including that performed by the model used in this paper, while the Livorno case was partially predicted by operational models.

Eliminato: (from both public and private sectors)

We use the RAMS@ISAC model (Regional Atmospheric Modelling System at Institute for Atmospheric Sciences and Climate of the Italian National Research Council), whose 3D-Var extension to the assimilation of RADAR reflectivity factor is shown in this paper for the first time.

Results for the two cases show that the assimilation of lightning and radar reflectivity factor, especially when used together, have a significant and positive impact on the precipitation forecast. For specific time intervals, the data assimilation is of practical importance for civil protection purposes because changes a missed forecast of intense precipitation (≥ 40 mm/3h) in a correct one. While there is an improvement of the rainfall VSF thanks to the lightning and radar reflectivity factor data assimilation, its usefulness is partially reduced by the increase of the false alarms, especially when both data area assimilated.

Keywords: data assimilation, lightning, radar reflectivity factor, RAMS@ISAC.

1. Introduction

Initial conditions of numerical weather prediction (NWP) models are a key point for a good forecast (Stensrud and Fritsch, 1994; Alexander et al., 1999). Nowadays limited area models are operational at the kilometric scale (< 5 km) and data assimilation of observations with high spatio-temporal resolution as lightning or radar reflectivity factor[1], is crucial to correctly represent the state of the atmosphere at local scale (Weisman et al., 1997; Weygandt et al., 2008). This is especially important over the sea, where the absence of local observations can misrepresent convection.

The assimilation of radar reflectivity factor is useful to improve the weather forecast considering the high spatio-temporal resolution of radar data.

First attempts to assimilate radar reflectivity factor are reported in Sun and Crook (1997, 1998), who expanded VDRAS (Variational Doppler Radar Analysis System) to include microphysical retrieval. Following these studies, several systems to assimilate radar observations, both Doppler velocity and reflectivity factor, were developed (Xue et al., 2003, Zhao et al., 2006; Xu et al., 2010). All these studies showed the stability and robustness of assimilating radar observations as well as the improvement of weather forecast.

In addition to direct methods, which assimilate the radar reflectivity factor adjusting the hydrometeor contents, there are indirect methods adjusting other variables. In particular, the method of Caumont et al. (2010) assimilates the relative humidity field. It consists of two different steps: a 1D retrieval of relative humidity (pseudo-profile), which depends on the radar reflectivity factor observations, followed by 3D-Var assimilation of the pseudo-profile. This method has the advantage to reduce the computational cost at the kilometric scale.

The choice of updating the moisture field directly is motivated by its greater impact on analyses and forecasts in comparison to that of hydrometeor-related quantities (e.g., Fabry and Sun, 2010).

Caumont et al. (2010) showed that the method improved the weather prediction of a heavy precipitation event in southern France and of an eight-day long assimilation cycle experiment.

The method was applied in other studies (Wattrelot et al., 2014, using AEROME model; Ridal and Dalbom, 2017; using HARMONIE model), or modified using 4D-Var in place of 3D-Var (Ikuta and Honda, 2011; using JNoVa model) showing its capability to improve the weather forecast. The methodology is also used in the operational context (Wattrelot et al., 2014).

Lightning is another important source of asynoptic data due to its ability to locate precisely the convection with few temporal gaps (Mansell et al., 2007). In the last two decades, there have been attempts to assimilate lightning into meteorological models both at low horizontal resolution, which

[1] Throughout the paper we use the expression radar reflectivity factor, which is the quantity provided by the radar (and expressed in $mm^6 m^{-3}$ or dBz) after conversion from the received power. The radar reflectivity factor is different from reflectivity and is obtained in the special case of Rayleigh scattering. Reflectivity is not the quantity that radars usually provide and display on their screens although most of people refer to it.

Eliminato: resolution of few kilometres

Eliminato: non-conventional

Eliminato: ,

Eliminato:

Eliminato: data

Eliminato: and model deficiencies

Eliminato: [2]

Eliminato:

Eliminato: repetition rate (asynoptic data) and the high spatial resolution (local scale)

Eliminato: the

Eliminato: Radar data are also assimilated in WRF (Weather Research and Forecasting model, Skamarock et al., 2008; Barker et al., 2012) both using 3DVar (Xiao et al., 2005, 2007; Barker et al., 2004) and 4DVar (Wang et al., 2013; Sun and Wang, 2012). The capability to assimilate radar data into WRF was recently applied to a heavy rainfall event over Central Italy by Maiello et al. (2014). They showed a notable and positive impact of the radar data assimilation on the precipitation forecast, also when radar data were assimilated together with conventional data (SYNOP and RAOB).

Eliminato:

Eliminato: acts on

Eliminato: method

Eliminato: Flashes are

Eliminato: their

Formattato: Giustificato

need a cumulus parameterization scheme to simulate convection, and at convection permitting scales.

First attempts to assimilate lightning in NWP models were based on relationships between lightning and rainfall rate estimated by microwave sensors on board polar satellites (Alexander et al., 1999; Chang et al., 2001; Jones and Macpherson, 1997; Pessi and Businger, 2009). In this approach, the rainfall rate was computed as a function of the density of lightning observations and then transformed into latent heat, which was assimilated. The results of these studies showed a positive impact of the lightning data assimilation on the forecast up to 24h also for fields at the large scale, as sea-level pressure.

Eliminato: The

Eliminato: f

The study of Papadopulos et al. (2005) used lightning to locate convection and the simulated water vapour profile was nudged towards vertical profiles recorded during convective events.

Eliminato: model

Mansell et al. (2007) modified the Kain-Fritsch (Kain and Fritsch, 1993) cumulus convective scheme to force convection when/where flashes are observed while the convective scheme was not activated in the model simulation, demonstrating the potential of lightning to improve the convection forecast. A similar approach was introduced by Giannaros et al. (2016) into WRF showing the positive impact of lightning data assimilation on the precipitation forecast up to 24h for eight convective events occurred over Greece.

Fierro et al. (2012) introduced a methodology to assimilate lightning at convection-resolving scales by modifying the water vapour mixing ratio simulated by the WRF according to a function depending on the flash-rate and on the simulated graupel mixing ratio. The water vapour could be assimilated by nudging (Fierro et al., 2012) or 3D-Var (Fierro e al., 2016).

Eliminato: permitting

Qie et al. (2014), using WRF, adopted the methodology of Fierro et al. (2012) to assimilate ice crystals, graupel and snow, showing promising results for deep convective events in China.

Eliminato: extended

Fierro et al. (2015) studied the performance of the Fierro et al. (2012) method for 67 days spanning the 2013 warm season over the CONUS giving a statistically robust estimation of the performance of the method. The computationally inexpensive lightning data assimilation method improved considerably the short-term (≤ 6h) precipitation forecast of high impact weather.

Lynn et al. (2015) and Lynn (2017) also applied the method of Fierro et al. (2012) to boost the local thermal buoyancy where/when lightning is observed. Results show that lightning data assimilation improved lightning forecast. Importantly, Lynn et al. (2015) offer an approach to address spurious convection (i.e., convection removal), which is a more challenging problem to tackle.

Eliminato: ,

Eliminato: far

Federico et al. (2017a) implemented the methodology of Fierro et al. (2012) in RAMS@ISAC model, showing the systematic and significant improvement of the precipitation forecast at the very short range (3h) for twenty case studies occurred over Italy; the impact of lightning data assimilation for longer time ranges (6h-24h; Federico et al., 2017b) showed considerable impact on the 6h precipitation forecast, with smaller (negligible) effects at 12 h (24 h).

In this paper, we study the impact of radar reflectivity factor and lightning data assimilation on the very short term (3h) rainfall prediction for two case studies in Italy. We use the method of Fierro et al. (2012) to assimilate lightning and the method of Caumont et al. (2010) to assimilate the radar reflectivity factor. The case studies occurred in September 2017. The first case, hereafter also referred to as Serano, occurred on 16 September, was characterized by moderate-intense and localized rainfall. The second case, hereafter also referred to as Livorno, occurred on 09-10 September, and was characterized by deep convection and very intense precipitation in several parts of Italy. Even if the Livorno case occurred before the Serano case, we reverse the chronological order in the discussion, ordering the event from the less intense to the most intense.

Eliminato: over

The forecast of severe events at the local scale still remains a challenge because of the multitude of physical processes involved over a wide range of scales (Stensrud et al., 2009). The Serano case study, being localized in space, poses challenges in forecasting the exact position and timing of convection initiation; the Livorno event involves the interaction between a high impact storm and the complex orography of Italy, which is difficult to simulate at the local scale. For the above reasons the forecast of both events was challenging, as confirmed by the poor forecast of RAMS@ISAC. The difficulty to forecast timely and accurately the precipitation field is the reason for choosing them as test cases.

This paper presents for the first time the assimilation of the total lightning (intra cloud + cloud to ground) and radar reflectivity factor in RAMS@ISAC and shows how the assimilation of the radar reflectivity factor works together with total lighting data assimilation. Also, this paper shows that the precipitation forecast using cloud scale observations over complex terrain can be accurate, contributing to a number of works on the same subject.

Eliminato: how accurate in space and time can be

Eliminato: of the precipitation field

Eliminato: in this way

The paper is organized as follows: Section 2 gives details on the synoptic environment of the case studies showing daily precipitation, lightning and radar observations; Section 3 gives details on the meteorological model, lightning and radar data assimilation; Section 4 shows the results for three very short-term forecast (VSF), one for Serano and two for Livorno; Discussion and conclusions are given in Section 5. This paper has additional material where we discuss: a) how the lightning and radar reflectivity factors data assimilation impact the total water field evolution; b) the sensitivity of the results to the choice of key parameters of lightning data assimilation; c) the sensitivity of the results to two aspects of the radar formulation; d) the sensitivity of the results to two aspects of RAMS@ISAC setting; e) the impact of lightning data assimilation for a well predicted case study. Supplemental material gives also the form of the forward radar operator.

Eliminato: adjust

Eliminato: .

2. The case studies

2.1 The 16 September 2017 (Serano) case study

During the 16 September 2017 Italy was under the influence of a cyclone that developed to the lee of the Alps. The storm crossed Italy from NW to SE leaving light precipitation over most of the peninsula with moderate rainfall over Central Italy. Figure 1 shows the precipitation recorded by the Italian raingauge network on 16 September 2017. Light precipitation (< 5 mm/day) is reported by 1018 raingauges out of the 1666 stations measuring precipitation (≥ 0.2 mm/day) on this day. Fourteen stations over Central Italy recorded more than 50 mm/day. The maximum precipitation was 90 mm/day in Città di Castello (Umbria Region, Figure 1). Because the meteorological radar closest to the maximum precipitation is over mount Serano (Figure 1), hereafter this event will be referred to as Serano.

The synoptic condition during the event is shown in Figure 2. At 500 hPa (Figure 2a) a trough, elongated in the SW-NE direction, extends over Western Europe and air masses are advected from SW towards western Alps. The interaction between the airflow and the Alps generates a low pressure to the lee of the Alps over Northern Italy.

The analysis at the surface (Figure 2b) shows the meteorological front represented by the equivalent potential temperature gradient between air masses advected over the Mediterranean Sea from NW and air masses advected from the South over the Tyrrhenian Sea. Notable is the feeding of warm unstable air masses towards Central Italy.

Infrared satellite images (Figure 3), from 00 UTC on 16 September to 00 UTC on 17 September, show the cold front structure moving slowly from NW to SE. Interestingly, at 00 UTC on 16 September, it is apparent the well-defined cloud system over Central Italy (red circle of Figure 3a), which caused most of the daily precipitation observed between 43.50 and 45.0 N.

Eliminato: in the six-hours 00 UTC-06 UTC on 16 September.

The well-defined cloud system over Central Italy is also shown in the radar Constant Altitude Plan Position Indicator (CAPPI) at 3 km above sea level at 02 UTC on 16 September (Figure 4). This CAPPI is formed by interpolating all the available data from the federated Italian radar network

Eliminato: evident

coordinated by the Department of Civil Protection (twenty-two radars, see Section 3.3 for their positions) and it is also referred to as the national radar composite (hereafter also mosaic). Several convective cells exceeding 35 dBz can be noted over central-northern Italy. Importantly, the cloud system over Central Italy shown by the satellite infrared channel at 00 UTC (Figure 3a) and that of the radar at 02 UTC have similar positions, showing that the cloud system was active for several hours over Central Italy.

Figure 5 shows the lightning recorded by the LINET network (Betz et al., 2009) on 16 September 2017. More than 105.000 flashes were recorded; most of them occurred in the afternoon and evening, but a secondary maximum occurred in the night, from 00 UTC to 06 UTC. In this phase, more than 3000 flashes were observed over Central Italy.

Eliminato: during the day

Eliminato: during

2.2 The 09-10 September 2017 (Livorno) case study

During the days 09 and 10 September 2017, Italy was hit by a severe storm characterised by intense and widespread rainfall over the country. Figure 6a shows the precipitation on 09 September recorded by the Italian raingauge network. Rainfall was intense over the Alps, where the maximum daily precipitation was observed (193 mm/day), and over Liguria, with precipitation of the order of 30-50 mm/day. One station over Tuscany reported 90 mm/day, showing that intense precipitation already started over the Region. The storm on 09 September was intense ; 20 raingauges reported more than 100 mm/day and 70 raingauges more than 60 mm/day. In most cases, this precipitation occurred in few hours.

Eliminato: intensity of the

Eliminato: high

Eliminato: because

Eliminato: , and, in

Eliminato: occurred

Eliminato: within

The following day (see Figure 6b) had higher rainfall. Precipitation occurred mainly over Central Italy, especially over Lazio, and over Northern Italy, in particular the North-East. In Tuscany, the two stations close to the sea, in the Livorno area, recorded about 150 mm/day mostly fallen in the hours between 00 and 06 UTC.

Eliminato: The rainfall on 10 September was abundant: and 60 raingauges recorded more than 100 mm/day.

Synoptic conditions leading to this storm are shown in Figure 7. At 500 hPa (Figure 7a) a trough extends from Northern Europe towards the Mediterranean. The interaction between the air-masses and Western Alps generated a pressure low to the lee of the Alps, which crossed the whole peninsula from NW to SE. It is noted the divergent flow over Central and Northern Italy favouring upward motions.

Eliminato: depression

At the surface, Figure 7b, the equivalent temperature gradient over the western Mediterranean is caused by the contrast between air masses pre-existing over the sea and air masses advected from France towards the Mediterranean. The pressure field at the surface advects air masses from the

Eliminato: it is evident

South over the Tyrrhenian Sea. These warm and humid air masses feed the cyclone during its development.

From a synoptic point of view, Livorno and Serano cases are similar and represent two cyclones developing to the lee of the Alps (Buzzi and Tibaldi, 1978). However, the Livorno case is more intense than Serano.

Eliminato: as shown by the larger rainfall occurred in the former case

Eliminato: .

The notable intensity of the Livorno case is confirmed by the lightning observations (Figure 8). During the evening of 9 September (after 18 UTC) about 38.000 flashes were recorded by LINET. On 10 September about 290.000 flashes were recorded over Italy, following the movement of the storm propagating from NW to SE. So, more than 300.000 flashes were recorded from 18 UTC on 09 September to 00 UTC on 11 September, which are more than three times those recorded for Serano.

Thermal infrared satellite images (channel, 10.8 micron; Figure 9) show the extension of the cloud coverage every 12 hours. It is well evident the cloud system associated with the cold front over Europe. More specifically, the satellite image at 00 UTC shows the cloud system over Livorno area (red circle in Figure 9b), before the most intense precipitation period over Tuscany (00-06 UTC), while Figure 9c shows the cloud system over Central Italy (orange circle), at the end of the period of intense precipitation over Lazio (06-12 UTC).

Eliminato: main

Eliminato: event

We conclude the synoptic analysis of the case study with two CAPPI at 3 km observed by the radar network of the Department of Civil Protection. The CAPPI in Figure 10a, at 00 UTC on 10 September, shows the cloud system over Tuscany with reflectivity factor up to 40 dBz. Other clouds cause rainfall over northern Italy. The CAPPI of Figure 10a is the last assimilated by the 00-03 UTC VSF on 10 September shown in Section 4.2.1.

Figure 10b shows the CAPPI of the national radar mosaic at 3 km above the sea level and at 06 UTC. The cloud system is moving towards Central Italy with reflectivity up to 45 dBz. Other cloud systems are apparent over northern Italy. Figures 10a-10b well represent the movement of the storm towards SE and Figure 10b shows the last CAPPI assimilated by the 06-09 UTC VSF shown in Section 4.2.2.

3.Data and Methods

3.1 RAMS@ISAC and simulations set-up

The RAMS@ISAC is used as NWP driver in this work. The model is based on the RAMS 6.0 model (Cotton et al., 2003) with the addition of four main features, as well as a number of minor improvements. First, it implements additional single moment microphysical schemes, whose performance is shown in Federico (2016): among them, the WSM6 (Hong and Lim, 2006) is used in this paper. Second, it predicts the occurrence of lightning following the diagnostic method of Dahl et al. (2011), the implementation being discussed in Federico et al. (2014). Third, the model assimilates lightning through nudging (Fierro et al., 2012, 2015; Federico et al., 2017a). Fourth, the model implements a 3D-Var data assimilation system (Federico, 2013, hereafter also RAMS-3DVar), whose extension to the radar reflectivity factor is presented in this paper (Section 3.3).

The list of the physical parameterisation schemes used in the simulations of RAMS@ISAC is shown in Table 1.

Considering the domains and the configuration of the grids (Figure 11 and Table 2), two different set-ups are used for Serano and Livorno. For the first case, we use the domains D1 and D2, while for Livorno we use also the domain D3. The first domain covers a large part of Europe and extends over the North Africa. Grid horizontal resolution is 10 km (R10). The second domain covers the whole Italy and part of Europe and the grid has 4 km horizontal resolution (R4). The third domain covers the Tuscany Region, has 4/3 km horizontal resolution (R1), and it is used for Livorno to represent with higher spatial detail the precipitation field over Tuscany. The fine structures of the precipitation field are smeared out over Tuscany using only domains D1 and D2. The operational implementation of the RAMS@ISAC model uses the domains D1 and D2 and no refinements for specific areas of Italy are used because Italy is a complex orography country and grid refinements for a specific event can be done only a-posteriori, i.e. after the occurrence of the event.

All domains share the same vertical grid. It covers the troposphere and the lower stratosphere. Vertical levels are more packed close to the ground. Among the 36 levels used in this paper 10 are below 1 km, 14 below 2 km and 17 below 3 km. The first vertical level is at 50 m above the surface in the terrain following coordinates used by RAMS@ISAC, the level 21 is at 5122 m. Above 6 km the model levels are about 1000 m apart, while the maximum allowed distance between two levels is 1200 m. The complete list of the vertical levels is shown in the supplemental material of this paper (Table S2).

The vertical grid is the same as the operational setting of RAMS@ISAC and is a compromise between vertical resolution and computing time. The number of vertical levels will be increased to 42, starting from September 2019, to better resolve the phenomena in this direction (Planetary Boundary Layer processes, vertical motions, interaction between air masses and orography etc.), nevertheless the current setting was successfully applied to the forecast of several heavy precipitation events over Italy. A sensitivity test, using 42 vertical levels for the Livorno case, shows similar results to those

Eliminato: main
Eliminato: For this domain, the
Eliminato: of the grid
Eliminato: extends over
Eliminato: The resolution and the extension of the grids in the vertical direction is the same for the three domains
Eliminato: The vertical grid
Eliminato: have different spacings and
Eliminato: 5
Eliminato: 8
Eliminato: 24
Eliminato: 5200
Eliminato: with a maximum of 1200 m for the vertical layer at the model top
Eliminato:
Eliminato:
Eliminato: In the future, t
Eliminato: increased
Eliminato: used
Eliminato: in the

reported in the next section. Details on this simulation can be found in the supplemental material of this paper.

Eliminato:

The nesting between the first and second domains is one-way, while the nesting between the second and the third domains is two-way.

VSF is implemented as shown in Figure 12. First a run with R10 configuration is performed using the 0.25° horizontal resolution GFS analysis/forecast cycle issued at 12 UTC as initial and boundary conditions. R10 run, which starts at 12 UTC on 16 September for Serano and at 12 UTC on 09 September for Livorno, lasts 36 h and doesn't assimilate neither radar reflectivity factor nor lightning. The R10 run is not updated after the acquisition of new data by the analysis system and this is a limitation of the results shown in this paper. However, a sensitivity test for Livorno case study shows that this limitation doesn't have a significant impact on the results presented in the next Section. Details on this experiment can be found in the supplemental material of this paper.

Starting from 12 UTC, ten VSF are performed using R4 for Serano and both R4 and R1 for Livorno. The VSF lasts 9h and uses R10 simulation as initial and boundary conditions (one-way nesting). The 9h forecast is divided into two parts: the first six hours are the assimilation stage when RAMS@ISAC simulation is adjusted by data assimilation, whereas the last three hours are the forecast stage, without data assimilation. During the assimilation stage, flashes are assimilated by nudging (Section 3.2), while radar reflectivity factor is assimilated every one-hour by RAMS-3DVar (Section 3.3).

Eliminato: Caumont et al. (2010),

It is noted that data assimilation is performed over the domain D2 (R4) only, and the innovations are transferred to the domain D3 (R1), for the Livorno case, by the two way-nesting. The domain D3 is used for the Livorno case to refine the resolution of the precipitation field over Tuscany and to show the spatial and temporal precision of the precipitation forecast over Tuscany using data assimilation. However, its usage is exceptional because, as stated above, Italy is a complex orography country and grid refinements for specific areas are used only after the occurrence of the event. For this reason, the domain D3 is usually not used in RAMS@ISAC and no statistics about the background error are available for this grid.

Because lightning and radar reflectivity factor are cloud scale observations, their assimilation at higher horizontal resolution by 3D-Var is foreseeable in future works.

The verification of the VSF for precipitation is done by visual comparison of the model output with the raingauge network of the Department of Civil Protection, which has more than 3000 raingauges all over Italy.

In addition we consider the FBIAS (Frequency Bias; range [0, + ∞)), where 1 is the perfect score, i.e. when no misses and false alarms occur), POD (Probability of Detection; range [0, 1], where 1 is the perfect score and 0 the worst value), ETS (Equitable Threat Score; range [-1/3,1], where 1 is the perfect score and 0 is a useless forecast), TS (Threat Score; range [0,1] where 1 is the perfect score and 0 the worst value). Scores are computed from 2x2 dichotomous contingency tables (Wilks, 2006) for different rainfall thresholds and for different neighbourhood radii. Moreover, performance diagrams (Roebber, 2009) are used to summarise the scores.

Eliminato: and

3.2 Lightning data assimilation

Lightning data are provided by LINET (LIghtning detection NETwork; Betz et al., 2009; www.nowcast.de) which has more than 500 sensors worldwide with the greatest density over Europe (more than 200 sensors). The network has a good coverage over Central Europe and Western Mediterranean (from 10 W to 35 E and from 30 N to 60 N). The area of good coverage includes the region considered in this paper.

LINET exploits the VLF/LF electromagnetic bands and provides measurements of both intra-cloud (IC) and cloud to ground (CG) discharges. IC strokes are detected as long as lightning occurs within 120 km from the nearest sensor thanks to an optimised hardware and advanced techniques of data processing (TOA-3D, Betz et al., 2004). According to Betz et al. (2009), LINET has a location accuracy of 125 m for an average distance of 200 km among the sensors verified by strikes into towers of known positions.

The good performance of the LINET network and its ability to detect IC strokes is shown in Lagouvardos et al. (2009) for a storm in southern Germany, while the good performance over Italy, including both CG and IC strokes, is discussed in Petracca et al. (2014).

The lightning data assimilation scheme is that of Fierro et al. (2012; 2014; 2015) and uses the total lightning, i.e. intra-cloud plus cloud to ground flashes.

The method starts by computing the water vapour mixing ratio q_v:

$$q_v = Aq_s + Bq_s \tanh(CX)(1 - \tanh(Dq_g^{\alpha})) \quad (1)$$

Where coefficients are set to A=0.86, B=0.15, C=0.30, D=0.25, α=2.2, q_s is the saturation mixing ratio at the model atmospheric temperature, and q_g is the graupel mixing ratio (g kg^{-1}). *X* is the number of total flashes (IC+CG) falling in a grid box of domain D2 (R4) in the past five minutes. The mixing ratio q_v of Eq. (1) is computed only for grid points where flashes are recorded. More specifically, for each grid point we consider the number of flashes falling in a grid box centred at the grid point in the last five minutes. The mixing ratio of Eqn. (1) is compared with that predicted by the model. If the mixing ratio of Eqn. (1) is larger than the simulated one, the latter is nudged towards the value of Eqn. (1), otherwise the modelled mixing ratio is left unchanged. This method can only add water vapour to the forecast.

The check and eventual substitution of the water vapour is performed every five minutes and it is made within the mixed phase layer zone (0 °C, -25°C), wherein electrification processes caused by the collision of ice and graupel are the most active (Takahashi 1978, Emersic and Sounders, 2010; Fierro et al., 2015).

The scheme of Fierro et al. (2012; 2015) was adapted to RAMS@ISAC in Federico et al. (2017a). In particular, the coefficient C of Eqn. (1) was rescaled from that of Fierro et al. (2012) considering the different spatio-temporal resolution of gridded lightning data; then the coefficient C was tuned (increased) by trials and errors considering two case studies of HyMeX-SOP1 (15 and 27 October 2012). The C constant was adapted subjectively as a compromise of increasing the hits and minimising false alarms. POD and ETS scores were considered as metrics for this purpose. Then, Eqn. (1) was applied to twenty case studies of HyMeX-SOP1 giving a statistically significant (90, or 95% depending on the rainfall threshold) improvement of the RAMS@ISAC precipitation VSF (3h).

Nevertheless, a definitive statistic on the performance of rainfall VSF to nudging formulation in RAMS@ISAC is missing and further studies are needed in this direction. Also, the optimal choice of the coefficients A, B, C, D and α is case dependent.

Fierro et al (2012) applied the method using the ENTLN network, which has a detection efficiency (DE) greater than 50% for IC over Oklahoma, where the ENTLN data were used. The emphasis on IC flashes in the set-up of Fierro et al. (2012) is given because observational and model studies have provided evidence that IC flashes correlate better than CG flashes with various measures of intensifying convection (updraft strength, volume, graupel mass flux etc.; MacGorman et al. 1989; Carey and Rutledge 1998; MacGorman et al. 2005; Wiens et al. 2005; Kuhlman et al. 2006; Fierro et al. 2006; Deierling and Petersen 2008; MacGorman et al. 2011). For these reasons methods using both IC and CG flashes perform better than those using CG only, being CG flashes correlated with the descent of reflectivity cores and the onset of the demise of the storm’ s updraft core (MacGorman and Nielsen, 1991).

The analysis of the case studies shows that IC strokes are about 30% of the total number of strokes reported by LINET. Also, the fraction of IC strokes to the total strokes depends on the position. For

Eliminato: spatial and

Eliminato:

Eliminato: the

Eliminato: considering

Eliminato: two opposite requests:

Eliminato: n exhaustive

Eliminato: is

Eliminato: that use

Eliminato: s

example, for the Serano case, the fraction of IC strokes detected by LINET over the area hit by the largest precipitation is more than 50% while over the Adriatic Sea it decreases to 10%.
It is also noted that DE for IC strokes cannot be reliably compared between LINET and ENTLN, because the area is different and the technical details about IC detection remain unclear (type of signals, VLF/LF or VHF, discrimination IC-CG).

For all the above reasons the application of the Fierro method to RAMS@ISAC is not straightforward and it is appropriate to study the dependence of the rainfall VSF to the nudging formulation. This subject is studied in the supplemental material of this paper (Section S.3) and the results show that the choice of the coefficient of Eqn. (1) used in this paper is reasonable.

It is finally noted that despite the limitations noted above, the lightning data assimilation, with the setting of this paper, had a significant and positive impact on RAMS@ISAC rainfall VSF (Federico et al., 2017a; 2017b).

3.3 Radar data assimilation

The method assimilates CAPPI of radar reflectivity factor operationally provided by the Italian Department of Civil Protection (DPC). Radar data are provided over a regular Cartesian grid with 1 km horizontal resolution and for three vertical levels (2, 3, 5 km above the sea level). The CAPPIs at 2, 3, and 5km can be considered as under-sampled vertical profiles. CAPPIs are composed starting from the 22 radars of the Italian Radar Network (Figure 13) 19 operating at the C-band (i.e., 5.6 GHz) and 3 at X-band (i.e., 9.37 GHz). Data quality control and CAPPI composition is performed by DPC. Data quality processing chain aims at identifying most of the uncertainty sources as clutter, partial beam blocking and beam broadening. The radar observations are processed according to nine steps detailed in Vulpiani et al. (2014), Petracca et al. (2018) and references therein.
Radial velocity is not assimilated into RAMS@ISAC because it is not operationally processed, the scan strategy being optimized for QPE purposes. Furthermore, the implementation of a radial velocity data assimilation scheme is under development in RAMS-3DVar and it is not currently available for testing. For these reasons, we didn't consider the assimilation of this parameter.
Before entering data assimilation, the Cartesian grid is downscaled to 5 km by 5 km in order to reduce the numerical cost of the data assimilation and the effect of correlated observation errors (Rohn et al., 2001). Thus, the radar grid (Figure 4, for example) is a Cartesian grid with 5 km grid-spacing and three vertical levels.

Eliminato: 2

Eliminato: as used in this paper

Eliminato: s

Eliminato: AR

Eliminato: reduced

Eliminato: by choosing one point every five of the Cartesian grid provided by DPC

Eliminato: to reduce

Eliminato: then

It is important to note that pure sampling of the data could result in implementation of errors (for example reflectivity given by insects or birds) or extremes. Creating superobservations would reduce this problem, the main drawback being the missing of very localised phenomena. While the aim of this paper is to present the update of the data assimilation system of RAMS@ISAC and its application to two challenging cases, the problem of using superobservations will be considered in future studies because it impacts the results.

The methodology to assimilate radar reflectivity factor is that of Caumont et al. (2010), named 1D+3DVar, which is a two-step process: first, using a Bayesian approach inspired to GPROF (Goddard Profiling Algorithm; Olson et al., 1996; Kummerow et al., 2001), 1D pseudo-profiles of model variables are computed, then those pseudo-profiles are assimilated by 3DVar. Both steps are discussed below.

The first step computes a pseudo-profile of relative humidity weighting the model profiles of relative humidity around the radar profile (Bayesian approach). The pseudo-profile is computed by:

$$\mathbf{z}_\mathbf{o}^\mathbf{p} = \frac{\sum_i \mathbf{RH_i} W_i}{\sum_j W_j} \qquad (2)$$

Where RH_i is the RAMS@ISAC vertical profile of relative humidity at a grid point inside a square of 50*50 km^2 centred at the radar vertical profile, W_i is the weight of each profile and $\mathbf{z_o^p}$ is the relative humidity pseudo-profile. The weights are determined by the agreement between the simulated and observed reflectivity factor:

$$W_i = \exp\left\{-\frac{1}{2}\left[\mathbf{z_o} - h_z(x_i)\right]^T \mathbf{R_z^{-1}}\left[\mathbf{z_o} - h_z(x_i)\right]\right\} \qquad (3)$$

Where h_z is the forward observation operator, transforming the background column $\mathbf{x_i}$ into the observed reflectivity factor. The forward radar observation operator is taken from the RIP (Read/Interpolate/Plot) software (https://dtcenter.org/wrf-nmm/users/OnLineTutorial/NMM/RIP/index.php, last access 03 March 2019) and is given in the supplemental material of this paper (Section S8). It assumes a Marshall-Palmer hydrometeors size-distribution, Rayleigh scattering, and depends on the mixing ratios of rain, graupel and snow.

The matrix $\mathbf{R_z}$ in Eqn. (3) is diagonal and its value is $n\sigma^2$, where σ is 1 dBz and n is the number of available observations in the vertical profile (from 1 to 3). In this way, we give more weight to vertical profiles containing more data.

Eliminato: the

Eliminato: The summation is taken over all the grid points inside a square of 50*50 km^2 around the observed profile and the denominator is a normalisation factor.

Codice campo modificato

Eliminato: 4

The error of radar data is assumed small (1dBz) for two reasons: a) reflectivity data are carefully checked by the Civil Protection Department; b) the performance of control simulation, not assimilating any data, is rather poor for the case studies. This setting, however, could not be optimal for cases when the control forecast performs better. A sensitivity test using σ=5 dBz for the Livorno case showed small differences compared to σ=1 dBz. The results of this sensitivity test are detailed in the supplemental material of this paper (Section S4).

It is important to point out that the 50 km length-scale of the above step doesn't represent the horizontal correlation length-scale of the background error, which determines the horizontal spread of the innovations in the 3D-Var data assimilation (the latter length-scale is between 14 and 25 km depending on the level). The 50 km length-scale is used to set a square for computing the pseudo-profile of relative humidity (Eqn. (2)). This profile is given by a weighted average whose weights are determined by the agreement between the simulated and observed reflectivity factor. The larger the agreement the larger the weight. This distance is appropriate because the spatial error of meteorological models in simulating meteorological features, for example fronts, can be of this order. The control simulation of the two events considered in this paper confirms this choice.

The method is not able to force convection when the model has no rain, snow or graupel in a square around (50*50 km^2) a radar profile with reflectivity factor greater than zero. In this case, the pseudo-profile of relative humidity is assumed saturated above the lifting condensation level and with no data below (Caumont et al., 2010).

It is also noted that the method is able to reduce spurious convection when the reflectivity factor is simulated but not observed, because the pseudo-profile of relative humidity gives more weight to the drier relative humidity profiles simulated by RAMS@ISAC inside the 50*50 km^2 square centred at the radar profile. Of course, the ability to reduce spurious convection depends on the availability of dry model profiles around the specific radar profile (see the example below). Finally, if the observed profile is dry and the profile simulated by RAMS@ISAC is dry too, the pseudo-profile is not computed.

Codice campo modificato

In summary, pseudo-profiles are computed for each profile of the radar grid whenever reflectivity is observed or simulated.

The pseudo-profiles computed with the procedure introduced above, are then used as observations in the RAMS-3DVar data assimilation (Federico, 2013), minimising the cost-function:

$$J(\mathbf{x})=\frac{1}{2}(\mathbf{x}-\mathbf{x}_b)^T\mathbf{B}^{-1}(\mathbf{x}-\mathbf{x}_b)+\frac{1}{2}(\mathbf{z}_o^p-h(\mathbf{x}))^T\mathbf{R}^{-1}(\mathbf{z}_o^p-h(\mathbf{x})) \quad (4)$$

Where $\mathbf{x}$ is the state vector giving the analysis when J is minimized, $\mathbf{x}_b$ is the background, $\mathbf{B}$ and $\mathbf{R}$ are the background and observations error matrices, $\mathbf{z_o}^{\mathbf{p}}$ is the pseudo vertical profile computed by Eqn. (2) and h is the forward observation operator transforming the state vector (RAMS@ISAC water vapour mixing ratio) into observations. The cost function in RAMS-3DVar is implemented in incremental form (Courtier et al., 1994) and its minimization is performed by the conjugate-gradient method (Press et al., 1992). No multi-scale approach is used.

The background error matrix is divided into three components along the three spatial directions (*x, y, z*). The $\mathbf{B_x}$ and $\mathbf{B_y}$ matrices account for the spatial correlation of the background error. The correlations are Gaussian with length-scales between 14 and 25 km, depending on the vertical level. These distances are computed using the NMC method (Barker et al., 2012) applied to the HyMeX-SOP1 (Hydrological cycle in the Mediterranean Experiment – First Special Observing Period occurred in the period 6 September-6 November 2012; Ducroq et al., 2014) period. It is again stressed that the spread of the innovations along the horizontal spatial directions in the 3D-Var analysis is determined by the length scales of $\mathbf{B_x}$ and $\mathbf{B_y}$ matrices and varies between 14 and 25 km, depending on the level.

The $\mathbf{B_z}$ matrix contains the error for the water vapour mixing ratio, which is the control variable used in RAMS-3DVar. This error is about 2 g/kg at the surface and decreases with height. In particular, it is larger than 0.5 g/kg below 4 km, and less than 0.2 g/kg above 5 km. The vertical decorrelation of the background error depends on the level and can be roughly estimated in 500-2000 m. The observation error matrix $\mathbf{R}$ in Eqn. (4) is diagonal and observations' errors are uncorrelated. This choice is partially justified by under sampling the radar reflectivity factor observation by choosing one point every five grid points in both horizontal directions of the radar Cartesian grid. However, correlation observations errors have significant impact on the final analysis, as shown for example in Stewart et al. (2013), and different choices of the matrix $\mathbf{R}$ will be considered in future studies.

The value of the elements on the diagonal of $\mathbf{R}$ depends on the vertical level and are 1/4 of the diagonal element of the $\mathbf{B_z}$ matrix at the corresponding height. With these settings, larger weights are given to the observations than to the background and analyses strongly adjust the background towards observations. The background error matrix is computed using the NMC method (Parrish and Derber, 1992; Barker et al. 2004) applied to the HyMeX-SOP1 (Hydrological cycle in the Mediterranean Experiment – First Special Observing Period occurred from 6 September to6 November 2012; Ducroq et al., 2014). This choice is motivated by the fact that HyMeX-SOP1 contains several heavy precipitation events over Italy and the background error matrix is

Eliminato: By this choice, we give more credit representative of the convective environment of the cases considered in this paper. In particular, 10 out of 20 declared IOP (Intense Observing Period) of HyMeX-SOP1 occurred in Italy (Ferretti et al., 2014). In contrast, the period of September 2017, especially before the events selected in this study was characterised by fair and stable weather conditions over Italy and the background error matrix for September 2017 is less representative of the convective environment that characterise the events of this paper.

Because it is the first time that we show the assimilation of radar reflectivity factor in RAMS@ISAC, it is useful to discuss an example of analysis. We select the analysis of Livorno case study at 06 UTC. The observed CAPPI at 3km above sea level is shown in Figure 10b. The corresponding CAPPI simulated by the background is shown in Figure 14a. In general, the comparison between simulated and observed reflectivity factor highlights the difficulty of the model to represent convection properly. In particular, the model is able to represent the convection over Northern Italy but it has poor performance over Sardinia, south of Sicily and over Central Italy. The difference between the analysis and background relative humidity after and before the analysis is shown in Figure 14b (absolute values less than 1% are suppressed in the figure for clarity). Both positive (convection enhancing) and negative (convection suppressing) adjustments are found. Over Central Italy, Sardinia and South of Sicily relative humidity is increased because the model doesn't simulate the observed reflectivity (Figure 10b).The occurrence of this condition added most of the water vapour to the RAMS@ISAC simulation for the case studies of this paper. Over northern Italy the model is partially dried for two different reasons: over northwest of Italy because RAMS@ISAC simulates unobserved reflectivity, over north and northeast of Italy because the model simulates larger values of reflectivity factor compared to the observations. The RAMS-3DVar reduces the relative humidity field north of Corsica island, where the RAMS@ISAC predicts unobserved reflectivity, while RAMS-3DVar didn't suppress the unobserved convection west of Sardinia because the pseudo profiles computed over this area weren't appreciably drier than the background. Cross correlations among different variables of the data assimilation system are neglected in this study and the application of the RAMS-3DVar affects the water vapour mixing ratio only. Cross correlations among different variables can improve the performance of data assimilation system, and an example of their impact in the RAMS-3DVar is shown in Federico (2013). Nevertheless, the impact of cross correlations among different variables in the precipitation VSF will be explored in future works.

Because also lightning data assimilation adjusts the water vapour mixing ratio, it follows that the data assimilation presented in this study adjusts only this parameter.

Eliminato: On the contrary

Eliminato: characterized

Eliminato: shows

Eliminato: r is

Eliminato: able to d

Eliminato: ry

Despite the fact that both radar reflectivity factor and lightning adjust the water vapour mixing ratio, different impacts on the VSF can be expected *a-priori* because radar reflectivity factor and lightning are different types of observations and because they are used in different ways in the data assimilation system.

In particular, lightning is recorded when deep convection develops, while radar reflectivity factor is observed also for light stratiform rain. Flashes of ground based network, as LINET, are available over the open sea, even if with a reduced detection efficiency, while radar reflectivity factor is confined to the range of coastal radars in the network. Lightning has a seasonal dependence over Italy, with the maximum in summer and fall, while radar reflectivity factor is available in all seasons.

Also, differences in data assimilation of lightning and radar reflectivity factor play a role. In addition to the methods used to assimilate observations, lightning saturates the layer 0°C/-25°C where/when it is detected, while radar reflectivity factor can be assimilated by pseudo-profiles or by saturation above the lifting condensation level where observed reflectivity is greater than zero.

So, despite both observations adjust the same model prognostic variable, which is a drawback of the methodology presented in this paper, the impacts of lighting and radar reflectivity factor is expected to be different as will be evident from the results of this paper.

There are, however, advantages using the methodology presented in this paper. In addition to being simple, it doesn't rely on approximate relationship between radar reflectivity factor with hydrometeors mixing ratio, leaving to the model the task of evolving the water vapour added/subtracted. Also, the impact of the data assimilation on model results are substantial (Fabry and Sun, 2010; Caumont et al., 2010), as also shown by the results of this paper.

Lightning and radar data assimilation may produce sharp gradients in vertical direction caused by the addition of water vapour to specific layers. In the case of lightning, the water vapour is added by nudging to reduce sharp gradients. However, radar data assimilation, which accounts for the largest mass of water added to RAMS@ISAC (see Section S.2 of the supplemental material), directly adjusts the water vapour into the model. Our experience with RAMS@ISAC, however, shows that results are reliable and the sudden addition of water vapour doesn't cause shocks to the model simulation, despite the notable gradients of specific humidity.

It is finally noted that the data assimilation increase/decrease the water vapour into the model depending on the cases. The eventual increase/decrease of the forecasted rainfall depends on the physical and dynamical processes occurring into the meteorological model, without any specific tuning.

Formattato: Tipo di carattere:Corsivo

Formattato: Tipo di carattere:Colore carattere: Nero, Bordo:: (Nessun bordo)

Eliminato: 1

4. Results

In this section, we discuss the most intense phase of the Serano case, 03-06 UTC on 16 September, and two VSF forecasts, 00-03 UTC and 06-09 UTC on 10 September, for the Livorno case. The two VSF for Livorno correspond to the most intense phase of the storm in Livorno and to a very intense phase over Lazio region, Central Italy. The aim of the section is to show the notable improvement given by lightning and radar reflectivity factor data assimilation to the VSF.

Eliminato: the

We consider four types of VSF (Table 3): a) CTRL, without radar reflectivity factor and lightning data assimilation; b) LIGHT, assimilating lightning but not radar reflectivity factor; c) RAD, assimilating radar reflectivity factor but not lightning; d) RADLI, assimilating both lightning and radar reflectivity factor.

Several aspects of lightning and radar reflectivity factor data assimilation are considered in the supplemental material of this paper: a) the relative contribution to the total water mass given by lightning and radar reflectivity factor data assimilation (Section S.2); b) the sensitivity of the precipitation VSF to the nudging formulation (Section S.3); c) the sensitivity of rainfall VSF to two specific aspects of radar reflectivity factor data assimilation (Section S4); d) the sensitivity of rainfall VSF to RAMS@ISAC setting (Section S5); e) the impact of lightning data assimilation for a case study well predicted by the control forecast (Section S6); f) different plots of Figures 15-17 (Section S7) and g) the forward radar operator used in RAMS-3DVar (Section S8).

Formattato: Nessuno, Tipo di carattere:Inglese (Regno Unito), Bordo:: (Nessun bordo)

Formattato: Nessuno, Tipo di carattere:Inglese (Regno Unito), Bordo:: (Nessun bordo)

Formattato: Nessuna

Eliminato: In order to avoid excessive length two specific topics are considered in the supplemental material of this paper; specifically, we study: a) t

Eliminato: 1

Eliminato: 2

Formattato: Nessuno, Inglese (Regno Unito)

Eliminato: . Also, the supplemental material gives different plots of Figures 15-17 (Section S3) and the forward radar operator used in RAMS-3DVar (Section S4).

4.1 Serano: 03-06 UTC on 16 September 2017

In this period, an intense and localised storm hit central Italy, while light precipitation occurred over northern Italy (Figure 15a). Considering the storm over central Italy, 10 raingauges observed more than 30 mm/3h, 6 more than 40 mm/3h, 3 more than 50 mm/3h and 1 more than 60 mm/3h, the maximum observed value being 63 mm/3h.

The CTRL forecast, Figure 15b, misses the storm over central Italy and considerably underestimates the precipitation area over Northern Italy, giving unsatisfactory results.

The assimilation of the radar reflectivity factor improves the forecast, as shown in Figure 15c. In particular, RAD forecast shows localized precipitation (30-35 mm/3h) close to the area were the most abundant precipitation was observed. Maximum precipitation is underestimated. Also, the RAD forecast better represents the precipitation over Northern Italy compared to CTRL.

Eliminato: However, the m

The rainfall forecast of LIGHT, Figure 15d, shows some improvements compared to CTRL because the precipitation over central Italy has a maximum of 25-30 mm/3h, close to the area where the maximum precipitation was observed. LIGHT, however, has a worse performance compared to RAD because it underestimated the precipitation area over northern Italy. LIGHT underestimates the maximum precipitation in central Italy.

RADLI forecast, Figure 15e, has the best performance. The precipitation over central Italy is well represented because the maximum rainfall (40-45 mm/3h) is in reasonable agreement with observations, and also because the area of intense precipitation (> 25 mm/3h) is elongated in the SW-NE direction in agreement with raingauge observations. The precipitation over northern Italy is well represented by RADLI.

Performance diagram for 1 mm/3h and 30 mm/3h and for 4 km and 25 km neighbourhood radii is shown in Figure 15f. Different radii are considered to account for the well-known double penalty error (Mass et al., 2002; Mittermaier et al., 2013) caused by displacement errors of the detailed precipitation forecast in convection allowing grids. RADLI has the best performance thanks to the synergistic contribution of lightning and radar reflectivity factor data assimilation.

4.2 Livorno

The Livorno case study lasted for several hours starting at 18 UTC on 9 September 2017 and ending more than a day later. The most intense phase in Livorno and its surroundings was observed during the night between 9 and 10 September. In the following, we will show two representative VSF (3h), including the most intense phase in Livorno.

4.2.1 Livorno: 00-03 UTC on 10 September 2017

This period represents the most intense phase of the storm in Livorno. In particular, the raingauge close to the label A (Figure 16a) reported 151 mm/3h (Collesalvetti), while the one close to the label B measured 82 mm/3h. Among the 518 raingauges reporting valid data, 75 observed more than 10 mm/3h, 31 more than 20 mm/3h, 17 more than 30 mm/3h, 9 more than 40 mm/3h, and 6 more than 50 mm/3h.

The CTRL precipitation forecast is shown in Figure 16b. The forecast is poor because it misses the precipitation swath from the coast towards NE. A precipitation swath is forecasted about 50 km to the North of the real occurrence, but it is less wide compared to the observations.

Eliminato: Also, similarly to RAD,

Eliminato: s, giving a much better idea of the real storm intensity compared to RAD and LIGHT, as well as CTRL

Eliminato: Table 4 shows the ETS and POD scores for selected rainfall thresholds for different neighbourhood radii.

Eliminato: CTRL was unable to predict rainfall larger than 6 mm/3h. The comparison between RAD and LIGHT shows that assimilating radar reflectivity factor performs better than assimilating lightning. This behaviour, however, is not general and sometimes the assimilation of lightning has a better performance than assimilating radar reflectivity factor (see section 4.2.1).
In conclusion, for this VSF, the assimilation of lightning and radar reflectivity factor acted synergistically to improve the precipitation VSF and the simulation assimilating both data performs considerably better than simulations assimilating either lightning or radar reflectivity factor.

Eliminato: In conclusion, for this VSF, the assimilation of lightning and radar reflectivity factor acted synergistically to improve the precipitation VSF and the simulation assimilating both data performs considerably better than simulations assimilating either lightning or radar reflectivity factor.

The RAD forecast, Figure 16c, shows that the assimilation of radar reflectivity factor gives a clear improvement to the forecast. The largest precipitation in the coastal part of the swath (we searched for the maximum in the area with longitudes between 10.20E and 10.70E and latitudes between 43.10N and 43.60N) is 94 mm/3h. Another local maximum is in the southern part of the domain (label B of Figure 16a). The maximum location is well represented, but the forecast value (55 mm/3h) underestimates the observed maximum (82 mm/3h).

An improvement, compared to both CTRL and RAD, is given by the assimilation of lightning (Figure 16d). The maximum value close to Livorno, i.e. in the coastal part of the swath, is 158 mm/3h. LIGHT simulation shows the local maximum in the southern part of the domain (about 50 mm/3h), but the amount is underestimated.

Figure 16e shows the RADLI rainfall forecast. The precipitation swath from coastal Tuscany towards NE is more intense compared to LIGHT and RAD. The maximum rainfall accumulated close to Livorno is 186 mm/3h. Also, the second precipitation maximum in the southern part of the domain reaches 70 mm/3h in good agreement with observations (82 mm/3h). RADLI is the only run giving a satisfactory precipitation VSF over the south-eastern Emilia Romagna (north-eastern part of the domain), to the lee of the Apennines. It is also noted that the main precipitation swath forecasted by RADLI is too broad in the direction crossing the swath compared to the observations. This is confirmed by the FBIAS of RADLI (not shown), which is more than 3 for thresholds larger than 42 mm/3h.

The performance diagram (Figure 16f) shows that LIGHT has better scores than RAD for this VSF.

4.2.2 Livorno: 06-09 UTC on 10 September 2017

In this period, the most intense precipitation occurred over the coastal part of Lazio (Figure 17a). More in detail, among the 2695 raingauges reporting valid data over the domain of Figure 17a, 307 reported more than 10 mm/3h, 132 more than 20 mm/3h, 86 more than 30 mm/3h, 66 more than 40 mm/3h, 49 more than 50 mm/3h and 35 more than 60 mm/3h. Among the 35 raingauges measuring more than 60 mm/3h, 33 were over Lazio, showing the heavy rainfall occurred over the Region.

Some precipitation persisted over Tuscany but the rainfall is much lower compared to previous 6h (the rainfall over Tuscany between 03 and 06 UTC was very intense, not shown).

Figure 17b shows the rainfall simulated by CTRL. The forecast is unsatisfactory, mainly for the following two reasons: a) heavy precipitation is simulated over Tuscany (> 75 mm/3h), also close to

Eliminato:

Eliminato:

Eliminato: Also for this simulation there is a precipitation swath from coastal Tuscany to the Apennines, but the shape of the swath better resembles that observed.

Eliminato: apparent

Eliminato: The analysis of the scores (Table 5) confirms the results outlined above. CTRL has the lowest performance and the improvement given by the data assimilation to the VSF is apparent for POD and ETS for all thresholds and neighbourhood radii considered. For this specific VSF, lightning data assimilation gives a better improvement to rainfall forecast compared to RAD. RADLI has the best performance, especially for 25 km and 50 km neighbourhood radii, nevertheless it over forecast the precipitation field. Because ETS penalises false alarms, the value of this score for RADLI is sometimes lower than that of LIGHT.

Eliminato: *3*

Eliminato:

Eliminato: Other notable precipitation areas are over the NE of Italy (moderate to low amounts), over central Alps (moderate values) and over the whole Sardinia (small amounts).

the Livorno area; b) precipitation is missed over central Italy. The rainfall over NE of Italy is well represented in space, but overestimated.

Considering the evolution of CTRL forecast for the two VSF of Livorno, we conclude that it was able to predict abundant rain over Livorno, but the rainfall forecast was delayed compared to the real occurrence. A similar behaviour was found in Ricciardelli et al. (2018) using the WRF model, showing that the results of this paper for Livorno are likely not tied to the specific model used.

The rainfall simulated by RAD (Figure 17c) clearly improves the forecast compared to CTRL. First, the precipitation over Lazio is well predicted. Second, the precipitation over Tuscany is less than for CTRL, showing the ability of radar reflectivity factor data assimilation to dry the model when it predicts reflectivity that is not observed. This is confirmed by the inspection of the analysis of Figure 14b, the last analysis used before this VSF, which gives a decrease of the relative humidity over most of Tuscany and over the sea in front of Livorno. It is noted, however, that the area of intense rainfall (>60 mm/3h) is overestimated by RAD, showing a wet forecast. The wet bias of the RAD forecast is apparent in the representation of the rainfall VSF shown in the supplemental material of this paper (Figure S12).

LIGHT forecast, Figure 17d, shows a worse performance compared to RAD for this time period. The precipitation forecast is mainly over Tuscany, where it is overestimated, with a small precipitation spot over Lazio.

The precipitation forecast of RADLI, Figure 17e, represents very well the precipitation over Lazio, and the rainfall amount is better predicted compared to RAD. The precipitation over Sardinia is well represented by RADLI as well as the precipitation over Central Alps, giving the best results among all VSF.

Figure 17f shows the better performance of RAD compared to LIGHT for this precipitation VSF. RADLI has the best performance being closer to the upper right corner of the diagram.

To better understand the changes of the precipitation VSF to different data assimilation set-up, Figure 18 shows maps of water vapour mixing ratio averaged between 3 and 10 km at the end of the assimilation phase (06 UTC on 10 September 2017). It is important to note that those maps contain the effects of both data assimilation and model evolution.

The comparison between CTRL (Figure 18a) and RAD (Figure 18b) shows that RAD has a line of high water vapour values over Central Italy, extending over the Tyrrhenian Sea and Sardinia, which is not simulated by CTRL. This line results from both radar data assimilation and convection, which transports water vapour from lower to upper levels. The comparison between CTRL and RAD shows

Eliminato: few millimetres of precipitation are forecasted

Eliminato: very

Eliminato: and the rainfall values are up to 65 mm/3h, so RAD forecast well represents the main precipitation spot over Italy for this VSF

Eliminato: Third, the precipitation over central Alps is represented, even if located about 30 km to the East.

Eliminato: This is confirmed by the wet frequency bias of the RAD simulation, which is greater than 3 between 14 and 44 mm/3h.

Eliminato: 5

Eliminato: The analysis of the scores confirms the above results (Table 6). CTRL has a poor performance as shown by the POD and ETS values, close to zero, for all thresholds above 30 mm/3h and for all neighbourhood radii. The simulations assimilating radar reflectivity factor performs better than LIGHT, the difference being larger for higher rainfall thresholds and for smaller neighbourhood radii ... [1]

the substantial impact of radar reflectivity factor data assimilation on the model evolution despite we are not using relationship between hydrometeors mixing ratios and radar reflectivity factor in data assimilation.

LIGHT averaged water vapour (Figure 18c) over the Tyrrhenian Sea and west of Sicily is higher compared to CTRL because of lightning data assimilation and model processes. Convection develops over Tuscany, northern Lazio and NE of Italy, causing the increase of averaged water vapour in those areas.

Because RAD and LIGHT both assimilate water vapour it is important to highlight the differences between the two fields. First, LIGHT it is not able to represent a compact line of high water vapour over Central Italy that, in the following hours, caused high precipitation over Lazio. Second, averaged water vapour simulated by RAD is larger than for LIGHT over Central Italy, which is caused by a deeper convection developing in RAD than in LIGHT, as well as by the different contributions of data assimilation. Finally, RADLI (Figure 18d) is similar to RAD but it shares also features with LIGHT as the increase of water vapour over the Tyrrhenian Sea.

It is also interesting to compare vertical cross sections of relative humidity for different data assimilation set-up. Figure 19 show the longitude-height cross sections of relative humidity from different data assimilation configurations.

Comparing RAD with CTRL it is evident the difference of the relative humidity field over the Tyrrhenian Sea and western part of Italy (more specifically at longitudes between 10.5 and 12.5).

LIGHT shows two areas with high relative humidity: west of Corsica and over the Tyrrhenian Sea. The wet area west of Corsica is caused by the assimilation of lighting (Figure 8b) and it is not simulated by RAD because Corsica is not well sampled by the radar network and because of different model evolutions. Lightning data assimilation also increases the humidity over the Tyrrhenian Sea and on the western part of Italy, as shown by the comparison with CTRL, nevertheless their effect is lower compared to radar reflectivity data assimilation.

RADLI has features of both lightning and radar reflectivity factor data assimilation.

So, considering the results of Figure 18 and 19 as well as the rainfall VSF, the impact of lightning and radar reflectivity factor on the VSF can be very different despite they both adjust the water vapour mixing ratio.

5. Discussion and Conclusions

Spostato (inserimento) [1]

Eliminato: In particular, flashes are recorded when deep convection develops, while radar reflectivity factor is observed also for light stratiform rain. Flashes of ground based network, as LINET, are available over the open sea, even if with a reduced detection efficiency, while radar reflectivity factor is confined to the range of coastal radars in the network. Lightning has a seasonal dependence over Italy, with the maximum in summer and fall, while radar reflectivity factor is available in all seasons.

In this paper, we showed the impact of lightning and radar reflectivity factor data assimilation on the very short term precipitation forecast (3h) for two case studies occurred in Italy. We used RAMS@ISAC model, whose 3DVar extension to the assimilation of radar reflectivity factor is shown in this paper for the first time.

The first case study occurred on 16 September 2017 and it is a moderate case with localised rainfall over central Italy. It was chosen because the control forecast, i.e. without radar reflectivity factor or lightning data assimilation, missed the event. The second event, occurred on 9-10 September 2017, was characterised by exceptional rainfall over several parts of Italy. This event was partially represented by the control forecast. In particular, the forecast of the event was incorrect because: a) the control forecast was delayed compared to the observations; b) the control forecast missed the rainfall over central Italy (Lazio Region).

It is important to recall that the impact of the lightning data assimilation on the precipitation forecast of RAMS@ISAC was already studied for the HyMeX-SOP1 period (Federico et al., 2017a, 2017b), and a robust statistic is already available. The results of this study confirm the important role of the lightning data assimilation on the rainfall forecast for other two case studies. However, considering the assimilation of radar reflectivity factor, and its combination with lightning data assimilation in RAMS@ISAC, the results of this paper are new.

Because we analysed only two case studies, no definitive conclusions can be derived on the performance of RAMS@ISAC for radar reflectivity factor data assimilation. There are, however, few points worth of mention.

The VSF performance of RAMS@ISAC is systematically improved by the assimilation of radar reflectivity factor. This improvement is of paramount importance for some specific VSF (for example for the 00-03 UTC of Livorno), when the control forecast missed the event while it was correctly predicted by radar reflectivity factor data assimilation. Sometimes the improvement of reflectivity factor data assimilation has less impact on the precipitation forecast, as for the period 18-21 UTC on 9 September 2017 (Livorno, not shown, see the discussion paper Federico et al. (2018) for a description of this VSF). This suggests that there is room for improvement for all components of the VSF: observations, data assimilation, meteorological model.

Lightning and radar observations are different and both add value to the VSF. Some examples have been shown: the light precipitation over Northern Italy for Serano is well forecasted assimilating radar reflectivity factor, while it is not simulated assimilating flashes because they are too few in this area to force convection; lightning data assimilation is able to better represent the deep

Eliminato: a lower

Eliminato: space

Spostato in su [1]: In particular, flashes are recorded when deep convection develops, while radar reflectivity factor is observed also for light stratiform rain. Flashes of ground based network, as LINET, are available over the open sea, even if with a reduced detection efficiency, while radar reflectivity factor is confined to the range of coastal radars in the network. Lightning has a seasonal dependence over Italy, with the maximum in summer and fall, while radar reflectivity factor is available in all seasons.

Eliminato: For the above reasons,

Eliminato: For the above reasons,

Eliminato: the impact of the two kinds of data on the rainfall VSF is expected different.

convection occurring during the intense phase of the Livorno case (00-03 UTC), especially because it is able to force convection where it occurs, reducing false alarms. The ability of lightning data assimilation to reduce false alarms compared to RAD and RADLI it is shown by the fact that the ETS score for LIGHT is sometimes the best among all simulations (see also the Section S2 of the supplemental material of this paper). These results show also that the influence of different observations depends on the meteorological situation.

The model configuration assimilating both radar reflectivity factor and lightning (RADLI) is able to retain important features of both data assimilation. For example, the simulation of the Livorno case in the phase 06-09 UTC was able to simulate the heavy precipitation over Lazio thanks to the radar reflectivity factor data assimilation and the precipitation over Sardinia, as well as the moderate precipitation over central Alps, thanks to lightning data assimilation.

The property of RADLI to retain the precipitation features of both RAD and LIGHT it is shown by the POD score, which is the best, for most cases and thresholds, for RADLI.

Another interesting feature is the considerable improvement of the POD of RADLI compared to CTRL for the lowest thresholds.

It is also underlined that the data assimilated, both lightning and radar reflectivity factor, are available in real time and could be used for an operational implementation of the VSF.

It is worth noting that several sensitivity tests were conducted for the case studies, whose results are shown in the supplemental material. In particular, we studied the sensitivity of the rainfall VSF to: a) nudging formulation used for lightning data assimilation; b) increasing the observation error of radar reflectivity factor; c) changing the shape of the searching area to compute the relative humidity pseudo-profile; d) updating IC/BC as new observations are available; e) increasing the vertical resolution of RAMS@ISAC by using 42 vertical levels. All these sensitivity tests confirm the findings of this paper and generalise in some measure the finding of this paper.

The above results are promising and deserve future studies to better understand the role of radar reflectivity factor data assimilation and its interaction with lightning data assimilation to improve the precipitation forecast, especially at the very short range (0-3 h).

There are, however, less satisfactory aspects of assimilating both radar reflectivity factor and lightning data. In particular, the wet bias of RAD and RADLI forecast is the main drawback of the results of this paper. To reduce the moisture added by radar and lightning data assimilation further research is needed and different approaches are possible (Fierro et al., 2016). In particular: a) assimilating for a shorter time (0-6h in this paper); b) reducing the length-scales of the 3D-Var in the

Eliminato: s

Eliminato: All the

Eliminato: features

horizontal directions to limit the spreading of the innovations, or assuming an innovation equal to zero for grid points without lightning and with zero reflectivity factor; c) reducing the amount of water vapour added to the model (for example reducing the values of A and B constants for lightning data assimilation or relaxing the request of saturation when radar reflectivity is observed in areas where the model has zero reflectivity); d) adding moisture to a shallower vertical layer.

It is also noted that a combination of heating and moistening could provide the same buoyancy with less water vapour addition (Marchand and Fulberg, 2014) and this approach could be used in future studies.

In addition to the acquisition of more case studies, there are two directions of future development of this work. The lightning data assimilation can be formulated by 3DVar, using a strategy similar to the radar reflectivity factor in which pseudo-profiles of relative humidity are first generated where flashes are recorded, and then those profiles are assimilated by 3DVar. This methodology was already reported in Fierro et al. (2016). The assimilation of both radar reflectivity factor and lightning using RAMS-3DVar will be explored in future studies.

Another important point to study is how long the innovations introduced by data assimilation lasts in the forecast. While in this study we consider the VSF at 3h, future studies must explore longer time ranges. This kind of study was performed for lightning data assimilation (Fierro et al., (2015); Federico et al., 2017b; Lynn et al. (2015) among others) and for radar data assimilation (Hu et al. (2006); Jones et al. (2014), among others), using a rationale similar to that used in this paper.

Eliminato: 4

In general, the performance of the forecast and the impact of lightning and radar data assimilation decrease with forecasting time because boundary conditions propagate inside the domain and because model errors grow and eventually become dominant. Improving the data assimilation system also contributes to a longer resilience of model performance. The studies cited above showed that lightning and radar data assimilation can have an impact up to 24h depending on several factors (meteorological model, data assimilation, quality of the data, meteorological conditions, initial and boundary conditions).

Eliminato: of the propagation of

Eliminato: of

Eliminato: th

A study considering both radar reflectivity factor and lightning should be performed to understand the resilience of the innovations introduced by data assimilation.

ACKNOWLEDGMENTS

This work is a contribution to the HyMeX program. Part of the computational time used for this paper was granted by the ECMWF (European Centre for Medium range Weather Forecast)

Eliminato: range

throughout the special project SPITFEDE. LINET data were provided by Nowcast GmbH (https://www.nowcast.de/) within a scientific agreement between H.D. Betz and the Satellite Meteorological Group of CNR-ISAC in Rome.

This work was partially funded by the agreement between CNR-ISAC and the Italian Department of Civil Protection.

References

Alexander, G. D., Weinman, J. A., Karyampoudi, V. M., Olson, W. S., and Lee, A. C. L.: The effect of assimilating rain rates derived from satellites and lightning on forecasts of the 1993 superstorm, Mon. Weather Rev., 127, 1433–1457, 1999.

Barker, D.M., Huang, W., Guo, Y.-R., and Xiao, Q.N.: A Three-Dimensional Variational Data Assimilation System for MM5: Implementation And Initial Results, Monthly Weather Review, 132, 897-914, 2004.

Barker, D. M., Huang, X.-Y., Liu, Z., Aulignè, T., Zhang, X., Rugg ,S., Ajjaji, R., Bourgeois, A., Bray, J., Chen ,Y., Demirtas, M.,. Guo, Y.-R, Henderson, T., Huang, W, Lin, H.C., Michalakes, J., Rizvi, S., and Zhang, X.: The Weather Research and Forecasting (WRF) Model's Community Variational/Ensemble Data Assimilation System: WRFDA. Bull. Amer. Meteor. Soc., 93, 831–843, 2012.

Betz, H.-D., Schmidt, K., Laroche, P., Blanchet, P., Oettinger, P., Defer, E., Dziewit, Z., and Konarski, J.: LINET-an international lightning detection network in Europe, Atmos. Res., 91, 564– 573, 2009.

Betz, H. D., Schmidt, K., Oettinger, P., Wirz, M.: Lightning detection with 3D-discrimination of intracloudandcloud-to-grounddischarges. J.Geophys. Res. Lett. 31 L11108. doi:10.1029/2004GL019821, 2004.

Buzzi, A. and Tibaldi, S.: Cyclogenesis in the lee of the Alps: A case study. Q.J.R. Meteorol. Soc., 104: 271-287. https://doi.org/10.1002/qj.49710444004, 1978.

Carey, L. D., and S. A. Rutledge: Electrical and multiparameter radar observations of a severe hailstorm. J. Geophys. Res., 103, 13 979–14 000, doi:10.1029/97JD02626, 1998.

Caumont, O., Ducrocq, V., Wattrelot, E., Jaubert, G., and Pradier-Vabre, S.: 1D+3DVar assimilation of radar reflectivity data: a proof of concept, Tellus A: Dynamic Meteorology and Oceanography, 62:2, 173-187, https://www.tandfonline.com/doi/abs/10.1111/j.1600-0870.2009.00430.x, 2010.

Eliminato: thoughout

Formattato: Inglese (Stati Uniti)

Formattato: Inglese (Stati Uniti)

Codice campo modificato

Spostato (inserimento) [2]

Codice campo modificato

Spostato in su [2]: Carey, L. D., and S. A. Rutledge: Electrical and multiparameter radar observations of a severe hailstorm. J. Geophys. Res., 103, 13 979–14 000, doi:10.1029/97JD02626, 1998.

Chang, D. E., Weinman, J. A., Morales, C. A., and Olson, W. S.: The effect of spaceborn microwave and ground-based continuous lightning measurements on forecasts of the 1998 Groundhog Day storm, Mon. Weather Rev., 129, 1809–1833, 2001.

Chen, C. and Cotton, W.R.: A One-Dimensional Simulation of the Stratocumulus-Capped Mixed Layer, Boundary Layer Meteorology, 25, 289-321, 1983.

Cotton, W.R., Pielke Sr., R.A., Walko, R.L., Liston, G.E., Tremback, C.J., Jiang, H., McAnelly, R.L., Harrington, J.Y.m Nicholls, M.E., Carrio, G.G., and McFadden, J.P.: RAMS 2001: Current status and future directions, Meteorology and Atmospheric Physics, 82, 5-29,2003.

Courtier, P., Thépaut, J. N., and Hollingsworth, A.: A strategy for operational implementation of 4D-Var, using an incremental approach, Q. J. Roy. Meteorol. Soc., 120, 1367–1387, 1994.

Dahl, J. M. L., Höller, H., and Schumann, U.: Modeling the Flash Rate of Thunderstorms. Part II: Implementation. Monthly Weather Review, 139, 3112-3124, 2011.

Deierling, W., and W. A. Peterse: Total lightning activity as an indicator of updraft characteristics. J. Geophys. Res., 113, D16210, doi:10.1029/2007JD009598, 2008.

Ducrocq, V., Braud, I., Davolio, S., Ferretti, R., Flamant, C., Jansa, A., Kalthoff, N., Richard, E., Taupier-Letage, I., Ayral, P.-A., Belamari, S., Berne, A., Borga, M., Boudevillain, B., Bock, O., Boichard, J.-L., Bouin, M.-N., Bousquet, O., Bouvier, C., Chiggiato, J., Cimini, D., Corsmeier, U., Coppola, L., Cocquerez, P., Defer, E., Delanoë, J., Di Girolamo, P., Doerenbecher, A., Drobinski, P., Dufournet, Y., Fourrié, N., Gourley, J.J., Labatut, L., Lambert, D., Le Coz, J., Marzano, F.S., Molinié, G., Montani, A., Nord, G., Nuret, M., Ramage, K., Rison, W., Roussot, O., Said, F., Schwarzenboeck, A., Testor, P., Van Baelen, J., Vincendon, B., Aran, M., and Tamayo, J.: HYMEX-SOP1 The Field Campaign Dedicated to Heavy Precipitation and Flash Flooding in the Northwestern Mediterranean. Bull. Amer. Meteor. Soc., 95, 1083–1100, https://doi.org/10.1175/BAMS-D-12-00244.1 , 2014.

Codice campo modificato

Emersic, C., and C. P. R. Saunders, 2010: Further laboratory investigations into the relative diffusional growth rate theory of thunderstorm electrification. Atmos. Res., 98, 327–340, doi:https://doi.org/10.1016/j.atmosres.2010.07.011, 2010.

Fabry, F., and Sun, J: For how long should what data be assimilated for the mesoscale forecasting of convection and why? Part I: On the propagation of initial condition errors and their implications for data assimilation. Monthly Weather Review, 138(1), 242–255, https://doi.org /2009mwr2883.1, 2010.

Federico, S.: Implementation of a 3D-Var system for atmospheric profiling data assimilation into the RAMS model: Initial results, Atmospheric Measurement Techniques, 6(12), 3563-3576, 2013.

Federico, S.: Implementation of the WSM5 and WSM6 Single Moment Microphysics Scheme into the RAMS Model: Verification for the HyMeX-SOP1, Advances in Meteorology, Volume 2016, 2016.

Federico, S., Avolio, E., Petracca, M., Panegrossi, G., Sanò, P., Casella, D., and Dietrich S.:Simulating lightning into the RAMS model: Implementation and preliminary results, Natural Hazards and Earth System Sciences, Volume 14, Number 11, p.2933-2950, 2014.

Federico, S., Petracca, M., Panegrossi, G., and Dietrich, S.: Improvement of RAMS precipitation forecast at the short-range through lightning data assimilation, Nat. Hazards Earth Syst. Sci., 17, 61–76, https://doi.org/10.5194/nhess-17-61-2017, 2017a.

Federico, S., Petracca, M., Panegrossi, G., Transerici, C., and Dietrich, S.: Impact of the assimilation of lightning data on the precipitation forecast at different forecast ranges. Adv. Sci. Res., 14, 187–194, 2017b.

Federico, S., Torcasio, R. C., Avolio, E., Caumont, O., Montopoli, M., Baldini, L., Vulpiani, G., and Dietrich, S.: The impact of lightning and radar data assimilation on the performance of very short term rainfall forecast for two case studies in Italy, Nat. Hazards Earth Syst. Sci. Discuss., https://doi.org/10.5194/nhess-2018-319, in review, 2018.

Ferretti, R., Pichelli, E., Gentile, S., Maiello, I., Cimini, D., Davolio, S., Miglietta, M. M., Panegrossi, G., Baldini, L., Pasi, F., Marzano, F. S., Zinzi, A., Mariani, S., Casaioli, M., Bartolini, G., Loglisci, N., Montani, A., Marsigli, C., Manzato, A., Pucillo, A., Ferrario, M. E., Colaiuda, V., and Rotunno, R.: Overview of the first HyMeX Special Observation Period over Italy: observations and model results, Hydrol. Earth Syst. Sci., 18, 1953–1977, https://doi.org/10.5194/hess-18-1953-2014, 2014.

Fierro, A. O., A. J. Clark, E. R. Mansell, D. R. MacGorman, S. Dembek, and C. Ziegler: Impact of storm-scale lightning data assimilation on WRF-ARW precipitation forecasts during the 2013 warm season over the contiguous United States. Mon. Wea. Rev., 143, 757–777, doi:https://doi.org/10.1175/MWR-D-14-00183.1, 2015.

Fierro, A.O., Gao, l., Ziegler, C. L., Calhoun, K. M., Mansell, E. R., and MacGorman, D. R.: Assimilation of Flash Extent Data in the Variational Framework at Convection-Allowing Scales: Proof-of-Concept and Evaluation for the Short-Term Forecast of the 24 May 2011 Tornado Outbreak. Mon. Wea. Rev., 144, 4373–4393,https://doi.org/10.1175/MWR-D-16-0053.1, 2016.

Fierro, A. O., J. Gao, C. Ziegler, E. R. Mansell, D. R. MacGorman, and S. Dembek: Evaluation of a cloud scale lightning data assimilation technique and a 3DVAR method for the analysis and short-term forecast of the 29 June 2012 derecho event. Mon. Wea. Rev., 142, 183–202, doi:10.1175/ MWR-D-13-00142.1, 2014.

Fierro, A. O., M. S. Gilmore, E. R. Mansell, L. J. Wicker, and J. M. Straka: Electrification and lightning in an idealized boundary-crossing supercell simulation of 2 June 1995. Mon. Wea. Rev., 134, 3149–3172, doi:10.1175/MWR3231.1, 2006.

Fierro, A. O., Mansell, E., Ziegler, C., and MacGorman, D.: Application of a lightning data assimilation technique in the WRFARW model at cloud-resolving scales for the tornado outbreak of 24 May 2011, Mon. Weather Rev., 140, 2609–2627, 2012.

Giannaros, T. M., Kotroni, V., and Lagouvardos, K.: WRFLTNGDA: A lightning data assimilation technique implemented in the WRF model for improving precipitation forecasts, Environ. Model. Softw., 76, 54–68, doi:10.1016/j.envsoft.2015.11.017, 2016.

Hong, S.Y., Lim, J.J.O.: The WRF single-moment 6-class microphysics scheme (WSM6). J. Korean Meteorol. Soc. 42, 129–151, 2006.

Hu, M., M. Xue, and K. Brewster: 3DVAR and cloud analysis with WSR-88D level-II data for the prediction of the Fort Worth, Texas, tornadic thunderstorms. Part I: Cloud analysis and its impact. Mon. Wea. Rev., 134, 675–698, doi:10.1175/MWR3092.1, 2006.

Ikuta, Y. and Honda, Y.: Development of 1D+4DVAR data assimilation of radar reflectivity in JNoVA. Tech. Report, 01.09–01.10. http://www.wcrp-climate.org/WGNE/BlueBook/2011/individual-articles/01_Ikuta_Yasutaka_WGNE2011_1D4DVAR.pdf, 2011.

Jones, C. D., and Macpherson, B.: A latent heat nudging scheme for the assimilation of precipitation into an operational mesoscale model, Meteorol. Appl., 4, 269–277, 1997.

Jones, T. A., J. A. Otkin, D. J. Stensrud, and K. Knopfmeier: Forecast evaluation of an observing system simulation experiment assimilating both radar and satellite data. Mon. Wea. Rev., 142, 107–124, doi:10.1175/MWR-D-13-00151.1, 2014.

Kain, J. S. and Fritsch, J. M.: Convective parameterization for mesoscale models: the Kain-Fritsch scheme. The representation of cumulus convection in numerical models, Meteor. Monogr. No. 46, Am. Meteor. Soc., Boston, 165–170, 1993.

Kuhlman, K. M., C. L. Zielger, E. R. Mansell, D. R. MacGorman, and J. M. Straka: Numerically simulated electrification and lightning of the 29 June 2000 STEPS supercell storm. Mon. Wea. Rev., 134, 2734–2757, doi:10.1175/MWR3217.1, 2006.

Kummerow, C., Hong, Y., Olson, W.S., Yang. S., Adler, R.F., McCollum, J., Ferraro, R., Petty, G., Shin. D.-B., and Wilheit, T.T.: The evolution of the Goddard profiling algorithm (GPROF) for rainfall estimation from passive microwave sensors. J. Appl. Meteor., 40, 1801–1820, 2001.

Lagouvardos, K., Kotroni, V., Betz, H.-D., and Schmidt, K.: A comparison of lightning data provided by ZEUS and LINET networks over Western Europe, Nat. Hazards Earth Syst. Sci., 9, 1713–1717, https://doi.org/10.5194/nhess-9-1713-2009, 2009.

Lynn, B. H., G. Kelman, and G. Ellrod: An evaluation of the efficacy of using observed lightning to improve convective lightning forecasts. Wea. Forecasting, 30, 405-423 doi:10.1175/ WAF-D-13-00028.1., 2015.

Lynn, B.H., 2017: The Usefulness and Economic Value of Total Lightning Forecasts Made with a Dynamic Lightning Scheme Coupled with Lightning Data Assimilation.Wea. Forecasting, 32, 645–663, https://doi.org/10.1175/WAF-D-16-0031.1 , 2017.

MacGorman, I. R. Apostolakopoulos, N. R. Lund, N. W. S. Demetriades, M. J. Murphy, and P. R. Krehbiel: The timing of cloud-to-ground lightning relative to total lightning activity. Mon. Wea. Rev., 139, 3871–3886, doi:10.1175/MWR-D-11-00047.1, 2011.

MacGorman, D. W. Burgess, V. Mazur, W. D. Rust, W. L. Taylor, and B. C. Johnson, 1989: Lightning rates relative to tornadic storm evolution on 22 May 1981. J. Atmos. Sci., 46, 221–251, doi:10.1175/ 1520-0469(1989)046,0221:LRRTTS.2.0.CO;2.

MacGorman, D.R. and K.E. Nielsen: Cloud-to-Ground Lightning in a Tornadic Storm on 8 May 1986. Mon. Wea. Rev., 119, 1557–1574, https://doi.org/10.1175/1520-0493(1991)119<1557:CTGLIA>2.0.CO;2, 1991.

MacGorman, W. D. Rust, P. Krehbiel, W. Rison, E. Bruning, and K. Wiens: The electrical structure of two supercell storms during STEPS. Mon. Wea. Rev., 133, 2583–2607, doi:10.1175/MWR2994.1, 2005.

MacGorman, W. D. Rust, P. Krehbiel, W. Rison, E. Bruning, and K. Wiens: The electrical structure of two supercell storms during STEPS. Mon. Wea. Rev., 133, 2583–2607, doi:10.1175/MWR2994.1, 2005.

Mansell, E. R., Ziegler, C. L., and MacGorman, D. R.: A lightning data assimilation technique for mesoscale forecast models, Mon. Weather Rev., 135, 1732–1748, 2007.

Marchand, M., and H. Fuelberg: Assimilation of lightning data using a nudging method involving low-level warming. Mon. Wea. Rev., 142, 4850–4871, doi:10.1175/MWR-D-14-00076.1, 2014.

Mass, C. F., Ovens, D., Westrick, K., and Colle, B. A.: Does increasing horizontal resolution produce more skilful forecasts?, B. Am. Meteorol. Soc., 83, 407–430, 2002.

Mellor, G., and Yamada, T.: Development of a Turbulence Closure Model for Geophysical Fluid Problems, Review of Geophysics and Space Physics, 20, 851-875, 1982.

Mittermaier, M., N. Roberts, and S. A. Thompson: A long-term assessment of precipitation forecast skill using the Fractions Skill Score. Meteor. Appl., 20, 176–186, doi:https://doi.org/10.1002/met.296, 2013.

Molinari, J., and Corsetti, T.: Incorporation of cloud-scale and mesoscale down-drafts into a cumulus parametrization: results of one and three-dimensional integrations, Monthly Weather Review, 113, 485-501, 1985.

Olson, W. S., Kummerow, C. D. , Heymsfield, G. M., and Giglio, L.: A method for combined passive-active microwave retrievals of cloud and precipitation profiles. J. Appl. Meteor., 35, 1763-1789, 1996.

Codice campo modificato

Eliminato: Maiello, I., Ferretti, R., Gentile, S., Montopoli, M., Picciotti, E., Marzano, F. S., and Faccani, C.: Impact of radar data assimilation for the simulation of a heavy rainfall case in central Italy using WRF–3DVAR, Atmos. Meas. Tech., 7, 2919-2935, https://doi.org/10.5194/amt-7-2919-2014, 2014.

Papadopoulos, A., Chronis, T.G., Anagnostou, E.N.. Improving convective precipitation forecasting through assimilation of regional lightning measurements in a mesoscale model. Mon. Weather Rev. 133, 1961-1977, 2005.

Parrish, D.F., and Derber, J.C.: The National Meteorological Center's Spectral Statistical Interpolation analysis system, Monthly Weather Review, 120, 1747-1763, 1992.

Pessi, A.T. and S. Businger: Relationships among Lightning, Precipitation, and Hydrometeor Characteristics over the North Pacific Ocean. J. Appl. Meteor. Climatol., 48, 833–848, https://doi.org/10.1175/2008JAMC1817.1 , 2009.

Petracca M., Casella D., Dietrich S., Milani L., Panegrossi G., Sanò P., Möhrlein M., Riso S. and Betz H.D. (2014), "Lightning strokes frequency homogenization for climatological analysis: application to LINET data records over Europe", 2nd TEA – IS Summer School, June 23 – 27, Collioure, France, 2014.

Petracca, M., L. P. D'Adderio, F. Porcù, G. Vulpiani, S. Sebastianelli, and S. Puca: Validation of GPM Dual-Frequency Precipitation Radar (DPR) rainfall products over Italy. J. Hydrometeor., 19, 907–925. https://doi.org/10.1175/JHM-D-17-0144.1., 2018.

Press, W. H., Teukolsky, S. A., Vetterling, W. T., and Flannery, B. P.: Numerical recipes in Fortran 77, second ed., Cambridge Uni- versity Press, Cambridge, 992 pp., 1992.

Qie, X., Zhu, R., Yuan, T., Wu, X., Li, W., and Liu, D.: Application of total-lightning data assimilation in a mesoscale convective system based on the WRF model, Atmos. Res., 145–146, 255–266, 2014.

Ricciardelli, E.; Di Paola, F.; Gentile, S.; Cersosimo, A.; Cimini, D.; Gallucci, D.; Geraldi, E.; Larosa, S.; Nilo, S.T.; Ripepi, E.; Romano, F.; Viggiano, M. Analysis of Livorno Heavy Rainfall Event: Examples of Satellite-Based Observation Techniques in Support of Numerical Weather Prediction. Remote Sens. 2018, 10, 1549, 2018.

Ridal, M., and Dahlbom, M.: Assimilation of multinational radar reflectivity data in a mesoscale model: a proof of concept, Journal of Applied Meteorology and Climatology, 56(6), 1739–1751, https://doi.org/10.1175/jamc-d-16-0247.1, 2017.

Roebber, P.J., 2009: Visualizing multiple measures of forecast quality. Wea. Forecasting, 24, 601-608.

Rohn, M., Kelly, G., Saunders, R. W.: Impact of a New Cloud Motion Wind Product from Meteosat on NWP Analyses and Forecasts, Monthly Weather Review, 129, 2392-2403, 2001.

Smagorinsky, J.: General circulation experiments with the primitive equations. Part I, The basic experiment, Monthly Weather Review, 91, 99-164, 1963.

Stensrud, D. J., and Fritsch, J. M.: Mesoscale convective systems in weakly forced large-scale environments. Part II: Generation of a mesoscale initial condition, Mon. Weather Rev., 122, 2068-2083, 1994.

Eliminato: ì

Codice campo modificato

Codice campo modificato

Codice campo modificato

Codice campo modificato

Formattato: Tipo di carattere:(Predefinito) Calibri, 12 pt, Inglese (Regno Unito), Bordo:: (Nessun bordo), Motivo: Trasparente

Formattato: A sinistra, Spazio Dopo: 0 pt, Interlinea: singola, Bordo:Superiore: (Nessun bordo), Inferiore: (Nessun bordo), A sinistra: (Nessun bordo), A destra: (Nessun bordo), Tra : (Nessun bordo), Barra : (Nessun bordo)

Eliminato: Skamarock, W. C., Klemp, J. B., Dudhia, J., Gill, D. O., Barker, D. M., Duda, M. G., Huang, X.-Y., Wang, W., and Powers, J. G.: A description of the Advanced Reasearch WRF Version 3. NCAR Technical Note, TN 475+STR, 113 pp., available at: http://www2.mmm.ucar.edu/wrf/users/docs/arw_v3.pdf (last access: November 2018), 2008.

Stensrud, D.J., M. Xue, L.J. Wicker, K.E. Kelleher, M.P. Foster, J.T. Schaefer, R.S. Schneider, S.G. Benjamin, S.S. Weygandt, J.T. Ferree, and J.P. Tuell: Convective-Scale Warn-on-Forecast System. Bull. Amer. Meteor. Soc., 90, 1487–1500, https://doi.org/10.1175/2009BAMS2795.1, 2009.

Codice campo modificato

Stewart, L. M., Dance, S. L., Nichols, N. K.: Data assimilation with correlated observation errors: experiments with a 1-D shallow water model, Tellus A: Dynamic Meteorology and Oceanography, 65:1, DOI: 10.3402/tellusa.v65i0.19546, 2013.

Codice campo modificato

Sun, J., and Crook, N. A.: Dynamical and Microphysical Retrieval from Doppler RADAR Observations Using a Cloud Model and Its Adjoint, Part I: Model Development and Simulated Data Experiments, J. Atmos. Sci., 54, 1642–1661, 1997.

Sun, J., and Crook, N. A.: Dynamical and Microphysical Retrieval from Doppler RADAR Observations Using a Cloud Model and Its Adjoint, Part II: Retrieval Experiments of an Observed Florida Convective Storm, J. Atmos. Sci., 55, 835–852, 1998.

Takahashi, T.: Riming electrification as a charge generation mechanism in thunderstorms. J. Atmos. Sci., 35, 1536–1548, doi:https://doi.org/10.1175/1520 0469(1978)0352.0.CO;2, 1978.

Eliminato: Sun, J. and Wang, H.: Radar data assimilation with WRF 4DVar. Part II: comparison with 3D-Var for a squall line over the US Great Plains, Mon. Weather Rev., 11, 2245–2264, https://doi.org/10.1175/MWR-D-12-00169.1, 2012.

Vulpiani, G., A. Rinollo, S. Puca, and M. Montopoli: A quality-based approach for radar rain field reconstruction and the H-SAF precipitation products validation. Proc. Eighth European Radar Conf., Garmish-Partenkirchen, Germany, ERAD, Abstract 220, 6 pp., http://www.pa.op.dlr.de/erad2014/programme/ ExtendedAbstracts/220_Vulpiani.pdf (last access January 2019), 2014.

Codice campo modificato

Walko, R.L., Band, L.E., Baron, J., Kittel, T.G., Lammers, R., Lee, T.J., Ojima, D., Pielke Sr., R.A., Taylor, C., Tague, C., Tremback, C.J., and Vidale, P.L.: Coupled Atmosphere-Biosphere-Hydrology Models for environmental prediction, Journal of Applied Meteorology, 39, 931-944, 2000.

Wattrelot, É., Caumont, O. and Mahfouf, J. F.: Operational implementation of the 1D+3D-Var assimilation method of radar reflectivity data in the AROME model. Monthly Weather Review, 142(5), 1852–1873. https://doi.org/10.1175/MWR-D-13-00230.1, 2014.

Eliminato: Wang, H., Sun, J., Zhang, X., Huang, X., and Auligne, T.: Radar data assimilation with WRF 4D-Var. Part I: system development and preliminary testing, Mon. Weather Rev., 141, 2224–2244, 2013.

Weisman, M. L., Skamarock, W. C., and Klemp, J. B.: The resolution dependence of explicitly modeled convective systems, Mon.Weather Rev., 125, 527–548, 1997.

Weygandt, S. S., Benjamin, S. G., Hu, M., Smirnova, T. G., and Brown, J. M.: Use of lightning data to enhance radar assimilation within the RUC and Rapid Refresh models. Third Conf. on Meteorological Applications of Lightning Data, 20–24 January 2008, New Orleans, LA, Amer. Meteor. Soc., 8.4, available at: https://ams.confex.com/ams/88Annual/webprogram/Paper134112.html (last access: 03 October 2018), 2008.

Wiens, K. C., S. A. Rutledge, and S. A. Tessendorf, A: The 29 June 2000 supercell observed during STEPS. Part II: Lightning and charge structure. J. Atmos. Sci., 62, 4151–4177, doi:10.1175/JAS3615.1, 2005.

Xu, Q., Wei, L., Gu, W., Gong, J., and Zhao, Q.: A 3.5-dimensional variational method for Doppler radar data assimilation and its application to phased array radar observations, Adv. Meteorol., vol. 2010, Article ID 797265, https://doi.org/10.1155/2010/797265, 2010.

Xue, M., Wang, D., Gao, J., Brewster, K., and Droegemeier, K. K: The Advanced Regional Prediction System (ARPS), storm scale numerical weather prediction and data assimilation, Meteor. Atmos. Phys., 82, 139–170, 2003.

Zhao, Q., Cook, J., Xu, Q., and Harasti, P. R.: Using radar wind observations to improve mesoscale numerical weather prediction, Weather Forecast, 21, 502–522, 2006.

Eliminato: Xiao, Q., Kuo, Y.-H., Sun, J., Chaulee, W., and Barker, D. M.: An Approach of RADAR Reflectivity Data Assimilation and Its Assessment with the Inland QPF of Typhoon Rusa (2002) at Landfall, J. Appl. Meteor. Climatol., 46, 14–22, 2007. ... [2]

TABLES

Table 1: RAMS@ISAC physical parameterisations used in this paper.

Eliminato: List of

Eliminato: for RAMS@ISAC

Physical parameterization	**Selected scheme**
Parametrized cumulus convection	Modified Kuo scheme to account for updraft and downdraft (Molinari and Corsetti, 1985). The scheme is applied to R10 only.
Explicit precipitation parameterization	Bulk microphysics with six hydrometeors (cloud, rain, graupel, snow, ice, water vapour). Described in Hong and Lim (2006).
Exchange between the surface, the biosphere and atmosphere.	LEAF3 (Walko et al., 2000). LEAF includes prognostic equations for soil temperature and moisture for multiple layers, vegetation temperature and surface water, and temperature and water vapour mixing ratio of canopy air.
Sub-grid mixing	The turbulent mixing in the horizontal directions is parameterised following Smagorinsky (1963), vertical diffusion is parameterised according to the Mellor and Yamada (1982) scheme, which employs a prognostic turbulent kinetic energy.
Radiation scheme	Chen-Cotton (Chen and Cotton, 1983). The scheme accounts for condensate in the atmosphere.

Table 2: Basic parameters of the RAMS@ISAC grids (R10, R4 and R1, corresponding, respectively, to the domains D1, D2 and D3). NNXP is the number of grid points in the WE direction, NNYP is the number of grid-points in the NS direction, NNZP is the number of vertical levels, DX is the size of the grid spacing in the WE direction, DY is the grid spacing in the SN direction. Lx, Ly, and Lz are the domain extensions in the NS, WE, and vertical directions. CENTLON and CENTLAT are the coordinates of the grid centres.

	R10, D1	**R4, D2**	**R1, D3**
NNXP	301	401	203
NNYP	301	401	203

NNZP	36	36	36
Lx	3000 km	1600 km	~270 km
Ly	3000 km	1600 km	~270 km
Lz	~22400 m	~22400 m	~22400 m
DX	10 km	4 km	4/3 km
DY	10 km	4 km	4/3 km
CENTLAT (°)	43.0 N	43.0 N	43.7 N
CENTLON (°)	12.5 E	12.5 E	11.0 E

Table 3: Types of simulations performed.

Experiment	Description	Data assimilated	Model variable impacted
CTRL	Control run	None	None
RAD	RADAR data assimilation	Reflectivity factor CAPPI (RAMS-3DVar)	Water vapour mixing ratio
LIGHT	Lightning data assimilation (A=0.85; B=0.16 in Eqn. (1))	Lightning density (nudging)	Water vapour mixing ratio
RADLI	RADAR + lightning data assimilation (A=0.86; B=0.15 in Eqn (1))	Reflectivity factor CAPPI (RAMS-3DVar) + Lightning density (nudging)	Water vapour mixing ratio

Eliminato: Table 4: ETS and POD scores for three different neighbourhood radii. Scores are computed over the domain D2.
ETS nearest neighboorhood (CTRL, RAD, LIGHT, RADLI) ... [3]

FIGURES

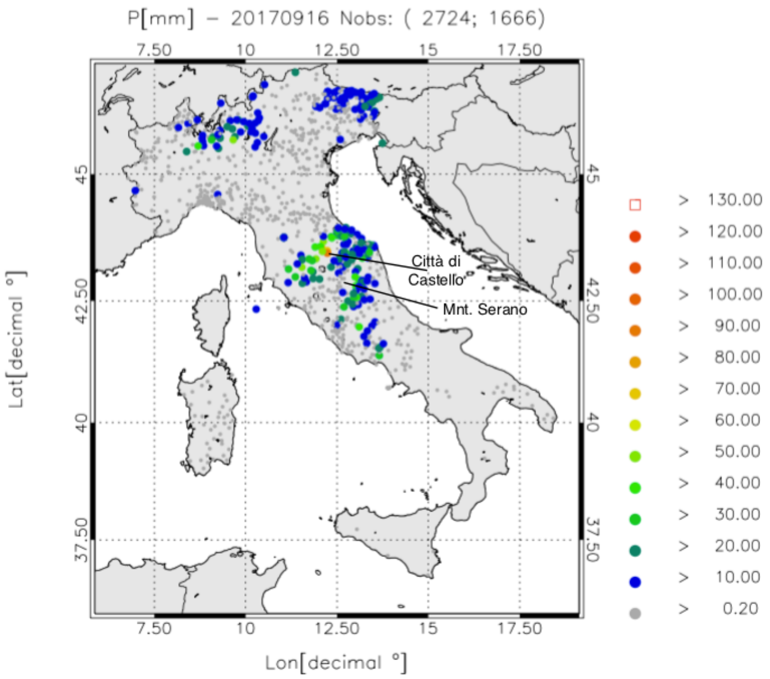

Figure 1: Daily precipitation (P) [mm] over Italy on 16 September 2017. Only raingauges observing at least 0.2 mm/day are shown. The first number in the figure title within brackets represents the available raingauges, while the second number represents raingauges observing at least 0.2 mm/day. The lowest precipitation class is represented by smaller dots, the largest by a red square. The locations of Città di Castello and Mount Serano are indicated.

Formattato: Centrato

Eliminato: 3h

Eliminato:

Formattato: Rientro: Sinistro: 0 cm, Prima riga: 0 cm

a)

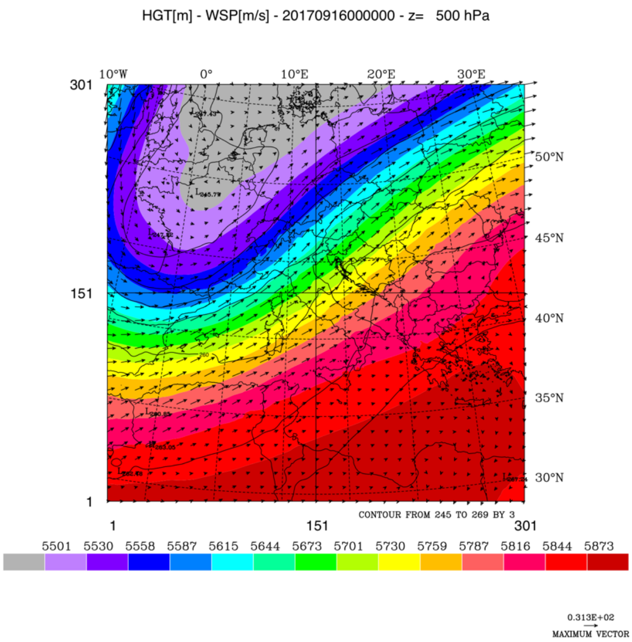

b)

Formattato: Centrato

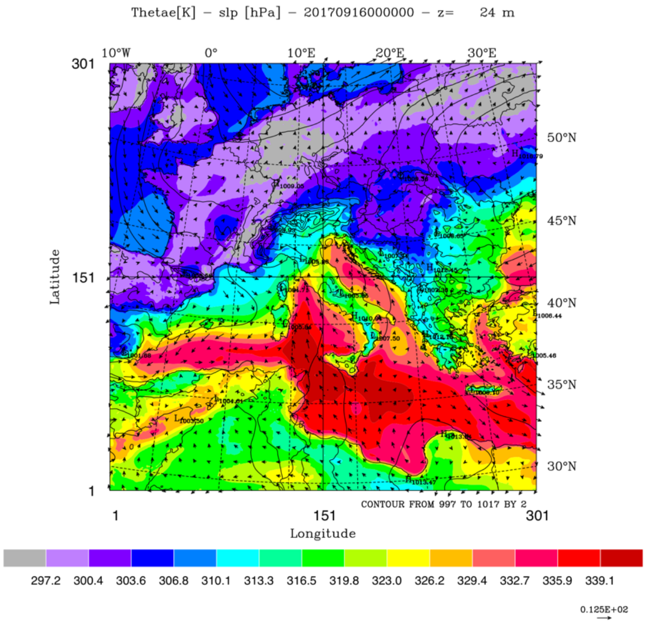

Figure 2: a) Geopotential height (filled contours), temperature (contours) and wind vectors at 500 hPa on 16 September 2017 at 00 UTC. Maximum velocity is 31 m/s; b) equivalent potential temperature (filled contours), sea-level pressure (contours) and wind vectors at 24 m above the surface (maximum value 13 m/s). A low-pressure patter is forming over northern Italy, with a front in the western Mediterranean.

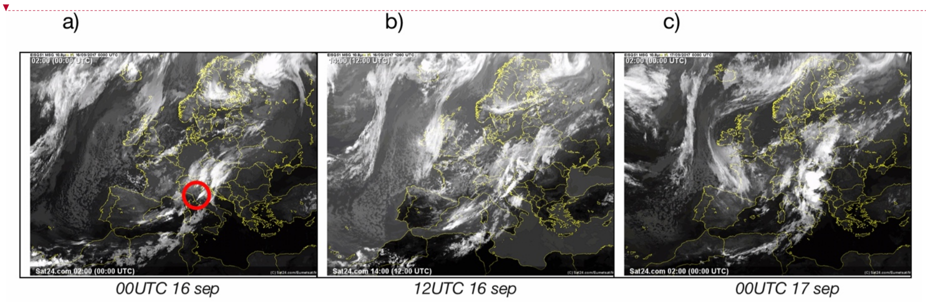

Figure 3: a) Satellite images (METEOSAT second generation) of the infrared channel, 10.8 micron, at 00 UTC and 12 UTC on 16 September, and at 00 UTC on 17 September 2017. A well-defined cloud system is apparent inside the red circle of the image at 00 UTC on 16 September 2017.

Formattato: Centrato

Eliminato: first vertical level of RAMS@ISAC,

Eliminato:

Eliminato:

Eliminato: <#> b)
c)

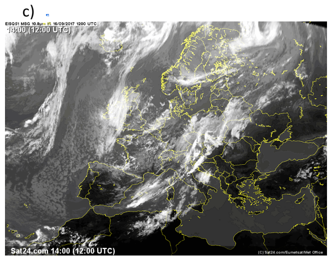

... [4]

Formattato: Tipo di carattere:(Predefinito) +Corpo tema (Calibri), Colore carattere: Automatico

Formattato: Tipo di carattere:(Predefinito) +Corpo tema (Calibri), Colore carattere: Automatico

Formattato: Tipo di carattere:(Predefinito) +Corpo tema (Calibri), Colore carattere: Automatico

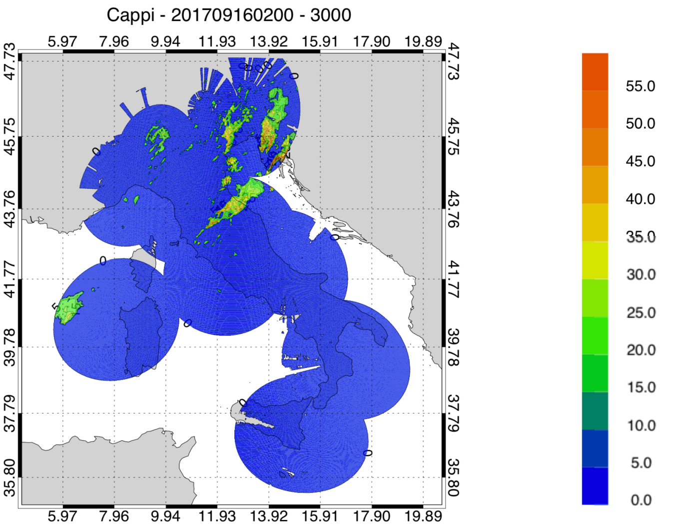

Figure 4: National radar mosaic at 3 km above the sea level observed at 02 UTC on 16 September 2017.

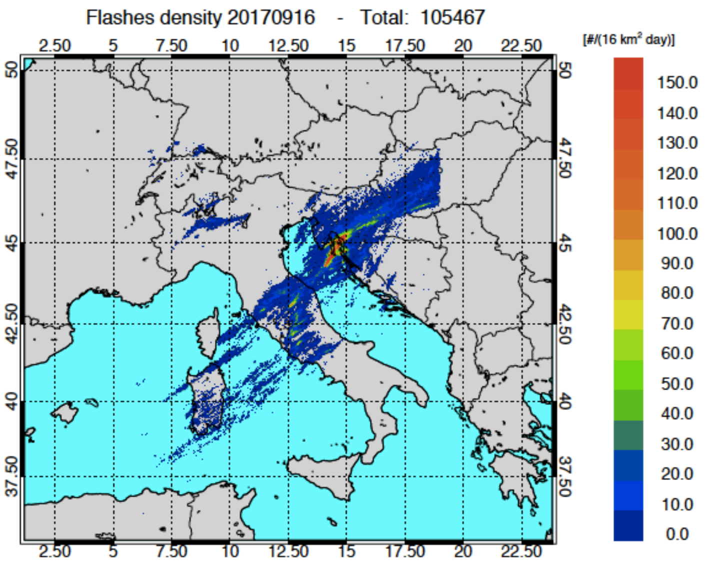

Figure 5: Lightning density (number of lighting per 16 km^2 for the whole day) recorded on 16 September 2017. The total number of flashes is shown in the title.

Eliminato: recorded

Eliminato: ... [5]

a)

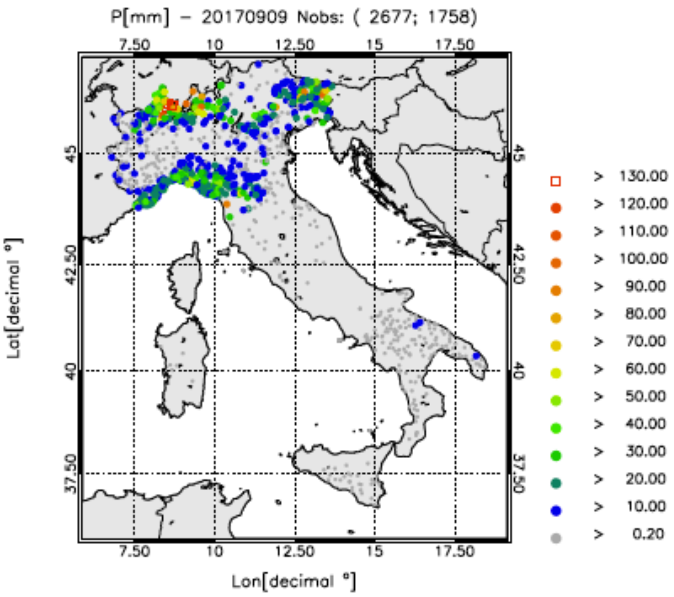

b)

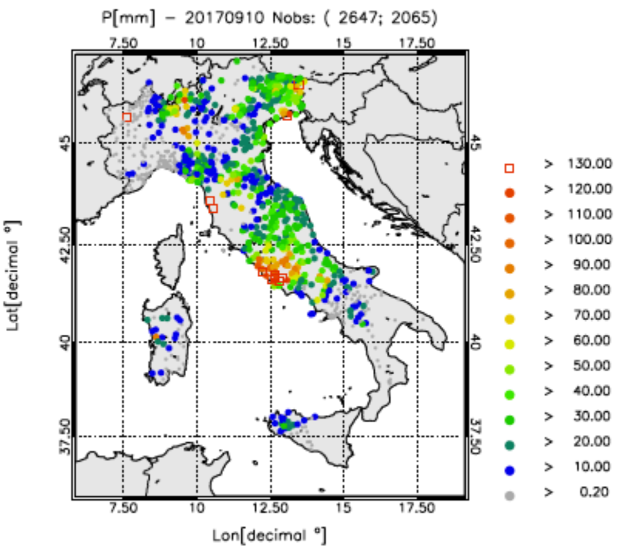

Figure 6: a) As in Figure 1 but for a) 9 September 2017 and b) 10 September 2017.

a)

b)

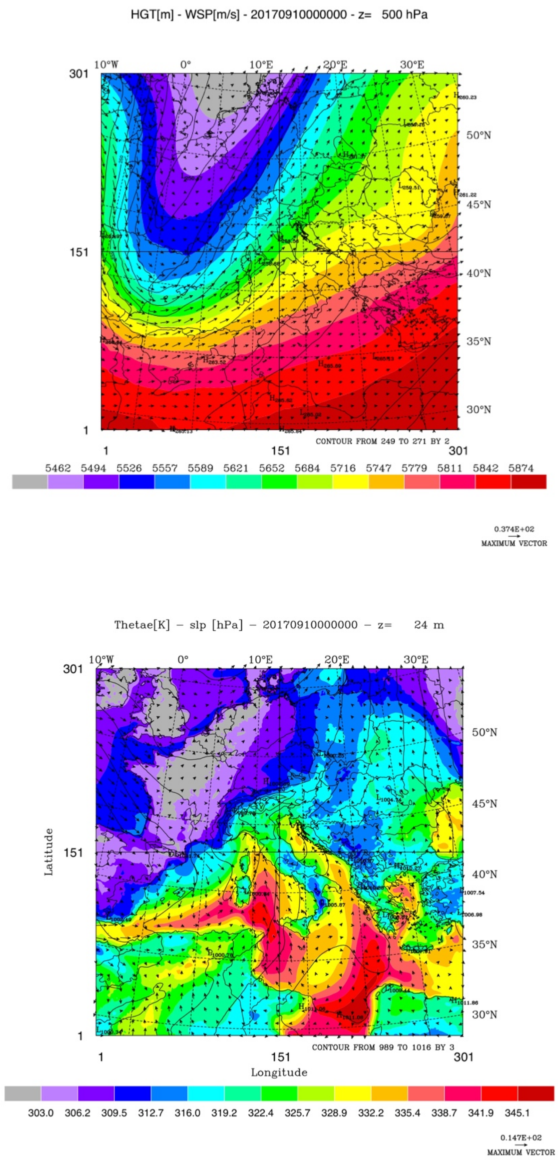

Figure 7: a) Geopotential height (filled contours), temperature (contours) and wind vectors at 500 hPa at 00 UTC on 10 September 2017. Maximum velocity is 37 m/s; b) equivalent potential temperature (filled contours), sea-level pressure (contours) and wind vectors at 24 m above the surface (maximum value 15 m/s).

Eliminato: (first vertical level,

Eliminato:

a)

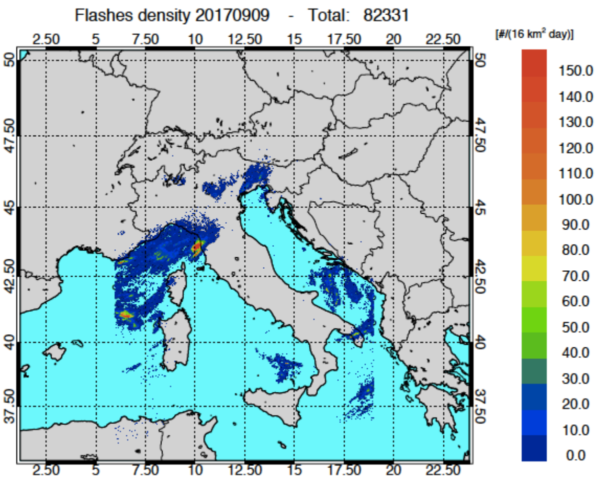

b)

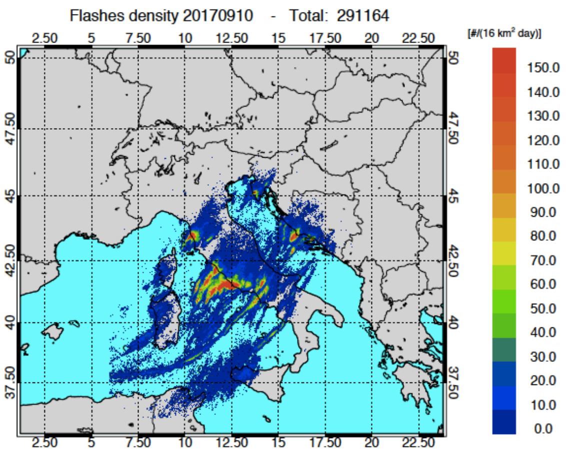

Figure 8: a) Lightning density (lightning number per 16 km^2 for the whole day) recorded on 09 September 2017; b) as in a) on 10 September 2017. The number of flashes on each day is shown in the title.

Eliminato: for
Eliminato: 9
Eliminato: recorded

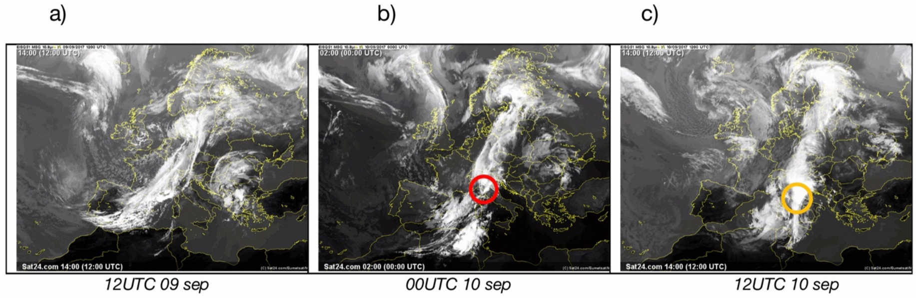

Figure 9: a) Satellite images (METEOSAT second generation) of the infrared channel, 10.8 micron, at 12 UTC on 9 September 2017, at 00 UTC and 12 UTC on 10 September 2017. The red circle in Figure 9b and the orange circle in Figure 9c show the Livorno and Lazio area, respectively.

a)

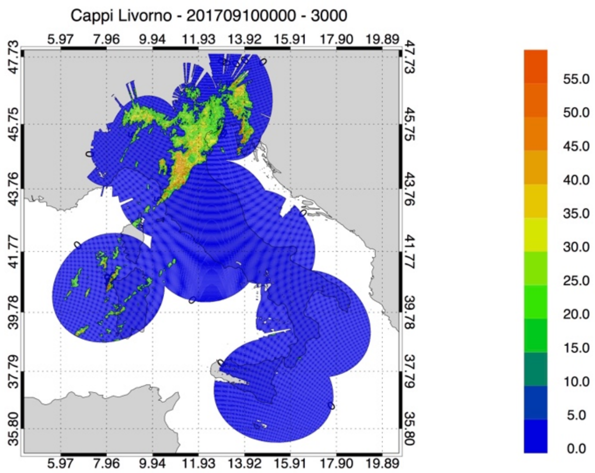

Eliminato:

Eliminato: <#> b)

c)

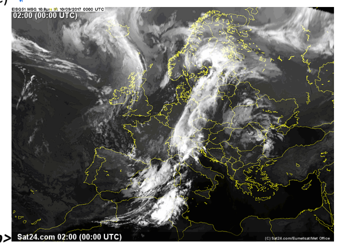

<sp> ... [6]

Formattato: Tipo di carattere:(Predefinito) +Corpo tema (Calibri), Colore carattere: Automatico

Formattato: Tipo di carattere:(Predefinito) +Corpo tema (Calibri), Colore carattere: Automatico

Formattato: Tipo di carattere:(Predefinito) +Corpo tema (Calibri), Colore carattere: Automatico

Eliminato: 00 UTC

Eliminato: ... [7]

b)

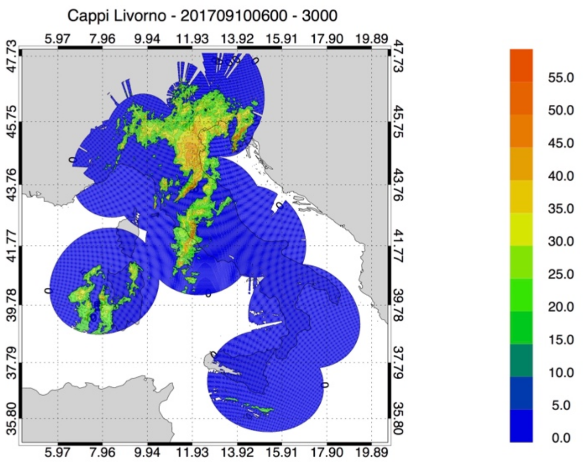

Figure 10: a) National radar mosaic at 3 km above the sea level observed at 00 UTC on 10 September 2017; b) as in a) at 06 UTC.

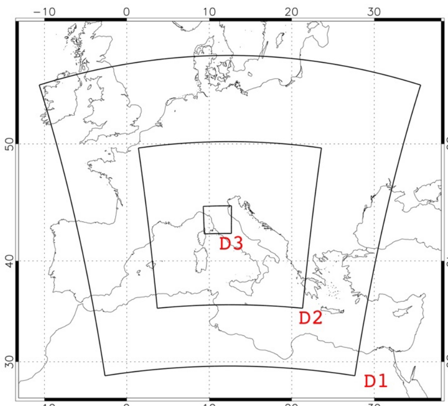

Figure 11: The three domains used in RAMS@ISAC. The model grid over domain D1 has 301 grid points in the NS and WE directions and has 10 km horizontal resolution, the model grid over domain D2 has 401 grid points in the NS and WE directions and has 4 km horizontal resolution. The model grid over domain D3 has 203 grid points in the NS and WE directions and has 4/3 km horizontal resolution. All grids have the same thirty-six vertical levels spanning the 0-22.4 km vertical layer.

Formattato: Interlinea: singola

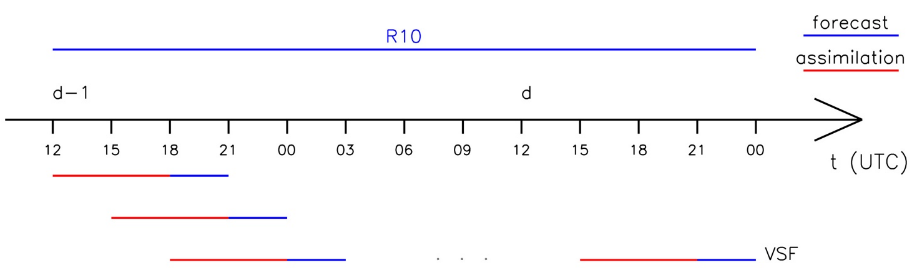

Figure 12: The implementation of RAMS@ISAC very short-term forecast.

Figure 13: The radar network of the Department of Civil Protection. Green radars operate with dual-polarisation, blue radars have single polarisation.

Eliminato: ... [8]

a)

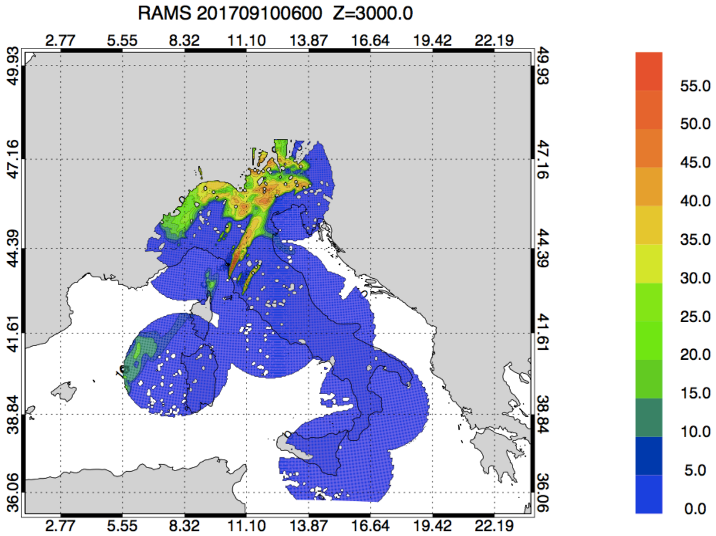

b)

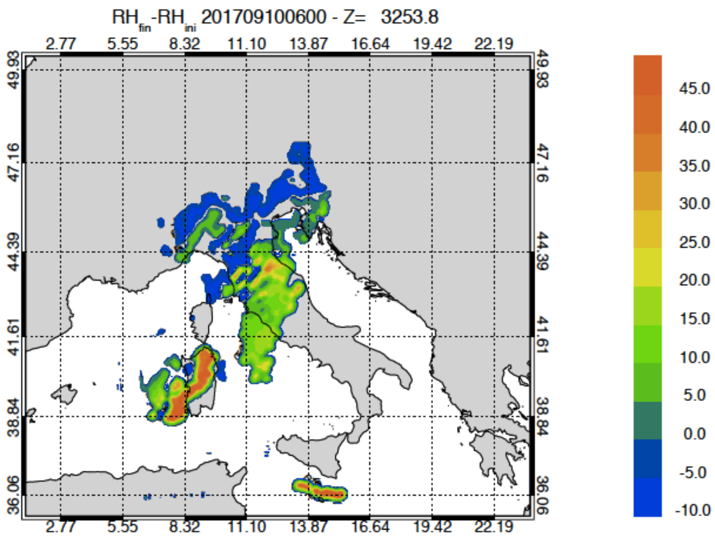

Figure 14: a) RAMS@ISAC reflectivity factor simulated 3 km above sea level at 06 UTC on 10 September 2017; b) relative humidity difference between the analysis and the background at 06 UTC at 3.2 km level in the terrain following vertical coordinate of RAMS@ISAC.

Formattato: Interlinea: singola

a)

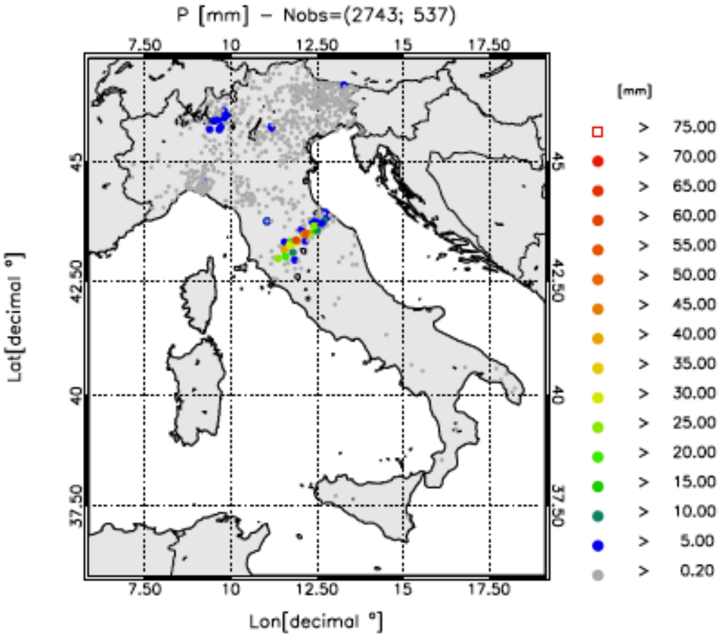
P [mm] – Nobs=(2743; 537)
Lat[decimal °]
Lon[decimal °]
[mm]
> 75.00
> 70.00
> 65.00
> 60.00
> 55.00
> 50.00
> 45.00
> 40.00
> 35.00
> 30.00
> 25.00
> 20.00
> 15.00
> 10.00
> 5.00
> 0.20

b)

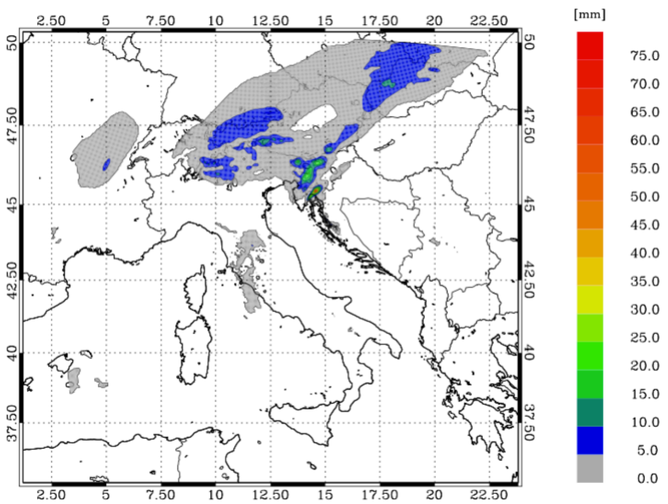
[mm]
75.0
70.0
65.0
60.0
55.0
50.0
45.0
40.0
35.0
30.0
25.0
20.0
15.0
10.0
5.0
0.0

c)

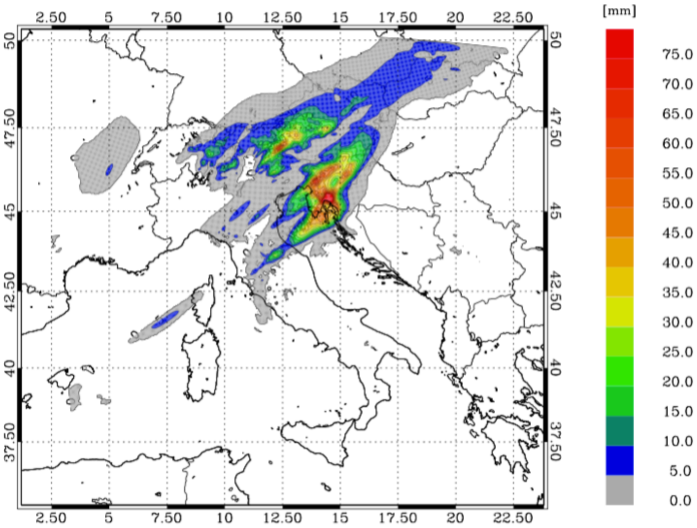
[mm]
75.0
70.0
65.0
60.0
55.0
50.0
45.0
40.0
35.0
30.0
25.0
20.0
15.0
10.0
5.0
0.0
2.50 5 7.50 10 12.50 15 17.50 20 22.50
50 47.50 45 42.50 40 37.50

d)

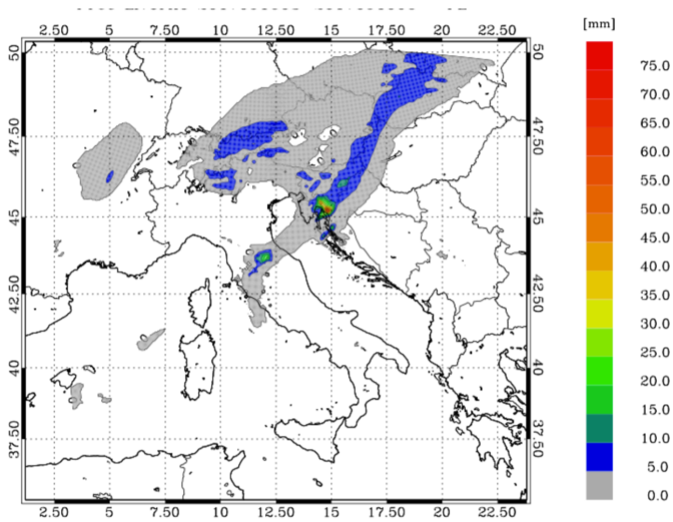
[mm]
75.0
70.0
65.0
60.0
55.0
50.0
45.0
40.0
35.0
30.0
25.0
20.0
15.0
10.0
5.0
0.0
2.50 5 7.50 10 12.50 15 17.50 20 22.50
50 47.50 45 42.50 40 37.50

e)

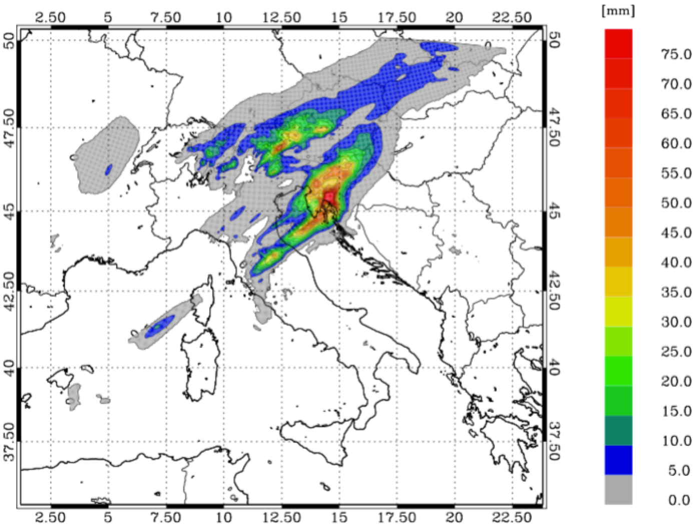
[mm]
75.0
70.0
65.0
60.0
55.0
50.0
45.0
40.0
35.0
30.0
25.0
20.0
15.0
10.0
5.0
0.0
2.50 5 7.50 10 12.50 15 17.50 20 22.50
50 47.50 45 42.50 40 37.50

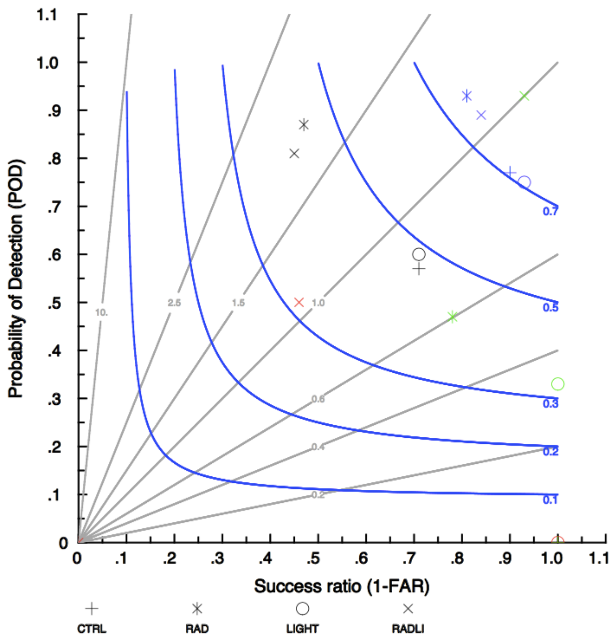
Probability of Detection (POD)
Success ratio (1-FAR)
CTRL
RAD
LIGHT
RADLI

Figure 15: a) rainfall reported by raingauges between 03 and 06 UTC on 16 September 2017. Only raingauges observing at least 0.2 mm/day are shown. The first number in the title within brackets represents the available raingauges, while the second number represents those observing at least 0.2 mm/3h; b) rainfall VSF of CTRL for the same time interval as in a); c) as in b) for RAD forecast; d) as in b) for LIGHT forecast; e) as in b) for RADLI forecast; f) performance diagram: black symbols are for the nearest neighbourhood and for 1mm/3h threshold; red symbols are for the nearest neighbourhood and for 30 mm/3h threshold; blue symbols are for 25 km neighbourhood radii and for 1 mm/3h threshold; green symbols are for 25 km neighbourhood radii and for 30 mm/3h threshold.

Eliminato: .

a)

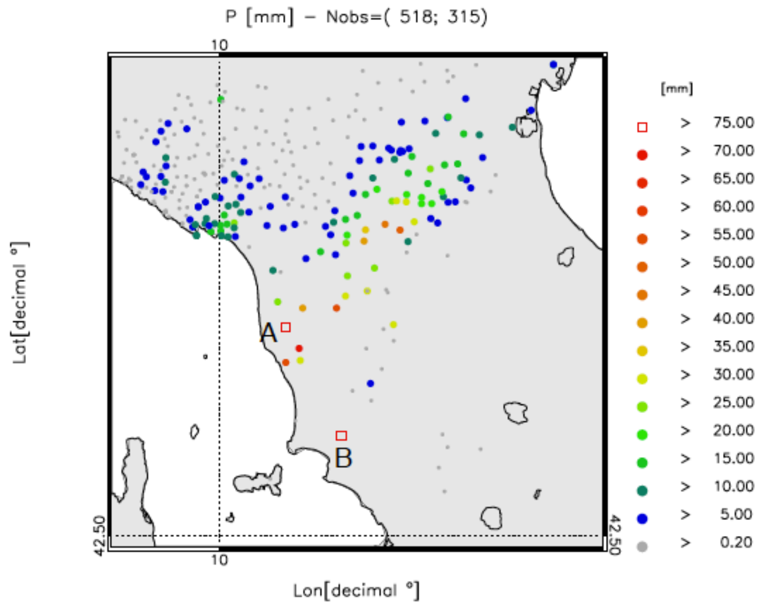

P [mm] - Nobs=(518; 315)
10
Lat[decimal °]
Lon[decimal °]
A
B
42.50
[mm]
> 75.00
> 70.00
> 65.00
> 60.00
> 55.00
> 50.00
> 45.00
> 40.00
> 35.00
> 30.00
> 25.00
> 20.00
> 15.00
> 10.00
> 5.00
> 0.20

b)

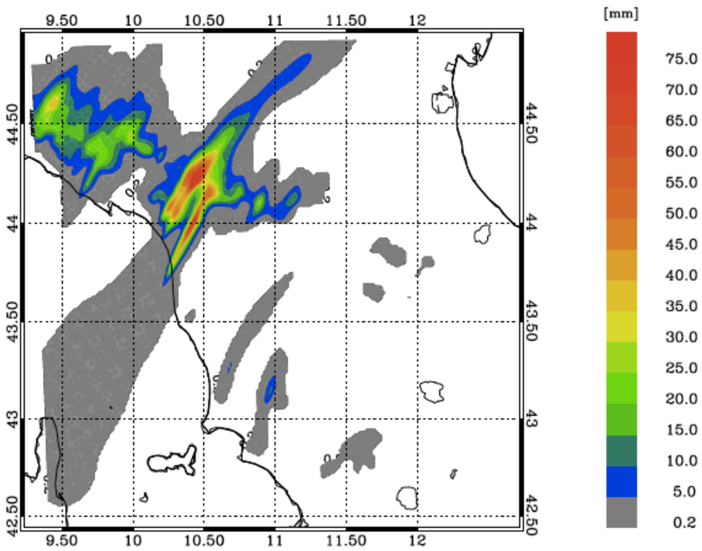

9.50
10
10.50
11
11.50
12
44.50
44
43.50
43
42.50
[mm]
75.0
70.0
65.0
60.0
55.0
50.0
45.0
40.0
35.0
30.0
25.0
20.0
15.0
10.0
5.0
0.2

c)

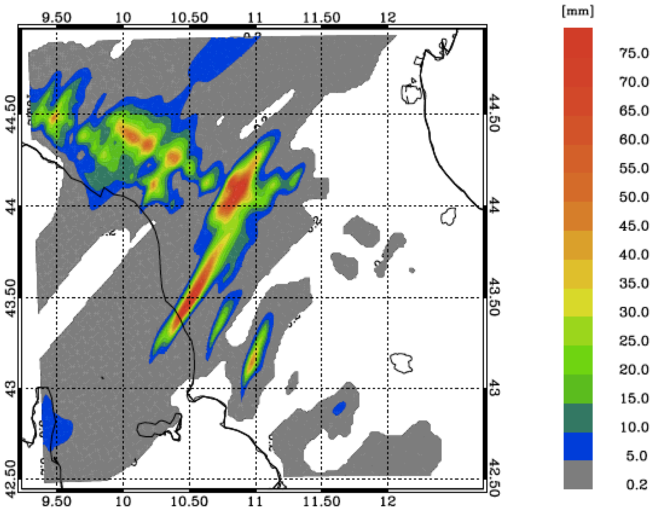
9.50 10 10.50 11 11.50 12
44.50
44
43.50
43
42.50
[mm]
75.0
70.0
65.0
60.0
55.0
50.0
45.0
40.0
35.0
30.0
25.0
20.0
15.0
10.0
5.0
0.2

d)

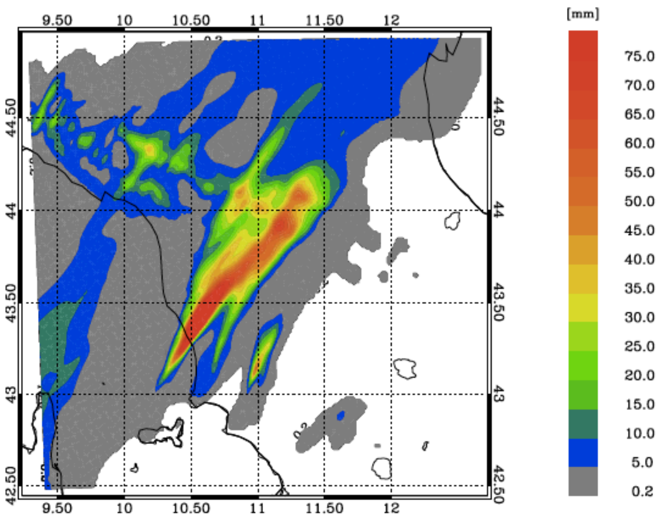
9.50 10 10.50 11 11.50 12
44.50
44
43.50
43
42.50
[mm]
75.0
70.0
65.0
60.0
55.0
50.0
45.0
40.0
35.0
30.0
25.0
20.0
15.0
10.0
5.0
0.2

e)

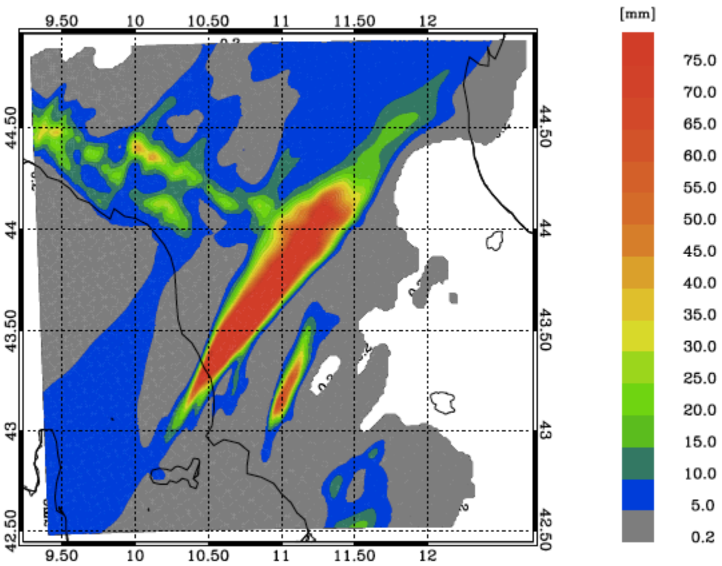

9.50
10
10.50
11
11.50
12
44.50
44
43.50
43
42.50
[mm]
75.0
70.0
65.0
60.0
55.0
50.0
45.0
40.0
35.0
30.0
25.0
20.0
15.0
10.0
5.0
0.2

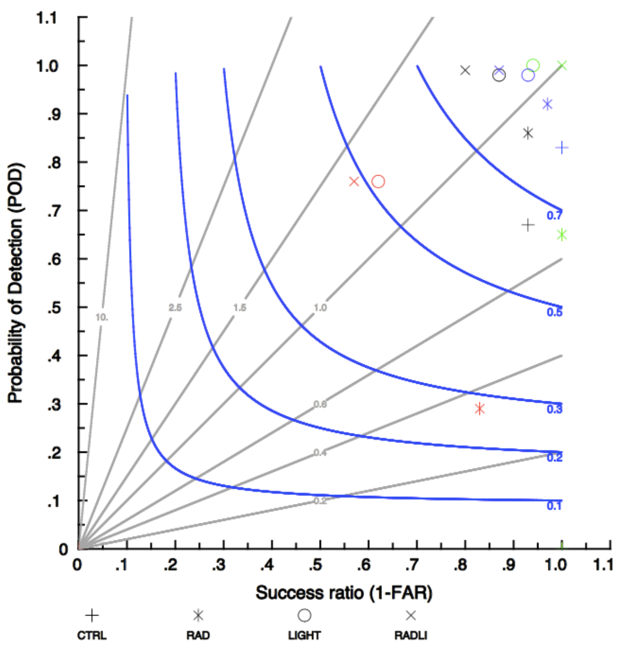

Figure 16: a) rainfall reported by raingauges between 00 and 03 UTC on 10 September 2017. Only stations reporting at least 0.2 mm/3h are shown. The first number in the title within brackets represents the number of raingauges available over the domain, while the second number shows those observing at least 0.2 mm/3h; b) rainfall VSF of CTRL for the same time interval as in a); c) as in b) for RAD forecast; d) as in b) for LIGHT forecast; e) as in b) for RADLI forecast. Labels A and B help to identify the positions of two rainfall maxima discussed into the text; f) performance diagram: black symbols are for the nearest neighbourhood and for 1mm/3h threshold; red symbols are for the nearest neighbourhood and for 30 mm/3h threshold; blue symbols are for 25 km neighbourhood radii and for 1 mm/3h threshold; green symbols are for 25 km neighbourhood radii and for 30 mm/3h threshold.

Formattato: Nessuno, Tipo di carattere:10 pt, Controllo ortografia e grammatica

Formattato: Centrato

Eliminato: .

a)

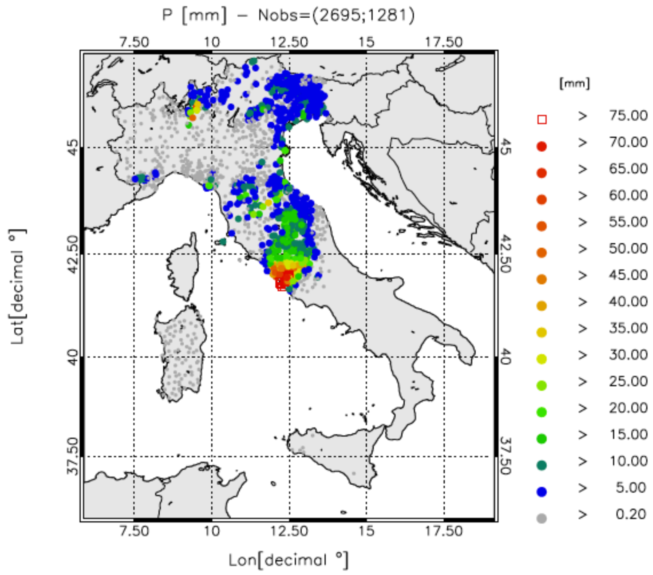
P [mm] – Nobs=(2695;1281)
7.50
10
12.50
15
17.50
45
42.50
40
37.50
Lat[decimal °]
Lon[decimal °]
[mm]
> 75.00
> 70.00
> 65.00
> 60.00
> 55.00
> 50.00
> 45.00
> 40.00
> 35.00
> 30.00
> 25.00
> 20.00
> 15.00
> 10.00
> 5.00
> 0.20

b)

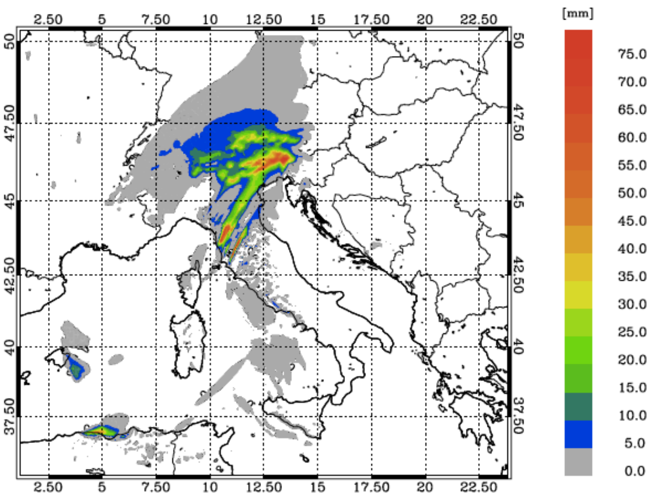
2.50
5
7.50
10
12.50
15
17.50
20
22.50
50
47.50
45
42.50
40
37.50
[mm]
75.0
70.0
65.0
60.0
55.0
50.0
45.0
40.0
35.0
30.0
25.0
20.0
15.0
10.0
5.0
0.0

c)

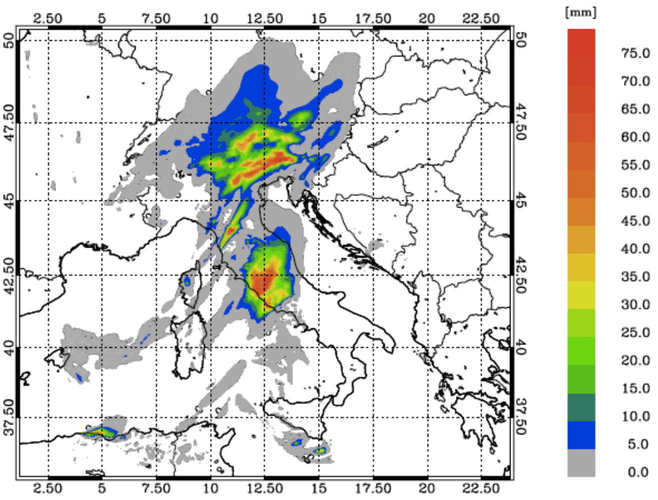

d)

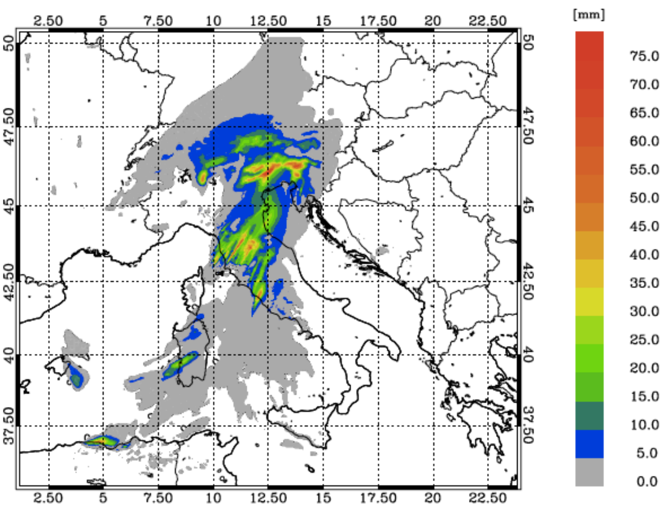

e)

Formattato: Centrato

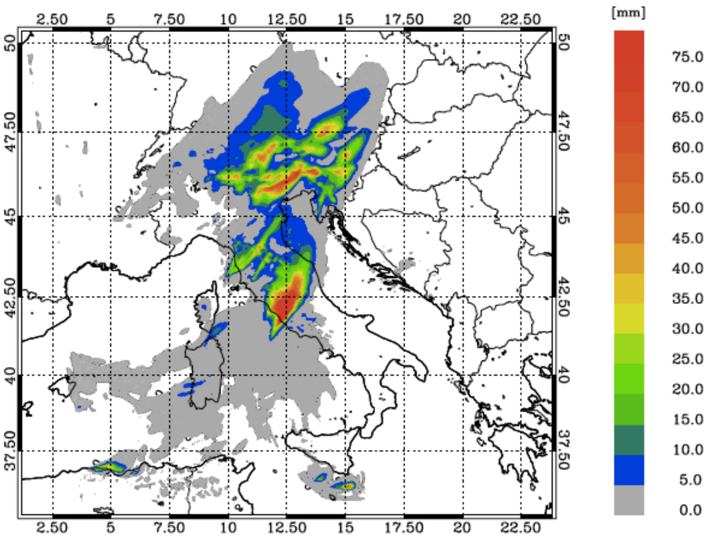

Eliminato: e)

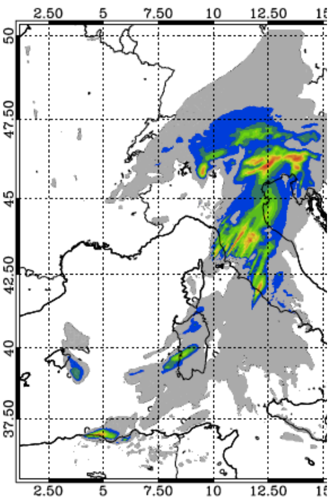

Eliminato:

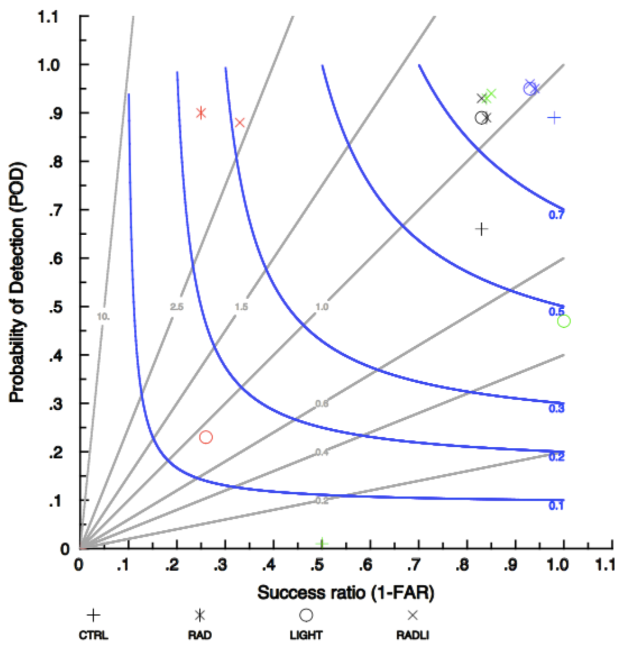

Figure 17: a) rainfall reported by raingauges between 06 - 09 UTC on 10 September 2017. For this time period 2695 raingauges reported valid observations in the domain, however only stations reporting at least 0.2 mm/3h are shown The first number in the title within brackets represents the number of raingauges available over the domain, while the second number shows those observing at least 0.2 mm/3h; b) rainfall VSF of CTRL in the same time interval as a); c) as in b) for RAD forecast; d) as in b) for LIGHT forecast; g) as in b) for RADLI forecast; f) performance diagram: black symbols are for the nearest neighbourhood and for 1mm/3h threshold; red symbols are for the nearest neighbourhood and for 30 mm/3h threshold; blue symbols are for 25 km neighbourhood radii and for 1 mm/3h threshold; green symbols are for 25 km neighbourhood radii and for 30 mm/3h threshold.

Formattato: Tipo di carattere:10 pt

Formattato: Centrato

a)

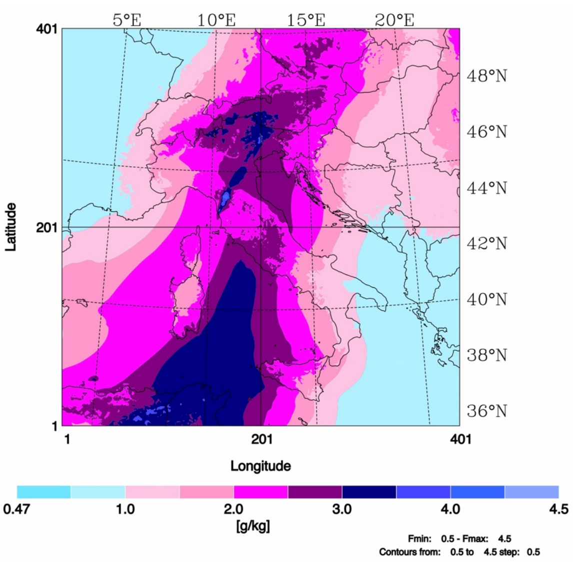

b)

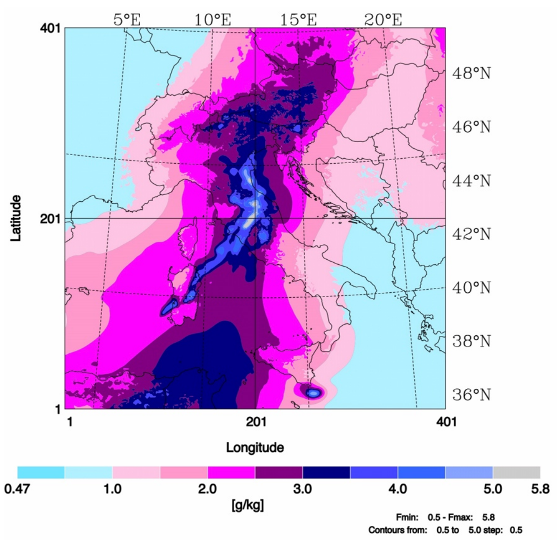

c)

Eliminato: . .

Formattato: Centrato

Formattato: Centrato

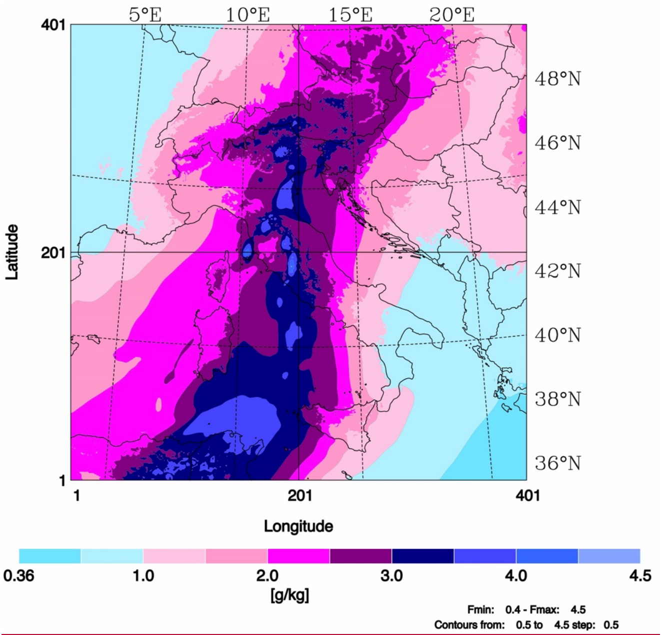

d)

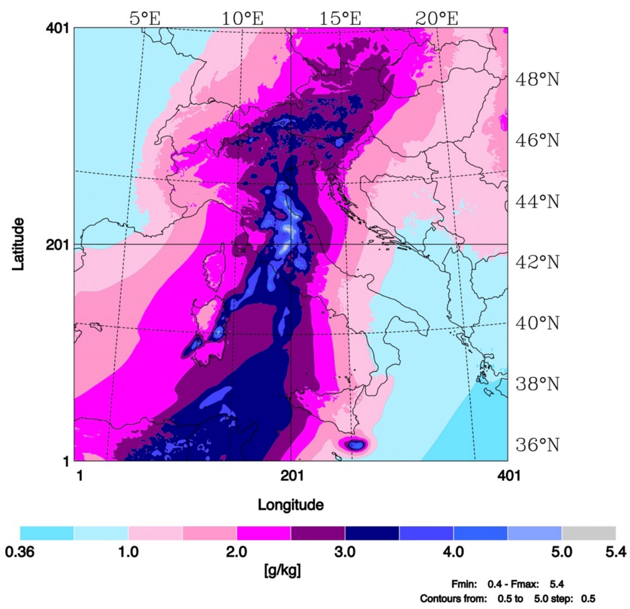

Formattato: Centrato

Formattato: Centrato

Figure 18: Water vapour mixing ratio averaged between 3 and 10 km at 06 UTC on 10 September 2017 for: a) CTRL; b) RAD; c) LIGHT; d) RADLI.

a)

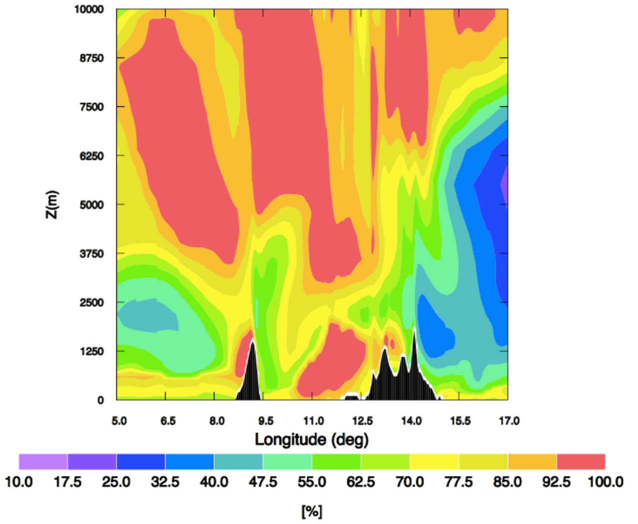

Formattato: Centrato

b)

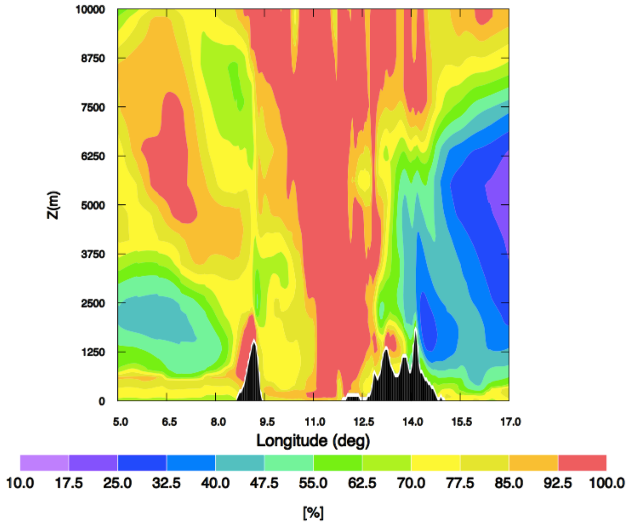

Formattato: Centrato

c)

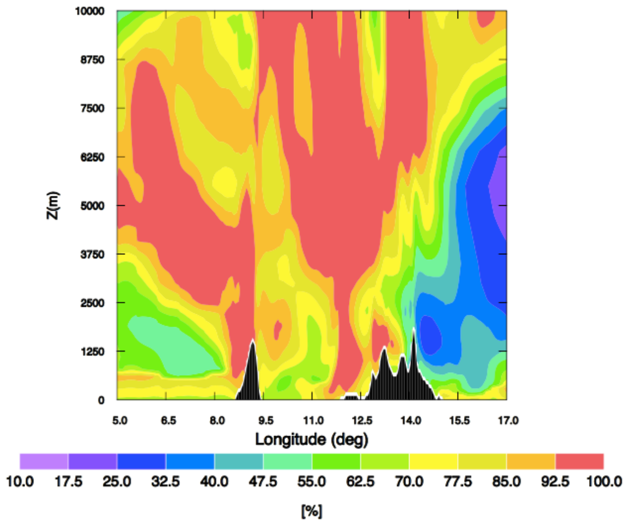

Formattato: Centrato

d)

Formattato: Centrato

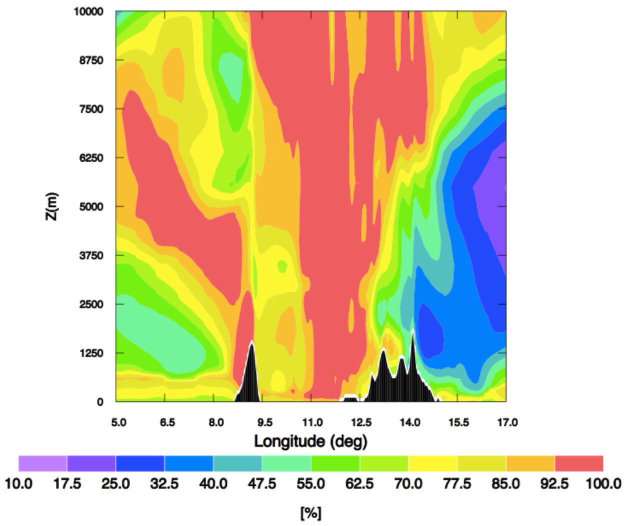

Formattato: Centrato

Figure 19: Relative humidity longitude-height cross-section at 42°N and at 06 UTC on 10 September 2017 for: a) CTRL; b) RAD; c) LIGHT; d) RADLI. Only the longitude range between 5 E and 17 E and the vertical range between 0 and 10 km are shown for clarity.

Formattato: Inglese (Stati Uniti)

Pagina 21: [1] Eliminato	stefano federico	05/06/19 12:22:00

The analysis of the scores confirms the above results (Table 6). CTRL has a poor performance as shown by the POD and ETS values, close to zero, for all thresholds above 30 mm/3h and for all neighbourhood radii. The simulations assimilating radar reflectivity factor performs better than LIGHT, the difference being larger for higher rainfall thresholds and for smaller neighbourhood radii. It is also notable the good performance of RADLI forecast for the nearest neighbourhood radii (ETS=0.43, POD=0.92) for the 50 mm/3h threshold.

Pagina 33: [2] Eliminato	stefano federico	11/06/19 07:25:00

Xiao, Q., Kuo, Y.-H., Sun, J., Chaulee, W., and Barker, D. M.: An Approach of RADAR Reflectivity Data Assimilation and Its Assessment with the Inland QPF of Typhoon Rusa (2002) at Landfall, J. Appl. Meteor. Climatol., 46, 14–22, 2007.

Xiao, Q., Kuo, Y.-H., Sun, J., and Lee, W. C.: Assimilation of Doppler RADAR Observations with a Regional 3DVAR System: Impact of Doppler Velocities on Forecasts of a Heavy Rainfall Case, J. Appl. Meteor., 44, 768–788, 2005.

Pagina 34: [3] Eliminato	stefano federico	04/06/19 11:44:00

Table 4: ETS and POD scores for three different neighbourhood radii. Scores are computed over the domain D2.

Threshold (mm/3h)	ETS nearest neighboorhood (CTRL, RAD, LIGHT, RADLI)	POD nearest neighbourhood (CTRL, RAD, LIGHT, RADLI)	ETS 25 km (CTRL, RAD, LIGHT, RADLI)	POD 25 km (CTRL, RAD, LIGHT, RADLI)	ETS 50 km (CTRL, RAD, LIGHT, RADLI)	POD 50 km (CTRL, RAD, LIGHT, RADLI)
1	(0.42,0.36,0.44,0.33)	(0.57,0.87,0.60,0.81)	(0.68,0.73,0.68,0.73)	(0.77,0.93,0.75,0.89)	(0.79,0.89,0.82,0.87)	(0.84,0.92,0.84,0.90)
6	(0.06,0.10,0.14,0.13)	(0.0,0.5,0.20,0.72)	(0.11,0.44,0.72,0.41)	(0.11,0.86,0.72,0.83)	(0.19,0.86,0.86,0.92)	(0.19,0.86,0.86,0.92)
10	(0.,0.05,0.,0.15)	(0.,0.26,0.,0.79)	(0.,0.66,0.58,0.74)	(0.0,0.84,0.58,0.89)	(0.,0.95,0.74,0.90)	(0.,0.95,0.74,0.90)
20	(0.,0.,0.,0.41)	(0.,0.,0.,0.8)	(0.0,0.41,0.33,0.87)	(0.,0.47,0.3,0.9)	(0.,0.73,0.80,1.0)	(0.,0.73,0.80,1.0)
30	(0.,0.,0.,0.31)	(0.,0.,0.,0.5)	(0.,0.,0.,0.90)	(0.,0.,0.,0.9)	(0.,0.,0.,1.0)	(0.,0.,0.,1.0)
40	(0.,0.,0.,0.)	(0.,0.,0.,0.)	(0.,0.,0.,0.33)	(0.,0.,0.,0.33)	(0.,0.,0.,0.50)	(0.,0.,0.,0.50)

Table 5: ETS and POD scores for three different neighbourhood radii. Scores are computed over the domain D3.

Threshold (mm/3h)	ETS nearest neighboorhood (CTRL, RAD, LIGHT, RADLI)	POD nearest neighbourhood (CTRL, RAD, LIGHT, RADLI)	ETS 25 km (CTRL, RAD, LIGHT, RADLI)	POD 25 km (CTRL, RAD, LIGHT, RADLI)	ETS 50 km (CTRL, RAD, LIGHT, RADLI)	POD 50 km (CTRL, RAD, LIGHT, RADLI)
1	(0.43,0.64,0.70,0.56)	(0.67,0.86,0.98,0.99)	(0.68,0.80,0.82,0.71)	(0.83,0.92,0.98,0.99)	(0.68,0.80,0.82,0.71)	(0.83,0.92,0.98,0.99)
6	(0.1,0.31,0.60, 0.49)	(0.24,0.58,0.89,0.95)	(0.49,0.70,0.91,0.96)	(0.55,0.76,0.96,0.97)	(0.49,0.70,0.91,0.96)	(0.55,0.76,0.96,0.97)
10	(0.11,0.33,0.56,0.54)	(0.19,0.56,0.75,0.80)	(0.48,0.76,0.91,0.97)	(0.52,0.79,0.92,0.97)	(0.48,0.76,0.91,0.97)	(0.52,0.79,0.92,0.97)
20	(0.02,0.30,0.52,0.59)	(0.03,0.39,0.74,0.81)	(0.18,0.73,0.97,0.93)	(0.19,0.74,0.97,0.97)	(0.18,0.73,0.96,0.93)	(0.19,0.74,0.97,0.97)
30	(0.,0.27,0.51,0.47)	(0.,0.29,0.76,0.76)	(0.,0.64,0.94,1.)	(0.,0.65,1.,1.)	(0.,0.64,0.94,1.)	(0.,0.65,1.,1.)
40	(0.,0.44,0.27,0.27)	(0.,0.44,0.56,0.67)	(0.,0.89,1.,1.)	(0.,0.89,1.,1.)	(0.,0.89,1.,1.)	(0.,0.89,1.,1.)
50	(0.,0.33,0.66,0.50)	(0.,0.33,0.67,0.67)	(0.,0.67,1.,1.)	(0.,0.67,1.,1.)	(0.,0.66,1.,1.)	(0.,0.67,1.,1.)

Table 6 ETS and POD scores for three different neighbourhood radii. Scores are computed over the domain D2.

Threshold (mm/3h)	ETS nearest neighboorhood (CTRL, RAD, LIGHT, RADLI)	POD nearest neighbourhood (CTRL, RAD, LIGHT, RADLI)	ETS 25 km (CTRL, RAD, LIGHT, RADLI)	POD 25 km (CTRL, RAD, LIGHT, RADLI)	ETS 50 km (CTRL, RAD, LIGHT, RADLI)	POD 50 km (CTRL, RAD, LIGHT, RADLI)
1	(0.41,0.63,0.61,0.65)	(0.66,0.89,0.89,0.93)	(0.79,0.83,0.82,0.83)	(0.89,0.95,0.95,0.96)	(0.88,0.92,0.93,0.94)	(0.93,0.97,0.98,0.98)
6	(0.2,0.4,0.39,0.47)	(0.43,0.82,0.77,0.88)	(0.45,0.63,0.71,0.76)	(0.63,0.90,0.95,0.96)	(0.72,0.86,0.88,0.92)	(0.82,0.96,0.97,0.96)
10	(0.,0.24,0.18,0.28)	(0.14,0.78,0.55,0.80)	(0.14,0.47,0.58,0.62)	(0.24,0.86,0.82,0.93)	(0.32,0.91,0.96,0.95)	(0.35,0.95,0.97,0.97)
20	(-0.03,0.18,0.13, 0.22)	(0.01,0.81,0.30,0.80)	(0.09,0.46,0.57,0.61)	(0.11,0.86,0.59,0.90)	(0.15,0.84,0.91,0.96)	(0.15,0.90,0.92,0.97)

30	(-0.02,0.22,0.13,0.28)	(0.,0.90,0.23,0.88)	(0.01,0.79,0.46,0.80)	(0.01,0.93,0.47,0.94)	(0.02,0.95,0.93,0.99)	(0.02,0.95,0.93,0.99)
40	(-0.1,0.24,0.08,0.36)	(0.,0.83,0.12,0.89)	(0.01,0.83,0.37,0.83)	(0.02,0.97,0.38,0.97)	(0.1,0.97,0.95,0.98)	(0.02,0.98,0.95,0.98)
50	(-0.01,0.27,0.,0.43)	(0.,0.67,0.,0.92)	(0.,0.90,0.,0.90)	(0.,0.94,0.,0.96)	(0.,0.96,0.,0.96)	(0.,0.96,0.,0.96)

Pagina 37: [4] Eliminato **stefano federico** **05/06/19 13:10:00**

b) c)

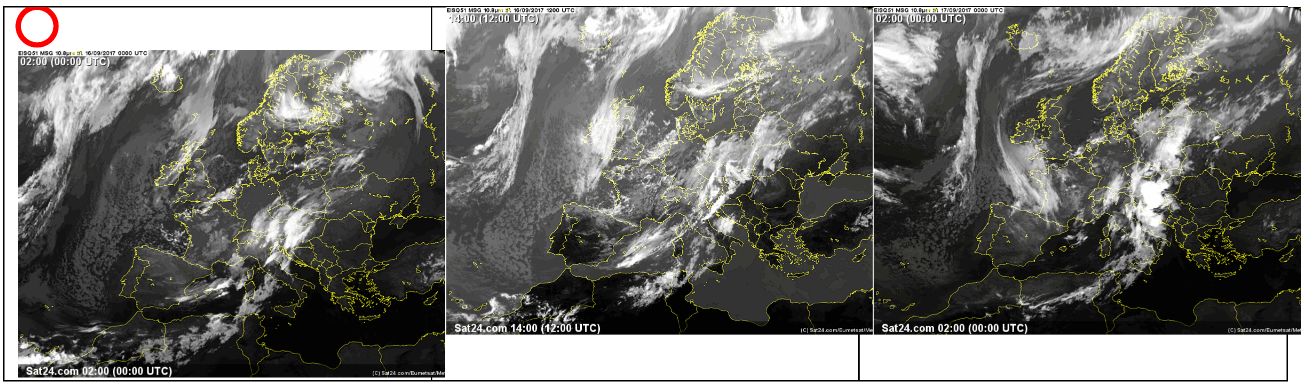

00UTC 16 sep *12UTC 16 sep* *00UTC 17 sep*

Pagina 38: [5] Eliminato **stefano federico** **12/06/19 07:32:00**

Pagina 42: [6] Eliminato stefano federico 05/06/19 13:11:00

b) c)

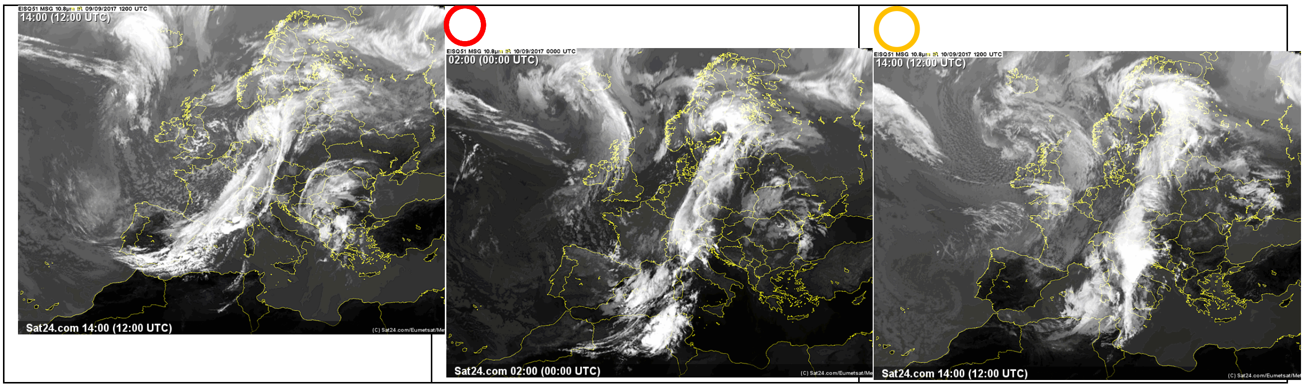

12UTC 09 sep *00UTC 10 sep* *12UTC 10 sep*

Pagina 42: [7] Eliminato stefano federico 12/06/19 07:33:00

Pagina 44: [8] Eliminato stefano federico 12/06/19 07:33:00

Supplemental material of the paper: nhess-2018-319

The impact of lightning and radar reflectivity factor data assimilation on the very short term rainfall forecasts of RAMS@ISAC: application to two case studies in Italy

Stefano Federico[1], Rosa Claudia Torcasio[1], Elenio Avolio[2], Olivier Caumont[3], Mario Montopoli[1], Luca Baldini[1], Gianfranco Vulpiani[4], Stefano Dietrich[1]

1. ISAC-CNR, via del Fosso del Cavaliere 100, Rome, Italy
2. ISAC-CNR, zona Industriale comparto 15, 88046 Lamezia Terme, Italy
3. CNRM UMR 3589, University of Toulouse, Météo-France, CNRS, 42 avenue G. Coriolis, 31057 Toulouse, France
4. Dipartimento Protezione Civile Nazionale Ufficio III - Attività Tecnico Scientifiche per la Previsione e Prevenzione dei Rischi, 00189 Rome

S1 Introduction

In this supplemental material, we discuss several sensitivity tests of lightning and radar reflectivity factor data assimilation. In particular: a) the contribution of data assimilation to the evolution of total water for each source of data is considered in Section S2; b) the sensitivity of rainfall VSF to the formulation of lightning data assimilation is discussed in Section S3; c) the sensitivity of rainfall VSF to two specific aspects of radar reflectivity factor data assimilation is considered in Section S4; d) the sensitivity of rainfall VSF to RAMS@ISAC setting is discussed in Section S5.

Section S6 shows the impact of lightning data assimilation for a case study well predicted by the control forecast, which doesn't assimilate neither lightning nor radar reflectivity factor. A different representation of the Figures 15-17 of the paper is provided in Section S7. The form of the forward radar operator is provided in Section S8. Conclusions are given in section S9. Table 1 shows the list of the simulations discussed in this supplemental material.

S2 Evolution of total water

Because both lightning data assimilation and radar reflectivity factor data assimilation adjust the water vapour mixing ratio (q_v), it is interesting to evaluate the contribution of each data source to the q_v adjustment including in this evaluation the assimilation phase (0-6 h).

Formattato: Numerazione: continua
Eliminato: Preliminary results of
Eliminato: t
Eliminato: 2
Formattato: Tipo di carattere:Non Grassetto
Formattato: Tipo di carattere:Non Grassetto, Inglese (Stati Uniti)
Formattato: Tipo di carattere:Non Corsivo, Inglese (Stati Uniti)
Formattato: Tipo di carattere:Non Corsivo, Inglese (Stati Uniti)
Formattato: Inglese (Stati Uniti)
Formattato: Inglese (Stati Uniti)
Formattato: Tipo di carattere:Non Corsivo, Inglese (Stati Uniti)
Formattato: Inglese (Stati Uniti)
Eliminato: *1*

Fierro et al. (2015) used the total water substance mass (accumulated precipitation + total hydrometeors and water vapour mass) to quantify the impact of lightning data assimilation by nudging. Here we use a similar approach. More specifically, we consider the forecasted accumulated precipitation and the total hydrometeors and water vapour mass averaged over the grid columns. Moreover, we averaged all VSFs for Serano and Livorno. Figure S1a shows the evolution of accumulated precipitation forecast, while Figure S1b shows the evolution of hydrometeors plus water vapour mass forecast

Figures S1a and S1b show that flashes add less water vapour compared to radar reflectivity factor data assimilation and, of course, RADLI has the largest impact. In particular, the total water mass added to the background at the end of VSF is 2.5%, 5.7% and 7.4% of the background value for LIGHT, RAD and RADLI, respectively.

Interestingly, the total water mass added by RADLI to the background is less than the sum of the total water masses added by RAD and LIGHT. This happens because RAMS-3DVar adds water to the background limiting the impact of nudging during the simulation and vice-versa.

Accumulated precipitation accounts for the largest part of the water mass added to the simulation, similarly to Fierro et al. (2015). At the end of the assimilation phase (6h), the evolution of the hydrometeors plus water vapour mass converges towards the background as boundary conditions propagate into the domain.

S3 Sensitivity to nudging formulation

As stated in Section 3.2 of the paper, the application of the Fierro et al. (2012) method to RAMS@ISAC is not straightforward. Furthermore, the optimal setting of the coefficients of Eqn. (1) (see the paper for the expression of the equation) depends on the case study. For these reasons, it is important to evaluate the sensitivity of the results to the nudging formulation. For this purpose, we show the variability of ETS and POD scores with A and B coefficients of Eqn. (1). The scores are computed considering all VSF of the two case studies for different configurations: A_76 has the coefficients A=0.76 and B=0.25; LIGHT has A=0.86 and B=0.15 (default setting), SAT has A=1.01 and B=0; RADLI has A=0.86 and B=0.15 (default setting).

Scores are computed for RAMS@ISAC second domain considering the nearest neighbourhood rainfall for all VSF of Serano and Livorno. ETS score (Figure S2a) shows that all configurations assimilating either lightning or radar reflectivity factor or both observations improve the forecast

Eliminato: For the 3D-Var approach, the impact of the contribution of data assimilation on q_v can be done using maps similar to Figure 14b. For example, Fierro et al. (2016) used the layer averaged q_v between 3 and 10 km to quantify the water vapour added to the WRF model by lightning data assimilation. However, because in this paper lightning are assimilated by nudging, this kind of representation is not practicable because it is difficult to separate the contribution of the nudging from model processes determining the evolution of q_v.

Eliminato: W

Eliminato: Also

Eliminato: T

Eliminato: the forecasted

Eliminato: is shown in Figure S1a

Eliminato: the

Eliminato: is shown in Figure S1b

Eliminato: Considering the

Eliminato: it is apparent

Eliminato: Importantly

Eliminato: 3D-Var

Eliminato:

Eliminato: In particular, in an already saturated atmosphere the nudging of lightning doesn't have any impact.

Eliminato: After

Eliminato: s

Eliminato: *2*

Eliminato: nudging method of

Eliminato: Also

Eliminato: interesting

Eliminato: to

Eliminato: changes in the

Eliminato: the

Eliminato:); CTRL, and RAD are as defined in Table S1

Eliminato: The s

Eliminato: VSF

for all thresholds. RADLI has the best ETS for rainfall intensity larger than 32 mm/3h in agreement with the results of the three VSF discussed in the paper.

The simulations assimilating lightning perform better than simulations assimilating radar reflectivity factor for thresholds below 32 mm/3h because they have less false alarms (not shown). A_76 has the worst score among all simulations assimilating lightning. The comparison between LIGHT and SAT shows mixed results: SAT performs better up to 32 mm/3h, while LIGHT is better for higher thresholds. This behaviour is confirmed by the POD (Figure S2b). A visual inspection of the model output reveals that, for high rainfall intensities, SAT generates spurious convection in some areas while misses convection in other areas that are correctly forecast by LIGHT.

Lynn et al. (2015) implemented a method suggested by Fierro et al. (2012) to suppress spurious convection in WRF (Weather Research and Forecasting Model). This method compares the lightning forecast during the assimilation period with observations to filter out spurious convection. The application of the methodology on 10 July 2013 improved the forecast of the squall line from Texas to Iowa, which was the focus of the forecast on that day; however, the application of the method to 19 and 21 March 2012 over the CONUS gave mixed results, improving the forecast in the first 6h and worsening it in the following hours.

The implementation of this method could be used in RAMS@ISAC in future applications of the nudging scheme, to suppress spurious convection.

It is finally noted that RAD and RADLI have high POD values for all thresholds, nevertheless their ETS is below that of LIGHT and SAT for rainfall intensities up to 32 mm/3h for RADLI and up to 42 mm/3h for RAD. This behaviour is caused by the larger number of false alarms in simulations assimilating radar reflectivity factor compared to those assimilating lightning. This result shows again that RAD and RADLI configurations have a wet bias. In particular, the frequency bias of RAD and RADLI configuration is about 3 for thresholds between 20 and 40 mm/3h.

S4 Sensitivity to radar formulation

In this section sensitivity tests involving two different settings of radar reflectivity factor data assimilation are performed: a) observation error (1 to 3 dBz for the default setting); b) the shape of the area used for computing the relative humidity pseudo-profiles.

We limit the discussion to the Livorno case, which is the most intense between the two events considered in the paper.

Eliminato: line
Eliminato: For rainfall lower than 32 mm/3h, the
Eliminato: ,
Eliminato: compared to those assimilating radar reflectivity factor
Eliminato: From the comparison of LIGHT and SAT with A_76, it is apparent that the latter has the worst performance
Eliminato: result
Eliminato: for larger rainfall intensities
Eliminato: e
Eliminato: lightning
Eliminato: after 6h
Eliminato: the
Eliminato: could be used,
Eliminato: implementation
Eliminato: up
Eliminato: (
Eliminato:)
Eliminato: (
Eliminato:)
Eliminato: given by
Eliminato: simulations

For the sensitivity to the radar reflectivity factor observation error, it is important to note that this error is used when computing the relative humidity pseudo profiles and not in RAMS-3DVar, where the NMC method (Parrish and Derber, 1992) is used. Because the model missed the event, the assimilation of radar reflectivity factor caused a model wetting. This humidity, however, is mainly added for the following reason: RAMS@ISAC doesn't simulate any reflectivity factor while the radars show positive values of reflectivity factor (for example most of the relative humidity added over central Italy and over Sardinia is produced by this occurrence). When this happens, the model is saturated above the LCL where the observed reflectivity factor is greater than zero and the error of radar observations is not used (the error of radar reflectivity factor is used for computing pseudo-profiles, which are used when the background provides already a good forecast of reflectivity factor). Although in general the error of radar reflectivity factor observations is important and a too small value could make the method too sensitive to radar observation, especially when combined with a pure sampling of the radar data as in our setting, this problem is less important for the case studies considered in this paper because they are missed by RAMS@ISAC.

The shape of the area used for computing relative humidity pseudo-profiles for the radar data assimilation is a square in this paper, according to Caumont et al. (2010). However, a circle is also a good choice for this shape because it considers grid points equidistant from the centre along the circumference. The impact of this geometry, however, is expected to be negligible because pseudo profiles are less important in the data assimilation of the cases considered in this paper, as explained above.

Figure S3 shows the precipitation forecast between 06 and 09 UTC on 10 September 2017 by the VSF assimilating radar with the default setting (RAD), by the VSF assimilating radar reflectivity factor with and error increased by 5 compared to the RAD simulation (in this case the radar reflectivity factor error varies between 5dBz and 15 dBz), and by the VSF using a circle with 50 km diameter for computing relative humidity pseudo-profiles (CIRC). There are small differences at the local scale but the precipitation VSF are very similar for different set-up. The POD and ETS scores computed for the ten VSF of the Livorno case (Figure S4) further confirm this result. Differences among RAD, RAD5 and CIRC are very small and increasing the radar reflectivity factor error or changing the shape of the area used for computing relative humidity pseudo-profiles has a minor impact on the rainfall VSF for the Livorno case study.

S5 Sensitivity to model formulation

In this section, we study the sensitivity of the rainfall VSF for the Livorno case to two aspects of the model formulation: a) updating initial (IC) and boundary conditions (BC) (RLAA simulation); b) increasing the number of vertical levels from 36 to 42 (simulations CTRL42 and ANL42).

The RLAA simulation uses updated IC/BC that assimilates new data as they become available. IC and BC for the R4 domain are interpolated from the output of R10 domain, and, in order to update IC and BC, analyses are done for the R10 domain.

These analyses assimilate radar reflectivity factor every one-hour by RAMS-3DVar and lightning by nudging, similarly to R4 domain. The background error matrix for the RAMS-3DVar for the R10 domain is obtained applying the NMC method to the HyMeX-SOP1 period.

Ten VSF are run with R10. Each VSF lasts 9h and data assimilation is performed for the first six-hours. Those VSF are used to create IC/BC for the RLAA simulations.

The impact of updating IC and BC for the R4 VSF is expected to be small for the setting of this paper.

The impact of BC is presumed low because both radar and lightning observations are inside the R4 domain.

Formattato: Inglese (Stati Uniti)
Formattato: Inglese (Stati Uniti)
Formattato: Inglese (Stati Uniti)

The impact of updating IC is also expected to be low because even if IC are substantially changed by the radar reflectivity factor data assimilation over the R10 domain, when the VSF starts on R4 an analysis is made assimilating radar reflectivity factor on R4 domain. So, if the IC for this VSF forecast on R4 are interpolated from the R10 background (setting of the paper) the innovations given by the analysis over the R4 at initial time are large; if IC are interpolated from an R10 analysis (RLAA setting), the innovations of the first analysis over the R4 domain are small, because IC already take into account for the radar reflectivity factor data assimilation. However, the final result is similar in both cases.

Formattato: Inglese (Stati Uniti)
Formattato: Inglese (Stati Uniti)
Formattato: Inglese (Stati Uniti)
Formattato: Inglese (Stati Uniti)
Formattato: Inglese (Stati Uniti)

The above considerations are confirmed by the results for the Livorno case. In particular, POD and ETS for the RLAA simulation are similar to those of RADLI forecast (Figure S5). POD for RLAA has slightly better performance (2-3%) compared to RADLI for specific thresholds, showing a positive impact of updating IC/BC as new data become available, nevertheless the impact is small and a detailed study, considering more cases, is needed to draw conclusions about this improvement.

Formattato: Inglese (Stati Uniti)

It is important to note, however, that if the observations are close to the edge of the domain or cross the domain, the impact of BC is expected to be more important than that found in this paper.

Formattato: Inglese (Stati Uniti)

To show the sensitivity of the results to the number of vertical levels we consider the simulation of the Livorno case using RAMS@ISAC with 42 levels (hereafter R_42) instead of 36 levels (R_36). This choice is motivated by the fact that RAMS@ISAC with 42 levels will be operational starting from

September 2019. R_42 has a higher vertical resolution than R_36. The complete list of levels used in R_36 and R_42 is reported in Table S2.

We simulated the Livorno case using R_42 and considering the assimilation of lightning and radar reflectivity factor data assimilation (ANL42). This experiment needed a control run using R_42 (CTRL42).

It is important to note that the background error matrix for RAMS@ISAC with 42 levels was interpolated/extrapolated from that of RAMS@ISAC with 36 levels (the application of the NMC method would require the simulation of the entire HyMeX-SOP1 period using R_42). While we believe that this choice is reasonable for this experiment, it could result in non-optimal adjustments given by RAMS-3DVar.

Figure S6a and S6b show, respectively, the rainfall VSF for CTRL and CTRL42 between 06 and 09 UTC on 10 September 2017, when the storm was active mainly over Lazio (Section 4.2.2 of the paper). The increasing of the number of levels did not result in an improvement of the precipitation forecast over Lazio. There are, however, differences at the local scale especially over Tuscany and NE of Italy. It is also notable the higher rainfall between Corsica and Italian peninsula for CTRL42. This feature is systematic for all VSF of the Livorno case and it is likely caused by a better representation of the interaction between the air-masses and the complex orography of Corsica in R_42. Figure S6c and S6d show the rainfall VSF between 06 and 09 UTC given by RADLI and ANL42. Differences between the two forecasts are small and at the local scale.

POD and ETS scores for R_42 considering the ten VSF of the Livorno case over the R4 domain are shown in Figure S5 for both CTRL42 and ANL42. The POD of CTRL42 is higher than that of CTRL but the improvement is small (2-3%). The POD of ANL42 is slightly worse than that of RADLI. Difference between RADLI and ANL42 could be the result of the specific case considered or a consequence of the non-optimal setting of RAMS-3DVar for ANL42.

The results for ETS score, which penalizes false alarms, show less differences between R_36 and R_42 settings.

Thus, the results of the experiment using 42 vertical levels in RAMS@ISAC are similar to those using 36 levels and show again the crucial role of lightning and radar reflectivity factor data assimilation for the successful forecast of the Livorno case.

S6 A well predicted case study

Formattato: Tipo di carattere:Corsivo

In this section, we show the impact of data assimilation for a case well predicted by the CTRL simulation, without lightning or radar reflectivity factor data assimilation. To keep the discussion concise, we limit the analysis to only lightning data assimilation.

The case study occurred on 5 November 2017 and was chosen because it is not very different from those of Serano and Livorno from a synoptic perspective. In particular, the storm was caused by a trough extending from northern Europe towards the Mediterranean. The interaction between the trough and the Alpine orography caused a low pressure over the Gulf of Genova (not shown). The storm propagated towards SE and, in these conditions, humid and unstable air masses were advected from the Tyrrhenian Sea towards the Italian mainland.

The convection developed over the Tyrrhenian Sea and over the Italian peninsula (especially on its western side), as shown by the lightning density observation on this day (Figure S7): more than 100.000 flashes were detected for this intense event. Moderate to heavy rainfall occurred in several parts of Italy. In particular, between 12 and 15 UTC intense precipitation fell around Rome (Figure S8a) with values greater than 50 mm/3h reported by several raingauges. Some areas of the city were flooded, and problems occurred in local transportation system in outdoor activities.

The intense precipitation over Rome is well predicted by the VSF of the CTRL forecast (Figure S8b), even if there is a shift to the north of the precipitation pattern (15-20 km). The intense precipitation over NE of Italy and the rainfall over Liguria and Tuscany are also well forecast.

Figure S8c shows the rainfall VSF for LIGHT simulation. The VSF follows a 6 h assimilation phase (6-12 UTC for this specific VSF), when more than 34000 flashes are assimilated in RAMS@ISAC following the method of Fierro et al. (2012). LIGHT rainfall VSF is similar to CTRL and lightning data assimilation has a lower impact on the rainfall VSF compared to Livorno or Serano case studies. Of course, considering the high number of assimilated lightning, there are differences between CTRL and LIGHT rainfall VSF, but they do not change substantially the forecast given by CTRL. Rainfall simulated by LIGHT is shifted to the south (15-20 km) compared to CTRL, in better agreement with observations. However, LIGHT VSF overestimates the area of intense precipitation (>30-40 mm/3h).

To discuss more in detail the lower impact of lightning data assimilation for the 5 November case study compared to Serano and Livorno, we consider the vertical cross section of relative humidity at 42°N (Figure S9a) and at the end of the assimilation phase (12 UTC). The vertical section shows very humid layers (relative humidity >92.5%). One of these layers is over the Tyrrhenian Sea (11 °E -12.5 °E). Considering that 0 °C and -25 °C isotherms heights are about 2500 m and 7000 m, it is expected a low impact of lightning data assimilation for this layer. This is confirmed by Figure S9b, which shows the same cross section of Figure S9a for LIGHT simulation. The humid layer over the Tyrrhenian Sea is slightly wider for LIGHT, but differences are overall small. The analyses of other fields, as the averaged specific humidity between 3 and 10 km, also show the low impact of lightning data assimilation for this VSF.

In conclusion, the analysis of the 5 November 2017 event, shows that the impact of lightning data assimilation is much lower when the CTRL VSF has a good performance. Interestingly, lightning data assimilation improves the rainfall forecast at the local scale even for well predicted events, while overestimates the precipitation. This is the main drawback of lightning data assimilation in RAMS@ISAC.

Formattato: Tipo di carattere:Non Corsivo, Inglese (Stati Uniti)

S7 New plots

Eliminato: *3*

Figures S10-S12 show a different representation of the Figures 15-17 of the paper. In particular, we show the rainfall predicted by RAMS@ISAC for the three VSF considered in the paper interpolated at the stations' positions. From Figure S12, in particular, is evident the overestimation of the precipitation field given by both RAD and RADLI (see also Section 4.2.2 in the paper).

Eliminato: 3

Eliminato: 5

Eliminato: of the paper in a different form

Eliminato: 5

S8 Forward radar operator

Eliminato: *4*

In the method of Caumont et al. (2010) there is the need to simulate reflectivity factor (in dBz) from the model output. To compute the reflectivity factor we use the forward operator of Stoelinga used in the RIP (Read/Interpolate/Plot) software of WRF (https://dtcenter.org/wrf-nmm/users/OnLineTutorial/NMM/RIP/index.php, last access 03 March 2019).

Codice campo modificato

The software assumes Rayleigh scattering regime (at C-band this assumption can be considered as valid for light to moderate rain) and includes the contribution of rain, snow and graupel. Particles are assumed spherical with constant density ($\rho_r = \rho_l$=1000 kg/m^3; ρ_s=100 kg/m^3; ρ_g =400 kg/m^3; *r* stands for rain, *l* for liquid, *s* for snow and *g* for graupel).

The size distribution of the hydrometeors follows an exponential distribution given by:

$$N(D) = N_0 e^{-\lambda D} \quad \text{(S1)}$$

Where N_0 is constant for each hydrometeor (N_{0r}=8x10^6,N_{0s}=2x10^7,N_{0g}=4x10^6 m^{-4}).

Using these assumptions, the reflectivity factor for rain Z_{er}, which is the sixth moment of the size distribution, is given by:

$$Z_{er} = \Gamma(7) N_{0r} \lambda^{-7} \quad \text{(S2)}$$

where Γ is the gamma function. The shape factor λ depends on the simulated mixing ratio (q_r) and it is given by:

$$\lambda_r = \left(\frac{\pi N_{0r}\rho_r}{\rho_a q_r}\right)^{1/4} \qquad \text{(S3)}$$

where ρ_a is the density of dry air.

In the case of snow, the reflectivity factor Z_{es} is given by:

$$Z_{es} = \Gamma(7) N_{0s} \lambda^{-7} \left(\frac{\rho_s}{\rho_l}\right)^2 \alpha \qquad \text{(S4)}$$

where α=0.224. The reflectivity factor for graupel is the same as (S4) with N_{0g} replacing N_{0s}, and ρ_g replacing ρ_s . Since the reflectivity factor, when expressed in mm^6/m^3, is an additive quantity, the contributions of rain, snow, and graupel can be added to obtain the reflectivity factor:

$$Z_{etot}=Z_{er}+Z_{eg}+Z_{es}$$

and in dBz is given by:

$$Z_e(dBz)=10\ log(Z_{etot}\ (\text{in mm}^6\text{m}^{-3}))$$

S.9 Conclusions

The analysis of the evolution of the total water mass shows that flashes add less water vapour to the VSF than radar reflectivity factor data assimilation. This, however, even if in agreement with other studies (Fierro et al., 2016) could be a result of the specific case studies.

The sensitivity of the rainfall VSF to the nudging formulation for lightning data assimilation shows that reducing the amount of water vapour added to RAMS@ISAC compared to the default set-up has a worse impact on ETS and POD. Nevertheless, assuming saturation (SAT) for grid points where lightning is observed gave mixed results. Spurious convection was generated in the SAT configuration, which decreased the performance of the model for thresholds larger than 34 mm/3h. A method proposed by Fierro et al. (2012) and used in Lynn et al. (2015) could be used in future implementations of the nudging scheme to suppress spurious convection.

Increasing the radar reflectivity factor error (RAD5) or changing the shape of the area used to compute pseudo-profiles (CIRC) had a minor impact on the rainfall VSF. Furthermore, updating IC/BC as new data are available (RLAA) and increasing the number of vertical levels in RAMS@ISAC (CTRL42, ANL42) gave minor changes to the rainfall VSF. Therefore, the sensitivity tests generalize the findings of the paper.

Formattato: Tipo di carattere:Non Grassetto, Corsivo

Eliminato: compared

Eliminato: to the

Eliminato: are

Eliminato: In particular, s

Finally, the results for a case study well predicted by the background show a limited impact of lightning data assimilation.

References

Caumont, O., Ducrocq, V., Wattrelot, E., Jaubert, G., and Pradier-Vabre, S.: 1D+3DVar assimilation of radar reflectivity data: a proof of concept, Tellus A: Dynamic Meteorology and Oceanography, 62:2, 173-187, https://www.tandfonline.com/doi/abs/10.1111/j.1600-0870.2009.00430.x, 2010.

Fierro, A. O., Mansell, E., Ziegler, C., and MacGorman, D.: Application of a lightning data assimilation technique in the WRFARW model at cloud-resolving scales for the tornado outbreak of 24 May 2011, Mon. Weather Rev., 140, 2609–2627, 2012.

Fierro, A. O., A. J. Clark, E. R. Mansell, D. R. MacGorman, S. Dembek, and C. Ziegler: Impact of storm-scale lightning data assimilation on WRF-ARW precipitation forecasts during the 2013 warm season over the contiguous United States. Mon. Wea. Rev., 143, 757–777, 2015. doi:https://doi.org/10.1175/MWR-D-14-00183.1.

Fierro, A.O., Gao, l., Ziegler, C. L., Calhoun, K. M., Mansell, E. R., and MacGorman, D. R.: Assimilation of Flash Extent Data in the Variational Framework at Convection-Allowing Scales: Proof-of-Concept and Evaluation for the Short-Term Forecast of the 24 May 2011 Tornado Outbreak. Mon. Wea. Rev., 144, 4373–4393, https://doi.org/10.1175/MWR-D-16-0053.1, 2016.

Lynn, B. H., G. Kelman, and G. Ellrod, 2015: An evaluation of the efficacy of using observed lightning to improve convective lightning forecasts. Wea. Forecasting, 30, 405-423 doi:10.1175/ WAF-D-13-00028.1.

Parrish, D.F., and Derber, J.C.: The National Meteorological Center's Spectral Statistical Interpolation analysis system, Monthly Weather Review, 120, 1747-1763, 1992.

Table S1: Simulations considered in this supplement material.

Experiment	Description	Data assimilated	Model variable impacted	Note
CTRL	Control run	None	None	/
RAD	RADAR data assimilation	Reflectivity factor CAPPI (RAMS-3DVar)	Water vapour mixing ratio	/

Eliminato:

Codice campo modificato

Codice campo modificato

Eliminato: Types of

Eliminato: s

Tabella formattata

LIGHT	Lightning data assimilation (A=0.86; B=0.15 in Eqn (1))	Lightning density (nudging)	Water vapour mixing ratio	/
RADLI	RADAR + lightning data assimilation (A=0.86; B=0.15 in Eqn (1))	Reflectivity factor CAPPI (RAMS-3DVar) + Lightning density (nudging)	Water vapour mixing ratio	/
A_76	Lightning data assimilation (A=0.76; B=0.25 in Eqn (1))	Lightning density (nudging)	Water vapour mixing ratio	/
SAT	Lightning data assimilation (A=1.01; B=0. in Eqn (1))	Lightning density (nudging)	Water vapour mixing ratio	/
RAD5	RADAR data assimilation.	Reflectivity factor CAPPI (RAMS-3DVar)	Water vapour mixing ratio	As RAD simulation but with the error of radar reflectivity factor increased by 5.
CIRC	RADAR data assimilation	Reflectivity factor CAPPI (RAMS-3DVar)	Water vapour mixing ratio	As RAD but with a circular shape to compute relative humidity pseudo-profiles

RLAA	RADAR + lightning data assimilation (A=0.86; B=0.15 in Eqn (1)).	Reflectivity factor CAPPI (RAMS-3DVar) + Lightning density (nudging)	Water vapour mixing ratio	As RADLI but with updated IC/BC as new data are available
CTRL42	Control run	None	None	As CTRL simulation but using 42 vertical levels
ANL42	RADAR + lightning data assimilation (A=0.86; B=0.15 in Eqn (1))	Reflectivity factor CAPPI (RAMS-3DVar) + Lightning density (nudging)	Water vapour mixing ratio	As RADLI simulation but using 42 vertical levels

Table S2: Vertical levels of RAMS@ISAC with 36 levels (default setting, R_36) and RAMS@ISAC with 42 levels (R_42).

RAMS@ISAC CONFIGURATION	LEVEL (m)
R_36	0, 50, 108, 174, 250, 337, 438, 553, 686, 839, 1015, 1217, 1450, 1718, 2025, 2379, 2786, 3254, 3792, 4411, 5122, 5941, 6882, 7964, 9164, 10364, 11563, 12764, 13964, 15164, 16364, 17564, 18764, 19964, 21164, 22364
R_42	0, 50, 106, 167, 235, 311, 396, 489, 593, 708, 836, 978, 1136, 1311, 1505, 1720, 1959, 2225, 2520, 2847, 3210, 3613, 4061, 4557, 5109, 5721, 6400, 7154, 7991, 8920, 9951, 1096, 12296, 13496, 14696, 15896, 17096, 18296, 19496, 20696, 21896, 23096

Formattato: Italiano

Formattato: Italiano

Eliminato: ... [1]

a)

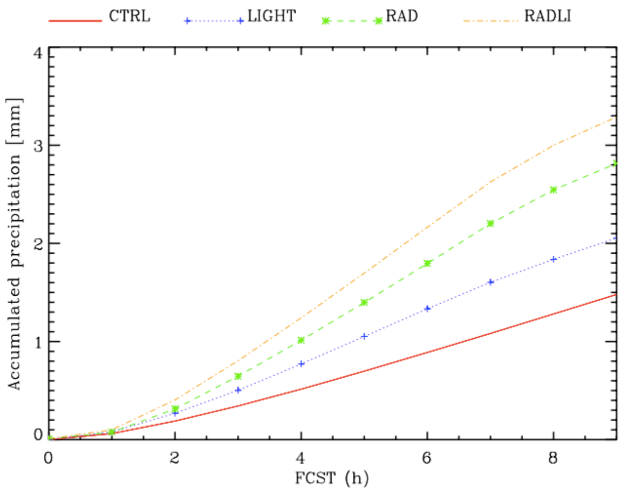

b)

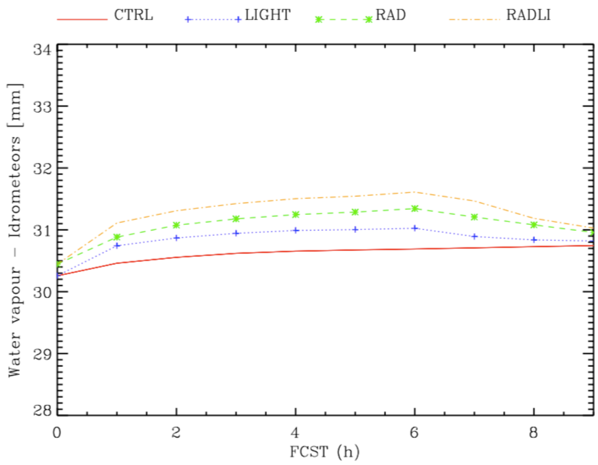

Figure S1: a) Evolution of accumulated precipitation for different model configurations and for all forecast hours; b) as in a) for the hydrometeors plus water vapour mass per unit area. All quantities are expressed in [mm] and are averaged over the number of grid columns.

Eliminato: the

Eliminato: The nearest neighbourhood is used to compute the dichotomous contingency tables.

a)

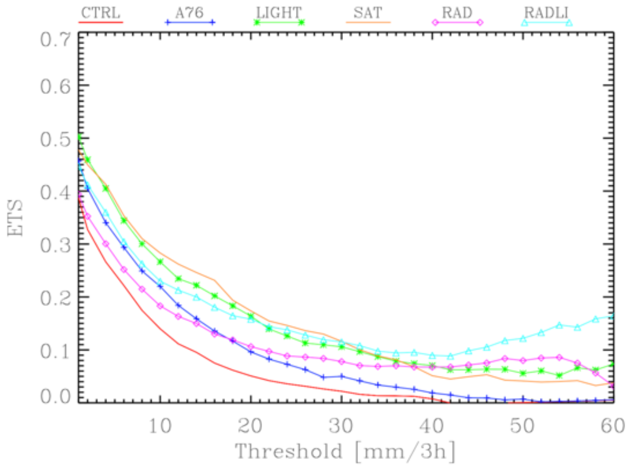

b)

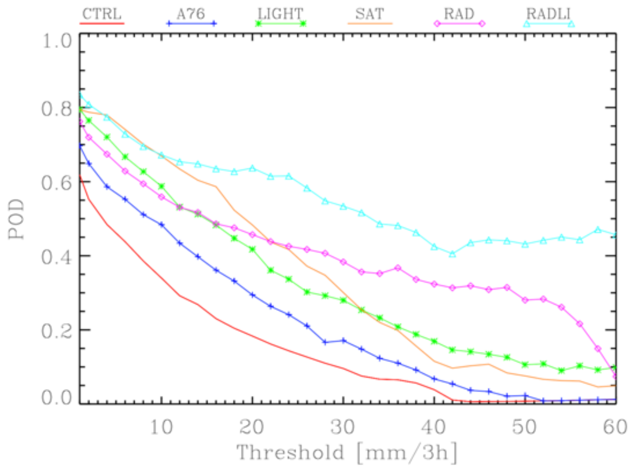

Figure S2: a) ETS score for all VSF considered in this paper; b) as in a) for the POD score. Scores are computed for the R4 domain considering all VSF for Livorno and Serano cases and using the nearest neighbourhood value. Scores are computed for the nearest neighbourhood and for the thresholds: 1mm/3h, 2mm/3h and then every 2 mm/3h up to 60 mm/3h.

Eliminato: The nearest neighbourhood method is used to compute scores.

a)

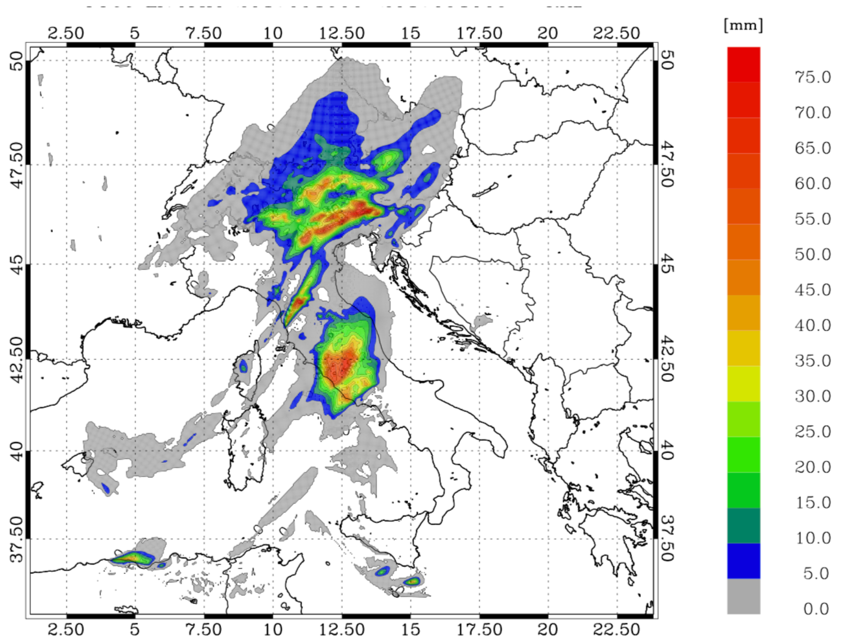
2.50 5 7.50 10 12.50 15 17.50 20 22.50
50 47.50 45 42.50 40 37.50
[mm]
75.0
70.0
65.0
60.0
55.0
50.0
45.0
40.0
35.0
30.0
25.0
20.0
15.0
10.0
5.0
0.0

b)

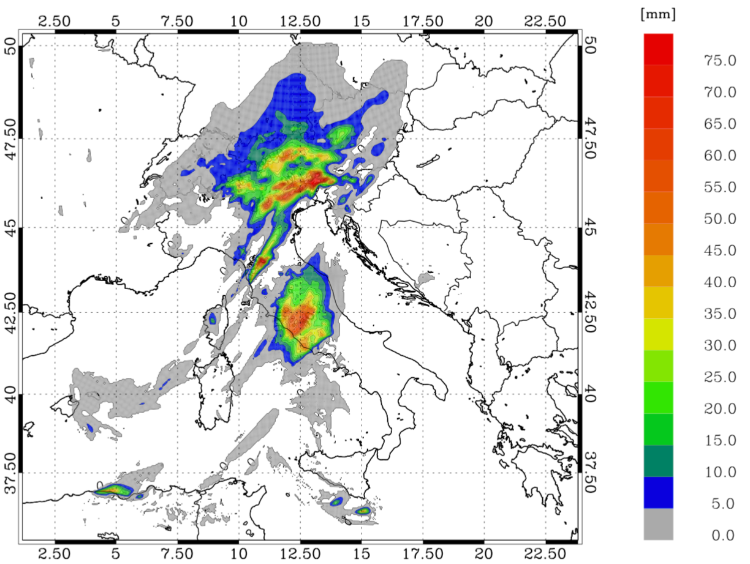

2.50
5
7.50
10
12.50
15
17.50
20
22.50
50
47.50
45
42.50
40
37.50
[mm]
75.0
70.0
65.0
60.0
55.0
50.0
45.0
40.0
35.0
30.0
25.0
20.0
15.0
10.0
5.0
0.0

Eliminato:

c)

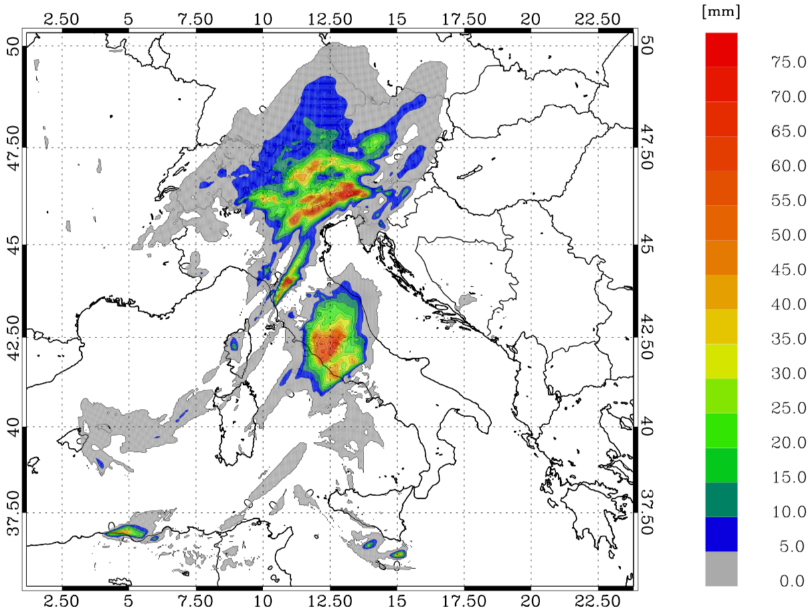

Figure S3: a) rainfall VSF between 06 and 09 UTC on 10 September for RAD; b) as in a) for RAD5; c) as in a) for CIRC.

a)

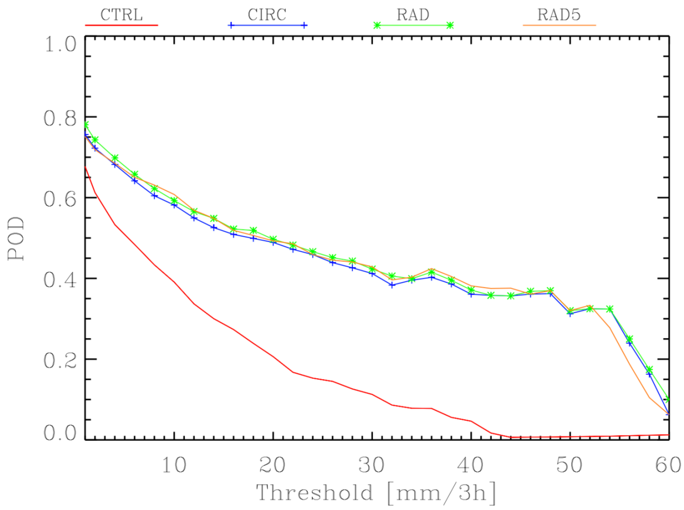

b)

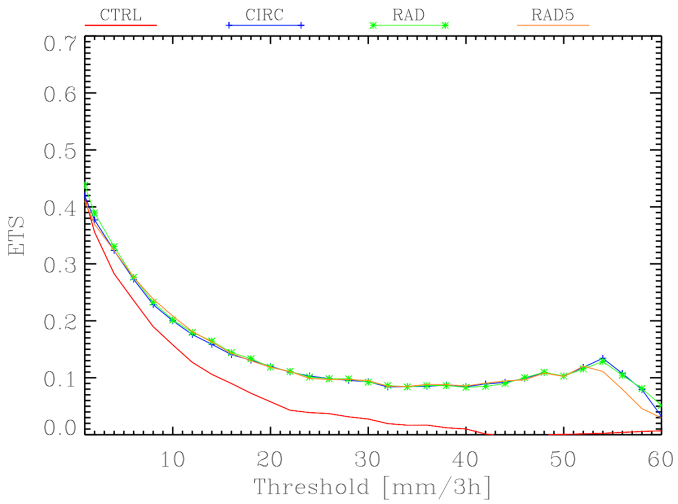

Figure S4: a) POD score for Livorno; b) as in a) for ETS score. CTRL is the control simulation, RAD is the simulation assimilating radar reflectivity factor, RAD5 is the simulation with a reflectivity factor error five times that of RAD; CIRC is the simulation using a circle for computing relative humidity pseudo-profiles. Scores are computed for the R4 domain considering the ten VSF of the Livorno case. Scores are computed

Eliminato:

Formattato: Normale, A sinistra, Rientro: Sinistro: 0,63 cm, Nessun elenco puntato o numerato

Formattato: Interlinea: singola

for the nearest neighbourhood and for the threshold of: 1mm/3h, 2mm/3h and then every 2 mm/3h up to 60 mm/3h, considering the R4 domain and the ten VSF of the Livorno case.

Formattato: Normale, Rientro: Sinistro: 0,63 cm, Nessun elenco puntato o numerato

a)

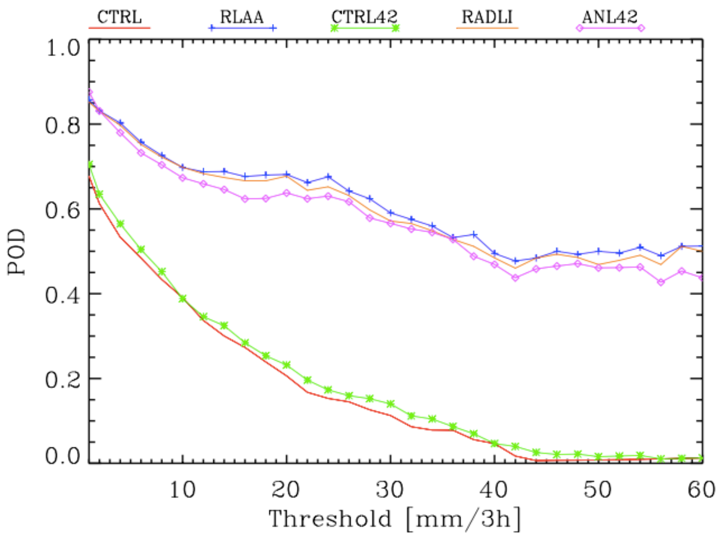

b)

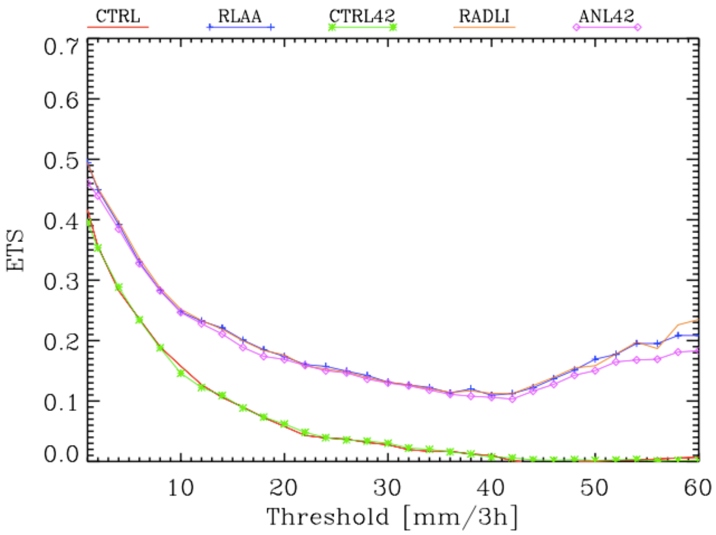

Figure S5: a) POD score for Livorno; b) as in a) for the ETS score. CTRL is the control simulation, RLAA is the simulations with updated IC/BC, CTRL42 is the control simulation using 42 model vertical level,

Formattato: Interlinea: singola

ANL42 is the simulation assimilating radar reflectivity factor and lightning and using 42 model vertical levels. Scores are computed for R4 domain considering all the ten VSF of the Livorno case. Scores are computed for the nearest neighbourhood and for the thresholds: 1mm/3h, 2mm/3h and then every 2 mm/3h up to 60 mm/3h.

Formattato: Normale, Nessun elenco puntato o numerato

a)

Formattato: Normale, Centrato, Rientro: Sinistro: 0,63 cm, Nessun elenco puntato o numerato

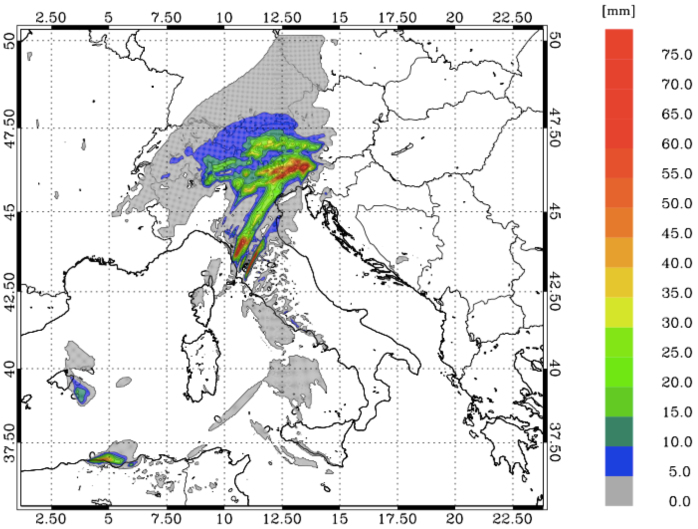

Formattato: Normale, Rientro: Sinistro: 0,63 cm, Nessun elenco puntato o numerato

b)

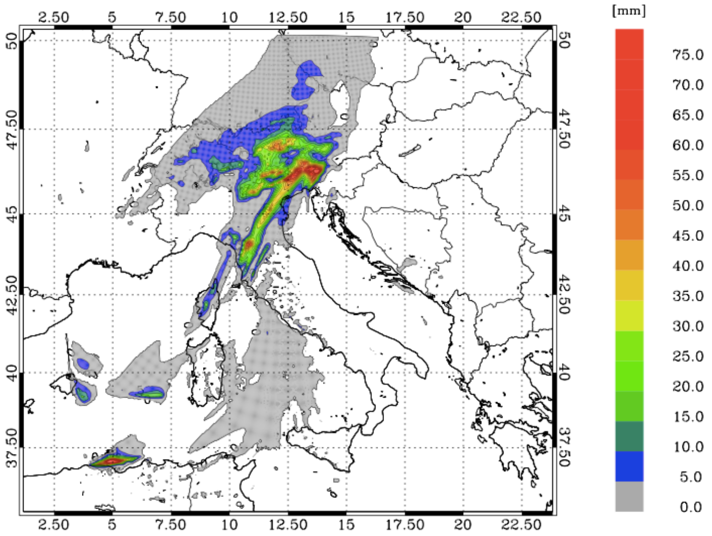

c)

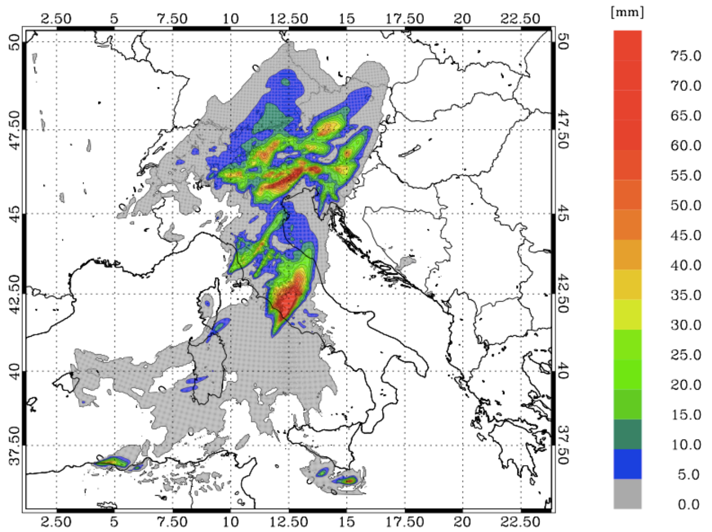

d)

Formattato: Normale, Centrato, Rientro: Sinistro: 0,63 cm, Nessun elenco puntato o numerato

Formattato: Normale, Rientro: Sinistro: 0,63 cm, Nessun elenco puntato o numerato

Formattato: Normale, Centrato, Rientro: Sinistro: 0,63 cm, Nessun elenco puntato o numerato

Formattato: Normale, Rientro: Sinistro: 0,63 cm, Nessun elenco puntato o numerato

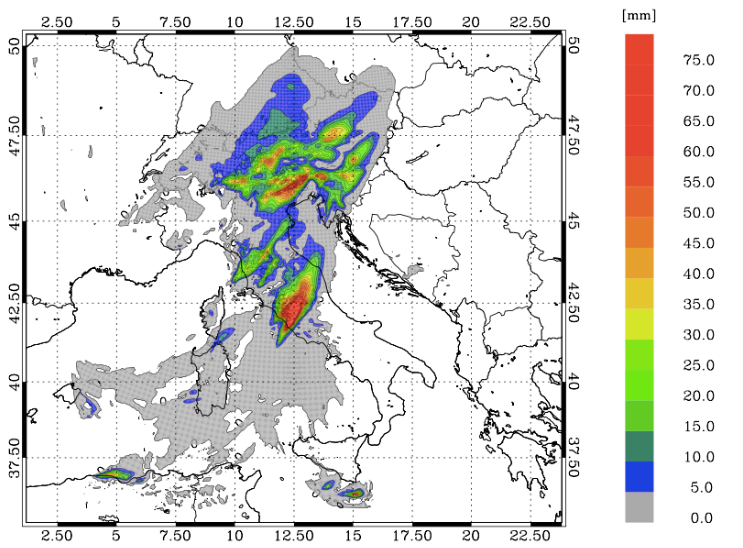

Formattato: Normale, Centrato, Rientro: Sinistro: 0,63 cm, Nessun elenco puntato o numerato

Formattato: Normale, Nessun elenco puntato o numerato

Figure S6: rainfall VSF between 06 and 09 UTC on 10 September for CTRL; b) as in a) for CTRL42; c) as in a) for RADLI; d) as in a) for ANL42.

Formattato: Interlinea: singola

Formattato: Normale, Rientro: Sinistro: 0,63 cm, Nessun elenco puntato o numerato

Formattato: Tipo di carattere:(Predefinito) Times New Roman, 12 pt, Colore carattere: Nero, Bordo:: (Nessun bordo)

Formattato: Centrato

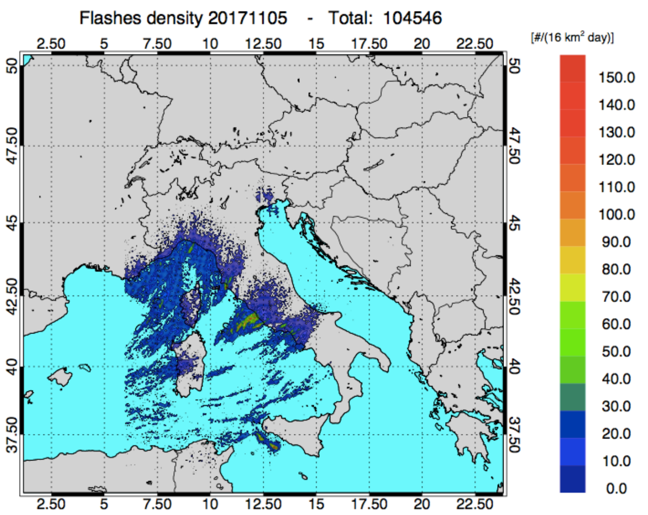

Figure S7: a) Lightning density (lightning number per 16 km^2 for the whole day) recorded on 05 November 2017. The total number of flashes is shown in the title.

Formattato: Tipo di carattere:11 pt

a)

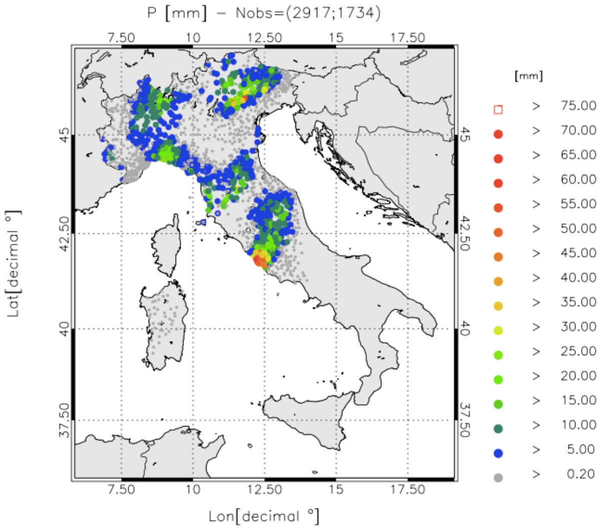

b)

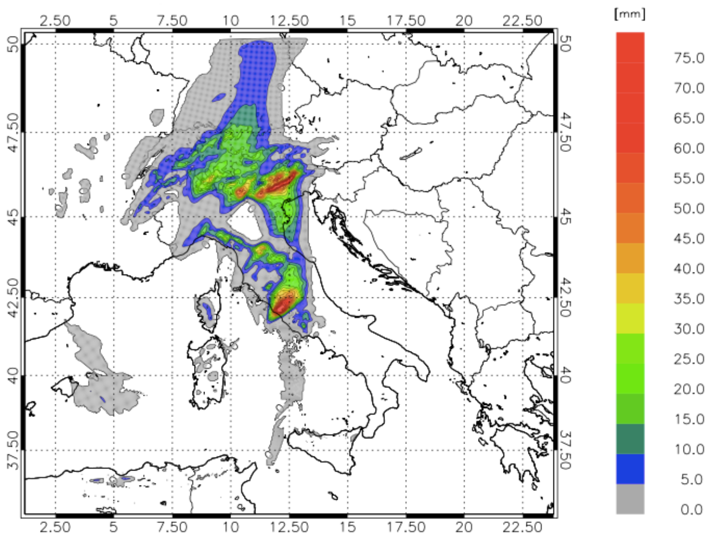

Formattato: Tipo di carattere:10 pt

Formattato: Centrato

Formattato: Tipo di carattere:10 pt

Formattato: Centrato

c)

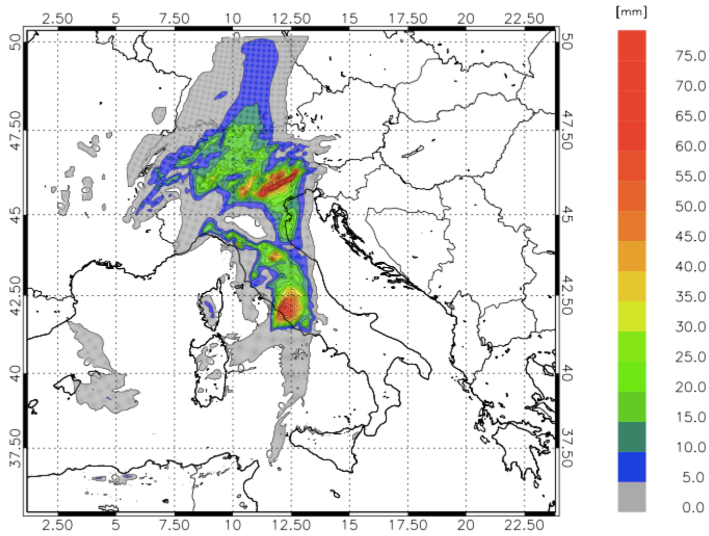

Figure S8: a) rainfall reported by raingauges between 12 and 15 UTC on 5 November 2017. Only stations reporting at least 0.2 mm/3h are shown. The first number in the title within brackets represents the number of raingauges available over the domain, while the second number shows those observing at least 0.2 mm/3h; b) rainfall VSF of CTRL for the same time interval as in a); c) as in b) for LIGHT forecast.

Formattato: Tipo di carattere:10 pt

Formattato: Centrato

Formattato: Tipo di carattere:11 pt

a)

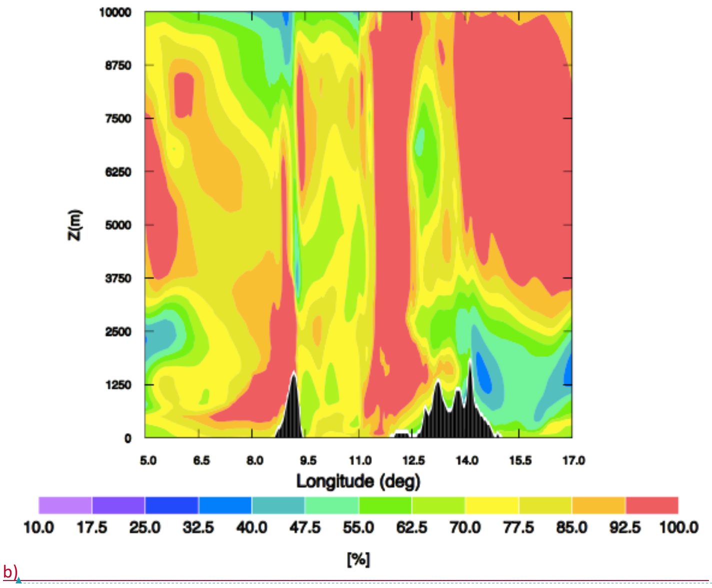

b)

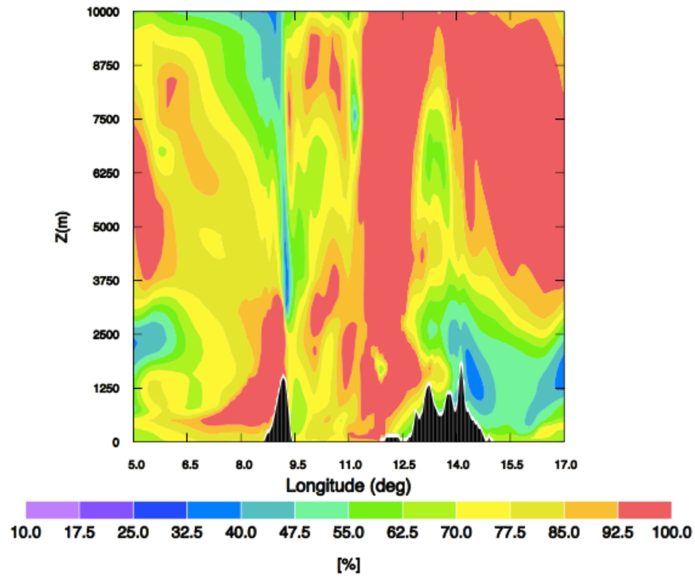

Formattato: Centrato

Formattato: Tipo di carattere:10 pt

Formattato: Tipo di carattere:10 pt

Figure S9: a) Relative humidity longitude-height cross-section at 42°N and at the end of the assimilation period (12 UTC on 5 November 2017) for the CTRL simulation; b) as in a) for LIGHT simulation. Only longitudes between 5 E and 17 E and altitudes between 0 km and 10 km are shown for clarity.

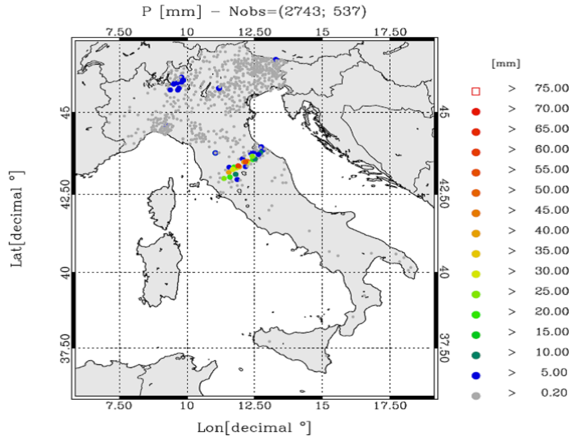

b)

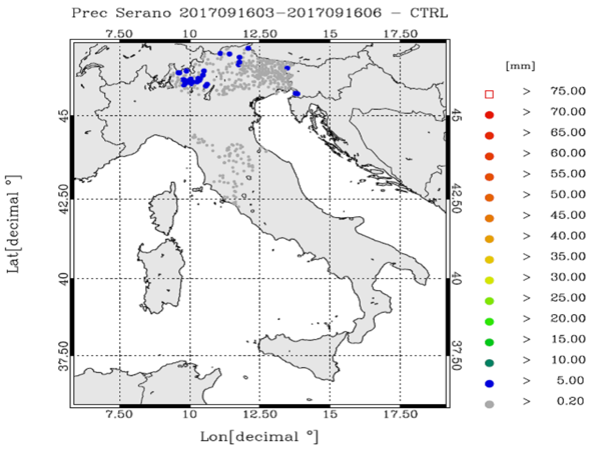

Formattato: Tipo di carattere:11 pt

Formattato: Tipo di carattere:11 pt

Formattato: Inglese (Regno Unito)

Formattato: Centrato

Formattato: Centrato

c)

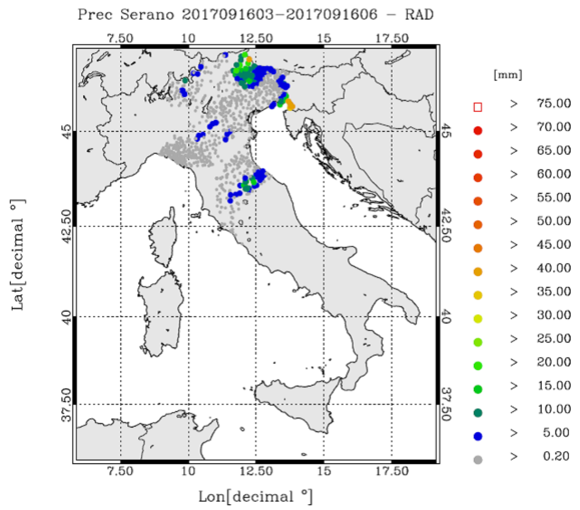

Formattato: Centrato

d)

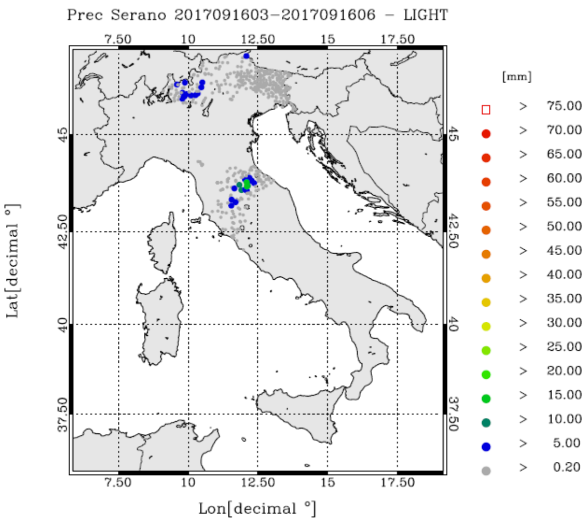

Formattato: Centrato

e)

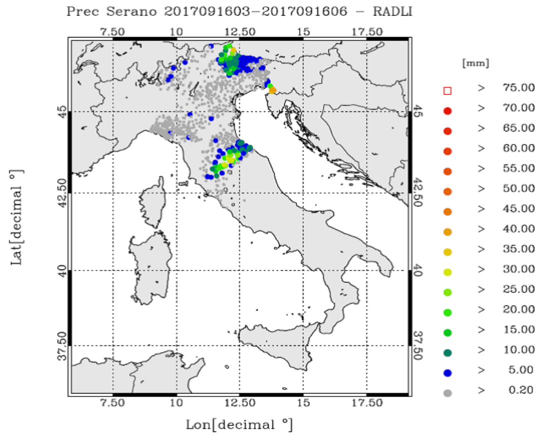

Formattato: Centrato

Figure S10: a) rainfall reported by raingauges between 03 and 06 UTC on 16 September 2017. Only raingauges observing at least 0.2 mm/day are shown. The first number in the title within brackets represents the available raingauges, while the second number represents those observing at least 0.2 mm/3h; b) as in a) for CTRL forecast; c) as in a) for RAD forecast; d) as in a) for LIGHT forecast; e) as in a) for RADLI forecast.

Formattato: Tipo di carattere:11 pt

Eliminato: 3

a) b)

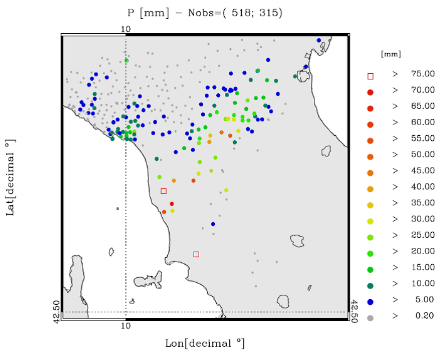

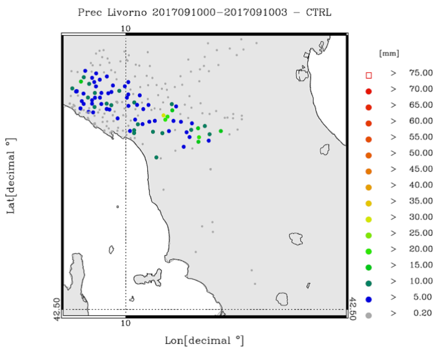

c) d)

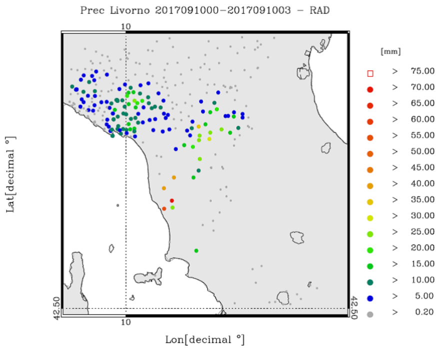

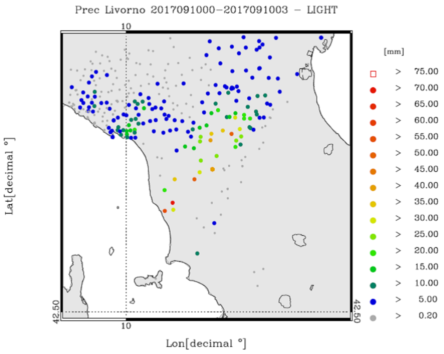

e)

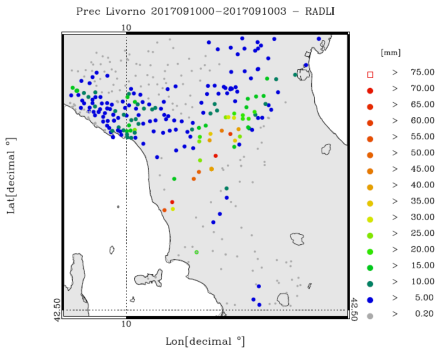

Figure S11: a) rainfall reported by raingauges between 00 and 03 UTC on 10 September 2017. Only stations reporting at least 0.2 mm/3h are shown. The first number in the title within brackets represents the number of raingauges available over the domain, while the second number shows those observing at least 0.2 mm/3h; b) as in a) for CTRL forecast; c) as in a) for RAD forecast; d) as in a) for LIGHT forecast; e) as in a) for RADLI forecast.

Formattato: Tipo di carattere:11 pt

Eliminato: 4

Eliminato: ... [2]

a)

Formattato: Centrato

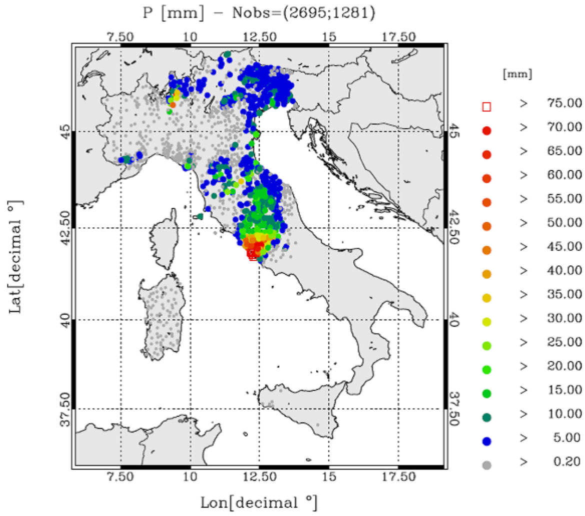

b)

Formattato: Centrato

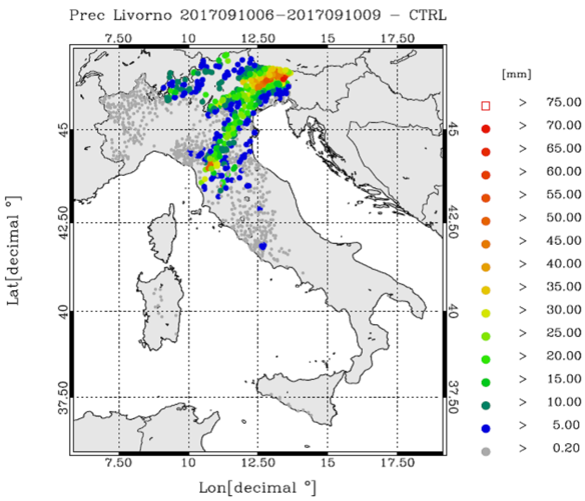

c)

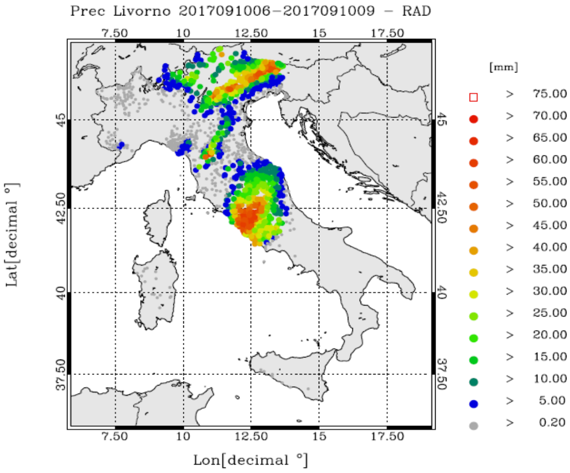

Formattato: Centrato

d)

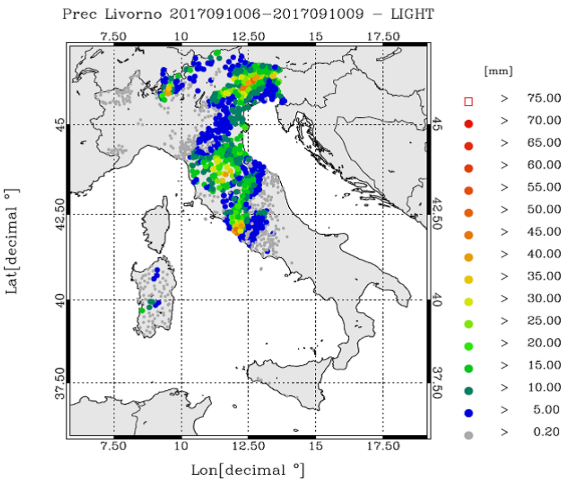

Formattato: Centrato

e)

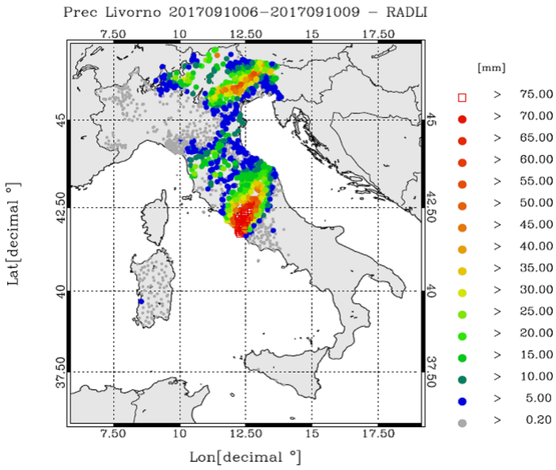

Formattato: Centrato

Figure S12: a) rainfall reported by raingauges between 06 and 09 UTC on 10 September 2017. For this time period 2695 raingauges reported valid observations in the domain, however only stations reporting at least 0.2 mm/3h are shown. The first number in the title within brackets represents the number of raingauges available over the domain, while the second number shows those observing at least 0.2 mm/3h; b) as in a) for CTRL forecast; c) as in a) for RAD forecast; d) as in a) for LIGHT forecast; g) as in a) for RADLI forecast.

Formattato: Tipo di carattere:11 pt

Eliminato: 5

Pagina 13: [1] Eliminato	stefano federico	06/06/19 16:13:00

Pagina 30: [2] Eliminato	stefano federico	06/06/19 16:19:00